Schweizerische Eidgenossenschaft
Confédération suisse
Confederazione Svizzera
Confederaziun svizra

Federal Department of the Environment, Transport, Energy and Communications DETEC

Swiss Federal Office of Energy SFOE
Energy Research and Cleantech Division

Final report dated 31.03.2021

ReVerDi

Platform to reduce fuel consumption and CO2 emissions of diesel power units using optimized operation and alternative fuels.

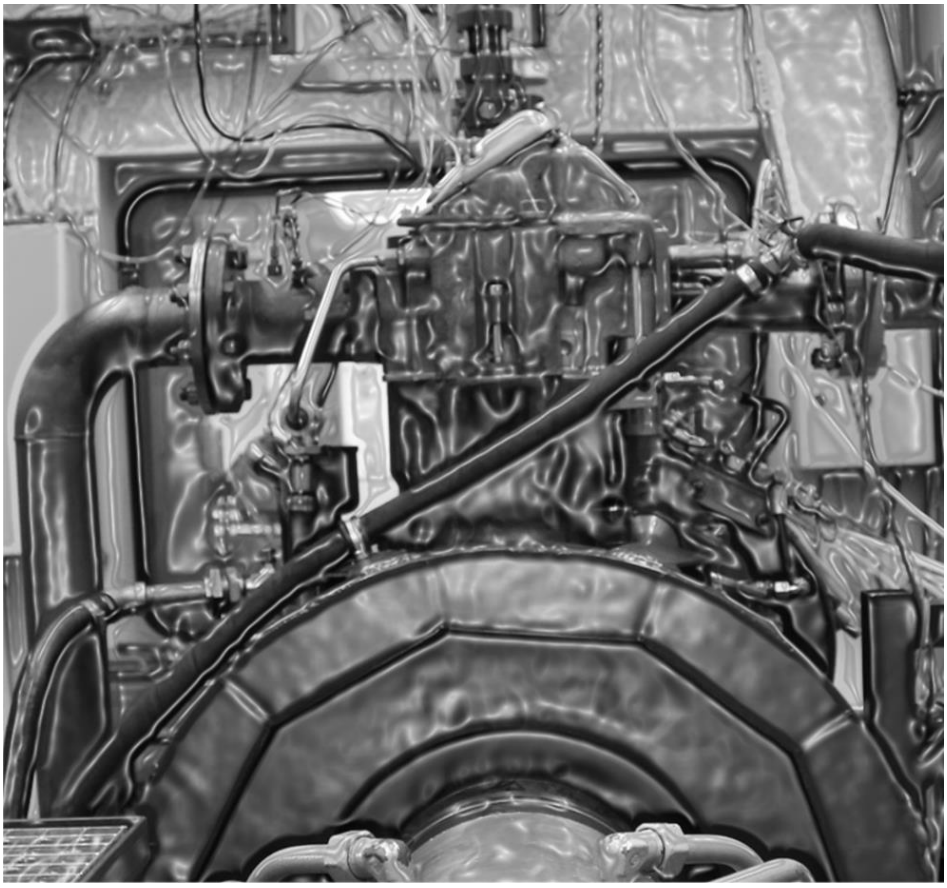

Source: ©LAV ETH 2015

Date: 31.03.2021

Location: Bern

Publisher:
Swiss Federal Office of Energy SFOE
Energy Research and Cleantech
CH-3003 Bern
www.bfe.admin.ch

Co-financing:
Neste Corporation
POB 95
00095 Neste, Finland

Subsidy recipients:
ETH Zürich, Institut für Energietechnik, LAV
Prof. Konstantinos Boulouchos
Sonneggstrasse 3
CH-8092 Zürich
www.lav.ethz.ch

EMPA
Überlandstrasse 129
8600 Dübendorf
www.Empa.ch

Vir2sense GmbH
Sihlbruggstrasse 109
CH-6340 Baar
www.vir2sense.com

combustion and flow solutions GmbH
Technoparkstrasse 1
CH-8005 Zürich
www.combustion-flow-solutions.com

Authors:
Christophe Barro, LAV, barro@lav.mavt.ethz.ch
Matteo Parravicini, LAV parravicini@lav.mavt.ethz.ch
Konstantinos Boulouchos, LAV, boulouchos@lav.mavt.ethz.ch
Panayotis Dimopoulos Eggenschwiler, EMPA, Panayotis.Dimopoulos@Empa.ch
Pangiotis Kyrtatos, V2S, kyrtatos@vir2sense.com
Christian Lämmle, CFS laemmle@combustion-flow-solutions.com
Stéphanie Schlatter, CFS, schlatter@combustion-flow-solutions.com

SFOE project coordinators:
Luca Castiglioni, luca.castiglioni@bfe.admin.ch

SFOE contract number: SI/501737-01 / 8100079

The authors bear the entire responsibility for the content of this report and for the conclusions drawn therefrom.

Zusammenfassung und wichtigste Ergebnisse

Die Reduktion von CO2 ist einer der grössten Aufgaben der jetzigen Generation. Eine Möglichkeit CO2 Emissionen zu reduzieren ist die Verwendung von Kraftstoffen mit einem geringeren CO2 Fussabdruck. Solche Kraftstoffe zeigen jedoch eine andere Verbrennungs- und Schadstoffbildungscharakteristik, sodass Anpassungen in der Motorsteuerung notwendig sind, um das volle Potential des Kraftstoffs auszuschöpfen. In diesem Projekt wird eine Simulationsplattform entwickelt, um das System Motor und Abgasnachbehandlung zu optimieren. Um dies zu erreichen wurden verschiedene Diesel-ähnliche Kraftstoffe in einem Einzylinder-Forschungsmotor getestet und detailliert die Charakteristiken bezüglich Verbrennung und Emissionen inklusive dem Energiebedarf der Partikelfilterregeneration erforscht und ausgewertet. Diese Charakteristika wurde modelliert und in ein GT Power Modell eines 6-Zylinder Motors integriert. Das Modell beinhaltet einen SCR (selective catalytic reduction) zur NOx Reduktion, sowie einen Partikelfilter (DPF), welcher seinen Energiebedarf zur Regeneration abhängig vom Kraftstoff und der Russmenge festlegt. Somit erlaubt die Plattform einen Vergleich der Motoreffizienz mit verschiedenen Kraftstoffen, inklusive Vorzüge bei Kraftstoffen mit z.B. geringerer Russneigung. Die verwenden Kraftstoffe waren paraffinische Diesel (HVO (Hydrotreated Vegetable Oil), GTL (Gas-to-Liquid) und Polyoxymethyldimethylether (OME_{3-6}), respektive deren Beimischung in Diesel oder untereinander.

Die wichtigsten Ergebnisse des Projekts sind folgend zusammengefasst:

Die Verbrennungs- und Emissionseigenschaften von Diesel-ähnlichen Kraftstoffen, welche potenziell erneuerbar sind, wurden herausgearbeitet und modelliert.

- Die alternativen Kraftstoffe haben punktuell andere Eigenschaften als Diesel, diese erlauben es den Nachteil des geringeren volumetrischen Heizwertes, welche alle getesteten Kraftstoffe aufweisen, auszugleichen. Bei den paraffinischen Kraftstoffen ist dies vor allem die hohe Zündwilligkeit als Folge der hohen Cetanzahl und die reduzierte Russbildung infolge Abwesenheit von aromatischen Verbindungen. Diese Eigenschaft ist auch vorteilhaft bei der benötigen Energie für die Regenration des Partikelfilters. Bei den Sauerstoffhaltigen Kraftstoffen verhindert der Sauerstoff Russbildung noch effektiver und die Luft-Kraftstoffmischung ist schneller.

Das Reduktionspotential bezüglich Verbrauchs und generell Betriebskosten eines Dieselmotors in Kombination mit der Abgasnachbehandlung (Partikelfilter und NOx SCR Katalysator) wurde für verschiede Kraftstoffe dargestellt. Für die verwendeten Kraftstoffe wurde folgendes maximales, sowie minimales Well-to-Wheel CO2-Einsparpotential ermittelt (Well-to-Tank dazu in Klammern):

- Diesel mit 20% HVO: 19.2% / 17.7% (18%)
- HVO: 90.2% / 89.6% (90%)
- Diesel mit 7% OME 6.1% / 3.8% (4%)
- 77% HVO mit 18% OME und 5% Stabilisator: 88.2% / 87.9% (88%)

Die CO2-Reduktion von rund 90% bei den paraffinischen Kraftstoffen ist dominiert durch die Well-to-Tank Eigenschaft des Kraftstoffs und nur minim verändert durch die Effizienz des Motors. Bei den Kraftstoffen mit hohem Dieselanteil liegt der Anteil, der gesteigerten Effizienz an die CO2 Reduktion bei bis zu 35%. Generell kompensiert oder überkompensiert die Optimierung die Nachteile des geringeren volumetrischen Heizwerts sehr gut. Die Resultate zeigen auch, dass es sich durchaus lohnen kann, Kraftstoffe mit geringerer Russneigung bei Motoren mit DPF einzusetzen. Nach der Optimierung wird bei HVO im Vergleich zum Betrieb mit Diesel eine höhere Abgasrückführrate (AGR) verwendet. Dies ist möglich, da trotz höherer AGR-Rate die Anzahl Regenerationen des DPF nicht erhöht wird. Dies wiederum führt zu einer geringeren Menge an Roh NOx-Emissionen ohne signifikante Verbrauchserhöhung. Die Reduktion in Roh-NOx ist direkt mit einer Einsparung von Harnstoff verbunden (in diesem Fall mehr als 50%). Allerdings ist dies nur auf das verwendete Setup anwendbar. Sobald sich zum Beispiel die Grösse oder Eigenschaften des DPF, des SCR oder anderen Komponenten ändern, so ändern sich auch die Resultate und das Einsparpotenzial des Kraftstoffs. Daher ist es auch Wichtig, dass die Plattform sehr modular aufgebaut ist und schnell auf ein System mit

anderen Komponenten (z.B. Hochdruck statt Niederdruck Abgasrückführung) abgeändert werden kann. Dies wurde demonstriert mit einer Reduktion des SCR um 50%. Dabei wurde das zuvor beschriebe Verhalten noch verstärkt.
Ein modulares Simulationssystem wurde entwickelt, um die Optimierung von Motor und Abgasnachbehandlung mit unterschiedlicher Komponentenanordnung und verschiedener Kraftstoffe zu ermöglichen. Nationale und internationale Motorenhersteller können direkt von den Projektergebnissen profitieren.

Summary and main findings

The reduction of CO2 emissions in transport and power generation is a key challenge of the current generation. One particular opportunity of CO2 reduction is the introduction of fuels with a smaller CO2 footprint. The combustion characteristics of such fuels are different and require engine settings modification to profit most from these characteristics. The aim of this project is to develop a simulation platform for optimizing the overall engine unit (engine with exhaust gas aftertreatment) of vehicles of all sizes for fuels with different characteristics. Therefore, different diesel like fuels have been tested in a single cylinder research engine to determine their detailed behavior with respect to combustion and emission characteristics, including required particulate filter regeneration energy. The combustion and emission formation process has been modelled and included into a GT Power model of a 6-cylinder heavy-duty engine. The model includes an SCR (selective catalytic reduction) for NOx reduction and a DPF (particulate filter), which requires energy for regeneration depending on the soot oxidation activity of each fuel which was determined through detailed analysis within this project. This model platform enables the comparison of engine efficiency when operating the engine with different fuels, including e.g. benefits from a fuel with lower tendency to form soot. The fuels tested include Hydrotreated Vegetable Oil (HVO), Gas-to-Liquid fuel (GTL) and polyoximethylene dimethylether (OME_{3-6}), which were tested neat and as blends with Diesel or among each other.
The main findings of this project are:
Different liquid diesel-like fuels which can be obtained by renewable sources show different combustion and emission characteristics.

- The fuels have different characteristics when compared to Diesel. For the paraffinic fuels, the ignitability is higher due to the high cetane number. In addition, soot formation is reduced due to absence of aromatic content, which leads to reduced energy consumption for the particulate filter regeneration. The oxygenated fuels inhibit soot formation even more effectively, and the air fuel mixing is faster, resulting in faster diffusion combustion.

The different fuel characteristics result in a potential to optimize diesel internal combustion engines including aftertreatment systems (Diesel particulate filter and NOx SCR catalyst) for operation with fuels of different composition. For the fuels investigated, the following maximum and minimum well-to-wheel CO2 reduction potential was found (well-to-tank in brackets):

- Diesel with 20% HVO: 19.2% / 17.7% (18%)
- HVO: 90.2% / 89.6% (90%)
- Diesel with 7% OME 6.1% / 3.8% (4%)
- 77% HVO with 18% OME and 5% stabilizer: 88.2% / 87.9% (88%)

The approx. 90% CO2 reduction found is dominated by the well-to-tank characteristics of the fuel itself and only small contribution originates from changes in engine operation. For fuels mixtures with small proportions of alternative fuels, the contribution to well-to-wheel improvements from the optimized engine operation is up to 35% of the total improvement observed. The optimization performed also compensates or even overcompensates for the smaller volumetric heating value of the alternative fuels, which otherwise would result in an engine efficiency decrease.
The final results show that engines with a DPF (i.e. used in applications where soot emissions are tightly regulated) can benefit from fuels which are less prone to form soot. After the optimization, in the case

of HVO at low load, a higher EGR (exhaust gas recirculation) rate can be applied in comparison to Diesel. The higher EGR rate does not increase DPF regeneration events and results in lower engine-out (before SCR) NOx emissions without a significant penalty in fuel consumption. The reduction in raw NOx reduces urea consumption (more than 50% in this case). This behaviour is even more apparent when the size of the SCR is reduced. As a general rule, it was determined that low sooting fuels are most beneficial when employing small particulate filters (where regeneration frequency is high), an efficient EGR path and a small NOx aftertreatement device.The latter has been demonstrated by an SCR size reduction of 50% which was investigated during the project.
The engine optimization for specific fuel compositions can be conducted at the engine design phase using engine modelling tools which have been developed within this project. Swiss and international engine manufacturers can directly benefit from the project's findings.

Contents

Abbreviations

DOC	Diesel Oxydation Catalyst
DOI	Duration of Injection
DPF	Diesel Particulate Filter
EGR	Exhaust Gas Recirculation
GTL	Gas to Liquid
HRR	Heat Release Rate
HVO	Hydrotreated/Hydrogenated Vegetable Oil
LHV	Lower Heating Value
ISEC	Indicated Specific Energy Consumption
NOx	Nitrogen Oxides (NO and NO2)
OME	Poly(oxymethylene) dimethyl ethers
SCR	Selective Catalytic Reduction
SOI	Start of Injection

1 Introduction

1.1 Background information and current situation

In order to meet the federal government's climate targets, measures to reduce CO2 emissions are required, as Figure 1 (SCCER-Mobility strategy) shows. In addition to more efficient mobility strategies, fuels with reduced or zero carbon emissions need to be introduced in order to reduce CO2 emissions arising from mobility, transportation and distributed power generation.

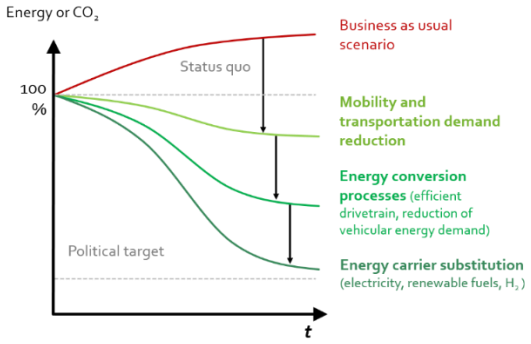

Figure 1: Different scenarios for the future development of CO2 emissions (SCCER-Mobility strategy)

Modern, electronically controlled engines have a large number of settings which allows their optimization depending on operating conditions and fuel used. These independent parameters need to be set based on an optimization for minimizing fuel consumption while simultaneously keeping other harmful emissions below the legislated limits. The optimization effort increases exponentially with the number of degrees of freedom of the motor. Due to the complexity of the processes and the number of independent parameters, the calibration of these engines has become exceedingly complex.
Past studies (e.g. the “MOVE” project [1]) have showed that the operation of a diesel engine can be optimized using a systematic approach. This was done using measurements of the engine on the test bench which cover the entire range of possible engine operation. As an alternative to measurements, as demonstrated in «MOVE», accurate models of the engine process can also be used, minimizing the calibration effort and cost.
As has been shown in past studies (e.g. the “Next Generation ICE” project [2]), in order to use alternative fuels most efficiently, engines need to be optimized based on the specific combustion and emission characteristics of each fuel. In order to perform this optimization using engine models, precise models which capture the combustion and emission characteristics of alternative fuels need to be developed. In addition to in-cylinder processes, it is important to understand the effect of the utilization of the fuels on the exhaust aftertreatment systems of the engine, in order to also take into account these in the overall optimization.

1.2 Purpose of the project

The aim of this project is to develop a simulation platform for optimizing the overall engine unit (engine with exhaust gas aftertreatment) of vehicles of all sizes for fuels with different characteristics. This platform contains models for predicting the combustion rate and engine-out emissions (NOx, soot), as well as the performance of the aftertreatment system for different fuels. The models need to provide accurate predictions, while being computationally efficient in order to be used for multi-parameter optimizations.
For the development of the models, different fuels which are expected to be commercially available in the near future will be tested in an experimental test rig (WP1). The different fuels to be tested are chosen based on their characteristics and reflect the expected future availability of renewable fuels; two paraffinic fuels (Hydrogenated Vegetable Oil and a Gas-to-Liquid fuel), Diesel- Poly(oxymethylene)

dimethyl ethers (OME) blends in various compositions and a blend of a paraffinic fuel with OME. Multiple reasons are taken into account to choose these fuels: The paraffinic fuels are already available on the market and show simultaneously the potential to emit lower amounts of soot due to the absence of aromatics. In addition, the fuels can be produced from renewable sources. The OME was chosen as a representative of oxygenated fuels, which have been proven to almost emit no soot. Also OME can be produced from renewable sources. In addition, the OME used show a higher density than Diesel. Since the paraffinic fuels fall out of the important EN590 regulation for Diesel fuels, due to their low density, a blend with OME is mixed to meet the EN590 regulation.
The engine measurements for all fuels will be then used in order to develop a methodology for online identification of the fuel characteristics (what we call a “fuel fingerprint”) based on measurements available on-board (WP2). In parallel to the engine measurements, the influence of the fuel emission characteristics on the aftertreatment requirements will be tested. This includes testing of the energy required for the regeneration of the particulate filter depending on operating conditions and fuel, in order for this effect to be included in the overall energy utilization of the engine unit (WP3).
In WP4, the engine measurements of combustion and emissions with different fuels are used for the development of combustion and emission models which reflect the characteristics of the individual fuels. The models have a physical basis in order to be able to be used for predictive simulations under varying operating conditions, but also as mentioned previously be computationally efficient in order to be used for multi-parameter optimizations.
In a final step in the project, the models will be integrated in a commercially available simulation software (GT-POWER) and will be used for the optimization of a full engine operating with different fuels (WP5). In the optimization, the optimal combination of all engine parameters for minimizing fuel consumption will be determined for a wide range of operating conditions. This optimization will show the potential benefits of using fuel-specific model-based optimization in a real application, with a particular focus on the potential for efficiency improvement and corresponding CO2 reduction using fuels with different characteristics.

1.3 Objectives

The overarching objective of the project is the development of a tuned simulation platform which allows the optimization of engine parameters for minimizing modern diesel engine fuel consumption for different renewable fuels. To achieve this, the project is divided into 6 work packages, which have individual objectives.

WP1: Measurement campaign on the single cylinder engine

Objective: To create a database for different fuels with a wide variety of operating conditions for:

a. Identification of combustion characteristics of different fuels, with particular focus on ignition and different phases of combustion (premixed, early mixing-controlled, late mixing-controlled)

b. Identification of emission characteristics of different fuels, with particular focus on NOx-soot tradeoff trends with varying injection and EGR settings

WP2: Fuel identification/fingerprint

Objective: To identify a fingerprint for the fuels being examined and their admixture with diesel so that, after analyzing these characteristic variables, the identification of the fuel is possible:

a. Determination of the parameters the measurement of which will allow fuel identification

b. Development of an algorithm to allow fuel identification using on-board measurements

WP3: Energy requirement of exhaust gas aftertreatment

Objective: Compilation of the energetic influences of regenerability of a particle filter as well as the required exhaust gas temperature of DOC. The influence of different fuels on the energetic requirements

of the exhaust aftertreatment system are to be examined. The focus lies on the particle filter and its periodic active regenerations. Thus the main goals are:

a. Examination of the different oxidative properties of the soot collected in a wall flow Particulate Filter (PF) with the different fuels
b. Experimental determination of the reactive (oxidative) parameters of the soot collected during engine operation with the different fuels
c. Assessment of the energetic requirements, in terms of heat to be externally (in terms of additional fuel consumption) provided in the exhaust gas, in order to regenerate PFs loaded with the soot of the different fuels

WP4: Platform for virtual sensors

Objective: The objective of this work package is to develop the fast combustion and emission models, which will be used for the optimization of the operating strategy. The models are developed with the aim to accurately depict changes in the heat release rate (HRR) and in the emissions with changes in operating conditions as well as for the different fuels tested in WP1. In order to do this, a detailed investigation of combustion characteristics was carried out, in order to determine the model parameters which need to be adjusted for an accurate depiction of heat release rate. In a second step, the emission models were developed to capture changes in the operating conditions and fuel characteristics, and were also tuned based on the engine measurements with different fuels.

The process of the overall model development and adaptation of the models is outlined below:

1) HRR Model:
   a) Concept evaluation
      i) Reverse calculation from a simplified mixing frequency to heat release rate and cylinder pressure
      ii) Connection of mixing rate to spray behaviour and stoichiometric air-to-fuel ratio
   b) Automatic mixing rate processing and separation in key characteristics
   c) Relationship between key characteristics and model parameters of fast model
   d) Tuning of model parameters for each fuel for the correct estimation of combustion rate
2) NOx Model:
   a) Model development using diesel fuel from existing models to capture operating condition changes
   b) Model parameter tuning for different fuels
3) Soot Model:
   a) Model development using diesel fuel from existing models to capture operating condition changes
   b) Model sensitivity analysis for different apparent fuel characteristics
   c) Model parameter tuning for different fuels

Expected findings:

a. Depiction of combustion characteristics for different fuels from WP1 measurements in a fast combustion model
b. Depiction of NOx emission characteristics for different fuels from WP1 measurements in a fast NOx emission model
c. Depiction of soot emission characteristics for different fuels from WP1 measurements in a fast soot emission model

WP5: Virtual sensors in GT-Power

Objective: Integration of the combustion and emission models developed in WP4 in GT-Power, and their use for multi parameter optimization of a full engine:

a. Integration of combustion and emission models into GT-Power
b. Testing of model performance vs measurements
c. Development of a full engine model in GT-Power
d. Optimization of full engine for different fuels at different steady-state load points

2 Procedures and methodology

The methodology and equipment used in this project is described in the sections below, with one sub-section for each work package.

2.1 WP1: Engine measurements (LAV)

A single cylinder MTU 396 heavy duty diesel engine was used for the present work. The engine is equipped with an independent EGR system powered by an electric blower. The intake pressure, as well as the exhaust pressure, can be set independently of the operating condition up to 4.5 bar and for that the compressed air system of the building hosting the testebench is used. The temperature at the inlet is set by an electric heater and a water-air intercooler. Two parallel fuel system are used. Both are equipped with a AVL fuel scale, a high pressure pump, and a NOVA high pressure pneumatic valve. The common rail is shared. The system is completed by a custom injector maufactured by Ganser CRS. The concentration of the exhaust gas species is measured online by an ABB AO2000 Series (CO, CO_2, HC, O_2) and an ECO PHYSICS CLD 82 M hrk1 (NOx). The particle size distribution was detected with a Cambustion DMS 500 and the total soot concentration is measured with an AVL Smoke Meter. The cylinder pressure is recorded with a resolution of 0.2°CA. A scheme of the testbench is shown in Figure 2.

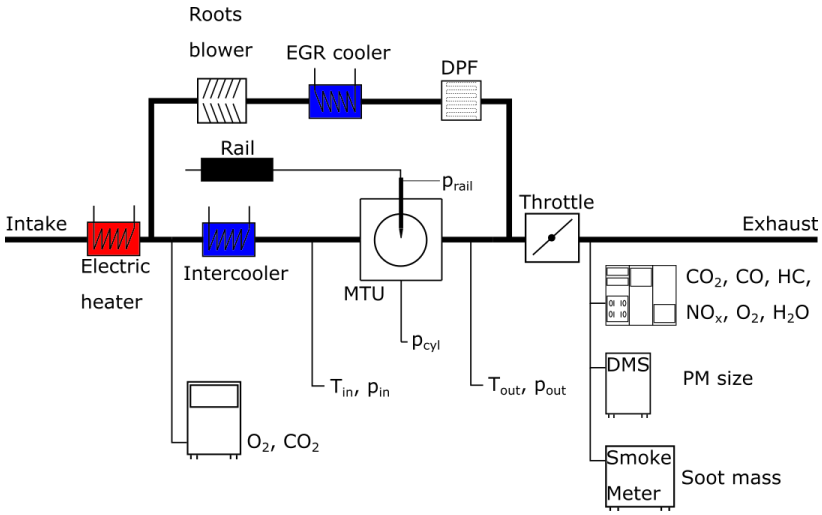

Figure 2: Scheme of the engine.

2.1.1 Fuels tested

As already in the introduction stated, the aim of this study is the investiagion of fuels with a smaller CO2 footprint than conventional Diesel. In order to allow a comparison of the finally a well-to-wheel analyis is required. The well-to-wheel analyis is separated into a well-to-tank analyis, to compare the CO2 footprint of the fuels and into a tank-to-wheel analysis to compare the engine efficiency with the different fuels. Based on conventional Diesel, neat Hydrogenated Vegetable Oil (HVO), a neat Gas-to-Liquid fuel (GTL, a fuel which is made from methane though a Fischer Tropsch conversion. The origin of methane can be

bio or fossil. In case of GTL it is fossil.) and OME_{3-6}, 5 blends where prepared: Diesel with 20% GTL (GTL20), Diesel with 7% (OME7), resp. 15% OME (OME15), Diesel with 20% HVO (HVO20) and 77% HVO with 18% OME and 5% of an stabilizer (R100). The well-to-tank CO2 reduction potential of these fuels is evaluated from literature OME from [3], HVO from [4] and [5]. The spread for the CO2 footprint is rather large since feedstock, energy and heat consumed can differ significantlly among the different producers. Neat OME3-6 shows a CO2 reduction potential of 70-90% (80% is used for further calculations, HVO shows a CO2 reduction potential of 50-90%. The HVO used is stated with ~8gCO2eq/MJ, which is about 10% of conventinal Diesel.
The blending ratio of OME7 and R100 were not chosen arbitrailry. Both the density and the viscosity of the two blends lie in the span of tolerance of the EN 590 standard for normal diesel oil (arctic diesel is allowed to have a lower density). In addition, the OME content is below a critical oxidation stability limit in combination with the stabilizer used. Figure 3 shows all the possible blends obtainable when mixing conventional diesel, HVO and OME. The orange area encloses all those blends whose viscosity is EN590 conform. The green surface repreents those compositions whose density is also compliant with the EN590 standard. The blue lines parallel to the OME-HVO line are potential “iso-renewability” lines. OME 7 lies on the Diesel-OME line and is on the upper limit of the standard EN590 regarding the density. HVO20 has a too low density to be in the green area while R100 is exactly on the fully renewable line OME-HVO and moreover at the lower density limit of EN590. The other blends are chosen in order to detect nonlinearities, if any, with respect to the blending ratio.

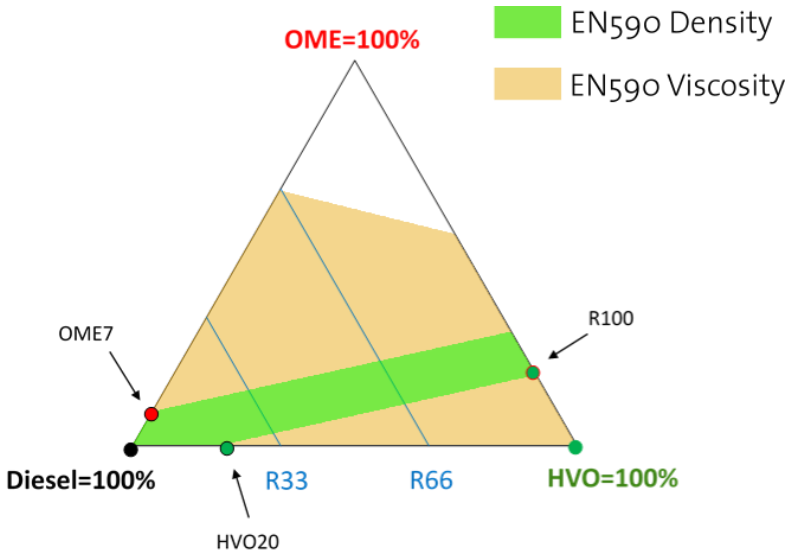

Figure 3: Triangle representing all the possible blends between Diesel, OME and HVO. The green area encloses the densities that are compliant with the EN590 standard. The orange surface represents the environment where also the viscosity is conform to the standard EN590.

2.1.2 Methodology

Apart from conventional diesel, which is available from the ETH building network, all the other 7 fuels investigated in the present study are pumped in the scale from a canister where they are continously stirred using an additional fuel pump.
The engine is started with conventional diesel. After having heated up the engine with approximately two liters of diesel, the fuel system is flushed with one liter of alternative fuel. Then 2 liters of alternative fuel are furhter burned into the engine after which the fuel being injected is considered to be pure test fuel. Once the measurement is concluded, the system is flushed again with diesel using the same procedure. This is done in order to exclude possible damages to the engine infrastructure due to corrosion.
The meaurement matrix is defined in order to cover a range of operating conditions as wide as possible. Five parameters were varied around a reference condition as shown in Figure 4. Intake pressure and

the exhaust pressure were kept constant at 2 bar and 1.9 bar, respectively. The intake temperature was chosen to be 50 °C for all the operating conditions. These variations span a measurement matrix of 60 operating conditions for every test fuel. The details of each operating condition (OC) is displayed in the appendix.

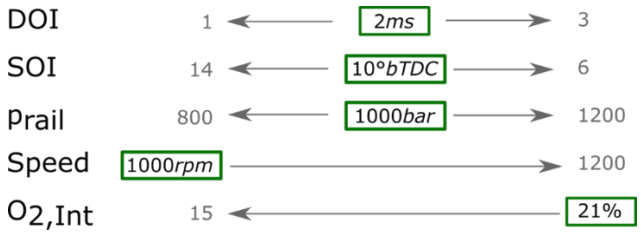

Figure 4: Measurement matrix. The reference condition is represented by the green boxes.

As shown in Table 1, different fuels have different lower heating values and different densities. This means that under constant injection parameters (duration of injection and fuel pressure), the amount of injected energy in form of fuel is different. In the present work this effect wasn't undesired. This situation corresponds to what would happen in a real application in the case the fuel is suddenly changed. Transient data (fuel pressure, cylinder pressure, intake pressure) are recorded and ensemble averaged over 144 engine cycles while all the rest of the data are averaged over 30s.

Table 1: Test fuels.

	Diesel	GTL20	GTL	OME15	OME7	HVO20	HVO	R100
Composition	100% Diesel	80% Diesel 20% GTL	100% GTL	85% Diesel 15% OME	93% Diesel 7% OME	80% Diesel 20% HVO	100% HVO	77% HVO 18% OME 5% Alcohol
LHV [MJ/kg]	43.5	43.57	43.8	39.89	41.89	43.6	43.8	38.61
Denstiy [kg/m^3]	827	817.3	778.3	859.9	842.3	817.6	780.2	820.9
CN [-]	56.1	61.1	82.4	<60	<57	61.2	82.8	75.1
Aromatics [wt%]	22.8	18.2	<0.1	19.4	21.2	8.3	<0.2	<0.2
Oxygen [wt%]	0	0	0	8.19	3.83	0	0	>8.19
Well-to-Tank CO2 red. [%]	0	n/a	n/a	9	4	18	90	~88

2.2 WP2: Fuel identification/"fingerprint" (LAV)

2.2.1 Fuel characterization

It would be a tremendous advantage for an engine to be able to recognize on-board the fuel being burned. This would allow an on-line adaption of the operating strategy to the used fuel in order to reduce the total cost of operation of the engine. Ideally, this recognition should be performed unsing the sensors

already available today in the majority of the internal combustion engines. This means that not all the measurements acccessible with the equipment available in the test rig can be used for that purpose.

2.2.2 On-board available data

An extensive research to assess the state of the art of today's engine or its expected evolution in the near future regarding the on-board data availability was not performed by the authors of the present study since it goes beyond the scope of the project. However, some assumptions based on experience were made. The following information is considered available:

- Exhaust gas temperature
- Intake temperature
- Exhaust pressure
- Intake pressure
- Engine speed
- Fuel pressure
- Electric injection timing (DOI, SOI)
- Crankshaft position
- Exhaust oxygen concentration
- Intake oxygen concentration
- Exhaust NOx concentration

Moreover, the soot mass emitted by the engine is assumed to be known as a result of the analysis of the temporal pressure drop evolution across the DPF in combination with a virtual sensor ([6, 7]). The concept of this combination is beyond the goal of the present investigation. For sake of simplicity, in the present investigation, a smoke meter has been used. Considering the above, and especially the fact that the cylinder pressure signal is not included in the set of available data, three measurable parameters were chosen to be used to perform the fuel recognition.
The nitrogen oxides emissions can directly be measured via a NOx sensor and the according conversion function from a current or voltage to ppm. NOx sensors are standard in today's engines since they are used for the control of the SCR system and/or EGR system. As explained above, also soot can be estimated assuming that the mass of soot trapped in the DPF causes a rise in the pressure drop across the DPF. Therefore, the soot-NOx trade-off, whose fitting line is shown later in Figure 38 for all the fuels, is accessible on-board.
The exhaust gas temperature (Figure 5) is easily measurable using a thermocouple, so it can be considered as an on-board available parameter. Typically, CI engines have wide-range lambda sensors, whose output (current or voltage) depend on the oxygen concentration of the environment where they are operated. Therefore, also the exhaust oxygen (Figure 5) concentration can be used as fuel characteristic parameter.

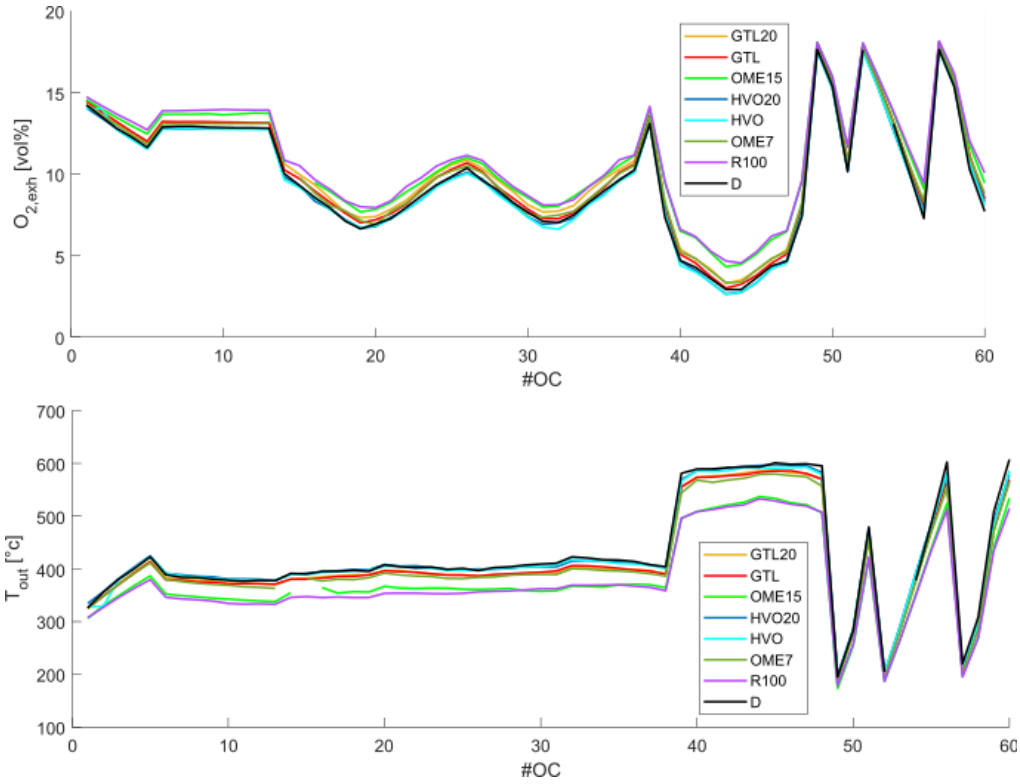

Figure 5: Oxygen concentration in the exhaust (top) and exhaust gas temperature (bottom) of all the operating conditions (OC) for all the tested fuels.

2.2.3 Development of the tools

Provided that a full recognition strategy that works under all circumstances would require a number of measurements much higher than the 60 operating conditions per fuel recorded in the present work, in the following three methods that could help coming closer to that goal will be presented. Measurable parameters (exhaust gas temperature, exhaust oxygen concentration, NOx concentration…) depend not only on the fuel used but also on the operating condition of the engine. This means that by looking at a single parameter it is difficult to tell one fuel apart from the other. To be able to extract some useful information from those data, it is necessary further processing them.

2.2.4 Combustion and lower heating value

One of the parameters that shows the biggest differences between fuels is the exhaust gas temperature (T_{exh}). The reasons are the different lower heating values (LHV) and the different combustion speeds. In particular, regarding the fuels testes in the present investigation, there is a trend according to which the higher the LHV, the lower the mixing frequency (ν_{mix}). This means that, for the set of fuels tested in the present study, the effects on T_{exh} of LHV and ν_{mix} act in the same direction. This, of course, is a coincidence and must not necessary hold true for other compounds.
Considering the above, the LHV of one fuel and the exhaust gas temperature are related by modelling the combustion with a simple approach. The cycle of the engine is modelled with an isentropic compression, a first isochoric process approximating the premixed combustion followed by an isobaric heat transfer that stands for the mixing controlled combustion, and finally an isentropic expansion to exhaust valve opening. The corresponding T-s-diagram is shown in Figure 6.

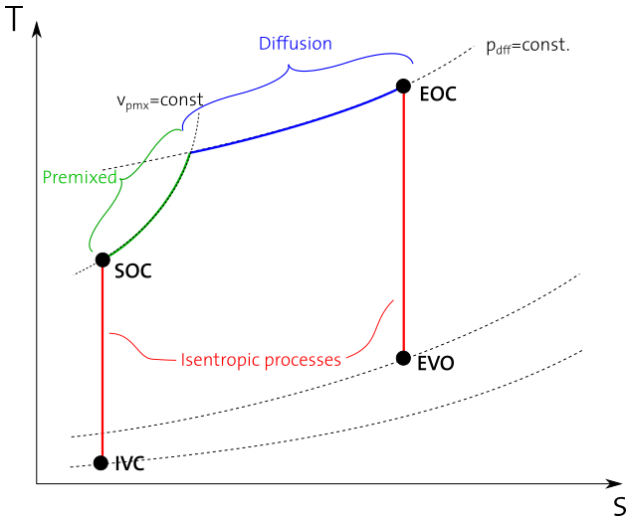

Figure 6: Scheme of the modelled high pressure cycle of the engine. IVC: Intake valve closing; SOC: Start of combustion; EOC: End of combustion; EVO: Exhaust valve closing.

First, the NASA polynomials [8] are used to compute the specific heat capacity under constant pressure C_p and constant volume C_v, and the isentropic coefficient γ at intake conditions. For simplicity, it is assumed that they remain constant throughout the entire cycle. Required inputs are the oxygen concentration $Y_{O_2,int}$ in the intake and the temperature. The nitrogen concentration $Y_{N_2,int}$ is known and constant $79vol\%$. If the rest is not zero, it is assumed to be a mixture of water and carbon dioxide coming from exhaust gas recirculation with the following proportions

$$Y_{CO_2} = \frac{x}{x + {}^{y}/_{2}} \cdot \left(1 - Y_{O_2,int} - Y_{N_2,int}\right) \quad (1)$$

$$Y_{H_2O} = \frac{{}^{y}/_{2}}{x + {}^{y}/_{2}} \cdot \left(1 - Y_{O_2,int} - Y_{N_2,int}\right) \quad (2)$$

where x and y are the number of carbon atoms and hydrogen atoms, respectively, in the fuel molecule (for diesel: $x = 1$, $y = 1.8$) . These results come from the general equation of combustion that states

$$C_xH_yO_z + \lambda\left(x + \frac{y}{4} - \frac{z}{2}\right)[O_2 + 3.76N_2] \leftrightarrow xCO_2 + \frac{y}{2}H_2O + \left(x + \frac{y}{4} - \frac{z}{2}\right)[(\lambda - 1)O_2 + 3.76\lambda N_2] \quad (3)$$

The intake process is modelled through a simple trapping efficiency factor η_{tr}:

$$p_{IVC} = p_{in} \cdot \eta_{tr} \quad (4)$$

with p_{IVC} being the cylinder pressure at intake valve closing and p_{in} the measured pressure in the intake manifold. The temperature of the charge right after IVC is assumed equal to the temperature measured in the intake duct.
From IVC to the start of injection SOI, the process continues with an isentropic compression where the pressure and the temperature evolve as follows

$$p_{SOI} = p_{IVC} \cdot \left(\frac{V_{IVC}}{V_{SOI}}\right)^{\gamma} \quad (5)$$

$$T_{SOI} = T_{IVC} \cdot \left(\frac{p_{IVC}}{p_{SOI}}\right)^{\gamma-1} \quad (6)$$

where: T: Temperature $[K]$
p: Pressure $[Pa]$
V: Cylinder volume $[m^3]$
IVC: Intake valve closing $[°CA]$
SOI: Start of injection $[°CA]$

In order to account for the opening delay of the injector, the value used for SOI is shifted by δ_{open} $[s]$ with respect to the electrical signal. The amount of injected mass m_{inj} is not directly available on-board and is therefore modelled with a semi-empirical approach. The Bernoulli equation is corrected by parameters taking into account the DOI dependant behaviour of the injector:

$$m_{inj} = \left(C_{1,inj} \cdot DOI \cdot \sqrt{2p_{rail}} + C_{2,inj}\right)^{C_{3,inj}} \quad (7)$$

where p_{rail} is the fuel pressure in Pa and $C_{1,inj}$, $C_{2,inj}$, and $C_{3,inj}$ are calibration parameters. In equation (7) the fuel density does not appear. The reason for this is that for one fuel the density is constant and therefore it is accounted for in $C_{1,inj}$.
The injection rate is obtained by dividing the injected mass m_{inj} by the hydraulic duration of injection DOI_{hyd} that is the sum of the electric DOI and a parameter taking in account the transients.
In order to determine that amount of injected fuel that is burned in premixed combustion, the ignition delay is needed. For that, the model described in [9] was adopted and minorly modified in order to account for the influence of the injection pressure:

$$\tau_{ig} = C_{1,ig} \cdot {V_{O_2}}^{C_{2,ig}} \cdot {p_{SOI}}^{C_{3,ig}} \cdot exp\left[\frac{E}{R \cdot T_{SOI}} \cdot {V_{arom}}^{C_{4,ig}}\right] \cdot \left(\frac{1}{\sqrt{p_{rail} - 500 \cdot 10^5}}\right)^{C_{5,ig}} \quad (8)$$

where: V_{O_2}: Cylinder oxygen concentration at SOI $[-]$
E: Activation energy $[kJ/(kg \cdot K)]$
R: Universal gas constant $[kJ/kg]$
$C_{1,\dots 5,ig}$: Calibration parameters $[-]$
p_{SOI}: Cylinder pressure at SOI [Pa]
T_{SOI}: Temperature at SOI [K]
V_{arom}: Aromatic content of the fuel [*wt*%]
p_{rail}: Fuel pressure [bar]

It is important to mention, that the injection model and the ignition delay model require a reference of the injected mass and the ignition delay under diesel conditions.
The fuel burning in premixed combustion is allocated as explained graphically in Figure 7. That amount of fuel that is injected before the ignition delay is assumed to burn premixed. The rest burns in mixing controlled regime.

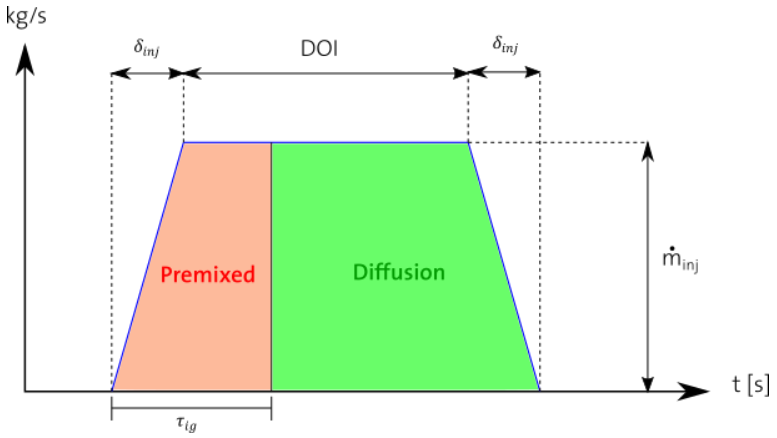

Figure 7: Injection delay and fuel allocation concept for premixed and diffusion combustion.

Between the start of injection and the actual start of combustion, it is assumed that pressure and temperature evolve following further the isentropic process (5) (6) and reaching p_{SOC} and T_{SOC}. As explained above, the premixed combustion is approximated with an isochoric heat transfer to the system. This means that the work on the piston is zero, since $dW = p \cdot dV$ and, per definition, $dV = 0$. The volume at which this heat release takes place is V_{pmx} and can be easily known if the corresponding position of the crankshaft is also known.
The change in internal energy of the system is given therefore by

$$\Delta U_{pmx} = m_{cyl} \cdot C_v \cdot \Delta T_{pmx} = HR_{pmx} - Q_{loss,pmx} = m_{pmx} \cdot LHV - Q_{loss,pmx}$$

(9)

with m_{pmx} being the mass of fuel burning in chemical controlled mode, and $Q_{loss,pmx}$ is the heat lost from the system during premixed combustion and it is assumed to be proportional to the heat released HR_{pmx}. Solving equation (9) for ΔT_{pmx} gives the increase of temperature during that phase and can be summed to T_{SOC} to obtain the temperature after the premixed combustion T_{pmx}. The pressure p_{pmx} after the premixed phase is calculated with the equation for ideal gases

$$p_{pmx} = \frac{m_{cyl} \cdot R \cdot T_{pmx}}{V_{pmx}}$$

(10)

The pressure p_{pmx} is kept constant throughout the entire diffusion combustion since it is approximated by an isobaric process. Accordingly, the change of internal energy of the system during diffusion combustion is given by

$$\Delta U_{dff} = m_{cyl} \cdot C_p \cdot \Delta T_{dff} = W_{dff} + HR_{dff} - Q_{loss,dff}$$

(11)

Analogously to the premixed combustion, the heat released in diffusion combustion HR_{dff} is nothing but the mass of fuel m_{dff} multiplied by the lower heating value of the fuel. Again, the heat lost through the walls and the piston $Q_{loss,dff}$ is arbitrarily modelled as proportional to HR_{dff}. The work is calculated as the volume difference between start and end of diffusion combustion multiplied by the (constant) pressure

$$W_{dff} = \Delta V_{dff} \cdot p_{pmx}$$

The start of diffusion combustion is delayed by δ_{dff} seconds with respect to the start of premixed combustion. Its duration Δt_{dff} in turn is calculated as the time it takes to the fuel mass m_{dff} to be consumed at a constant reaction rate HRR_{dff}:

$$\Delta t_{dff} = \frac{m_{dff} \cdot LHV}{HRR_{dff}} \quad (12)$$

The constant reaction rate HRR_{dff} is assumed equal to the maximum injection rate. The reason of this choice is that in the case of a hypothetic infinite injection in a constant conditions environment, the reaction rate must be as high as the injection rate to reach the steady state. At the end of combustion, the pressure and the temperature in the cylinder will be $p_{dff} = p_{pmx}$ and $T_{dff} = T_{pmx} + \Delta T_{dff}$. The subsequent expansion until exhaust valve opening is approximated to an isentropic process, similarly to the compression. Right before EVO, the temperature in the combustion chamber is therefore:

$$T_{EVO} = T_{dff} \cdot \left(\frac{V_{EOC}}{V_{EVO}}\right)^{\gamma-1} \quad (13)$$

where the subscript EOC indicates the instant of the end of combustion. Since the measuring matrix followed in the present work did not have an exhaust pressure variation, for keeping the model as simple as possible, the exhaust process is accounted for with a multiplication of T_{EVO} by a constant.

$$T_{out} = T_{EVO} \cdot C_{exh} \quad (14)$$

The model presented above was intended to be calibrated with conventional diesel operating conditions. This means for example, that when the LHV is needed, the value of the lower heating value of diesel is used. Moreover, all the calibration parameters are set according to the measurements performed with diesel.

2.2.5 Model calibration

An overview of the calibration parameters can be found in Table 2.The calibration of the model is performed using the measurements recorded with conventional diesel, as explained above. Of the 60 available operating conditions, 40 are randomly chosen for calibrating all the sub-models. The remaining 20 are used for the validation.

Table 2: Overview of the calibration parameters for the exhaust temperature model.

Name	Type	Model
η_{tr}	Multiplicative constant	Intake model
$C_{1,inj}$	Multiplicative constant	Injection model
$C_{2,inj}$	Additive constant	
$C_{3,inj}$	Exponential constant	
$C_{1,ig}$	Multiplicative constant	Ignition delay model
$C_{2,ig}$	Exponential constant	
$C_{3,ig}$	Exponential constant	
$C_{4,ig}$	Exponential constant	
$C_{5,ig}$	Exponential constant	
C_{exh}	Multiplicative constant	Exhaust model

The performances of the calibrated injection model (7) are shown in Figure 8. The model delivers reasonably good results, with an error of at most 4% under prediction.

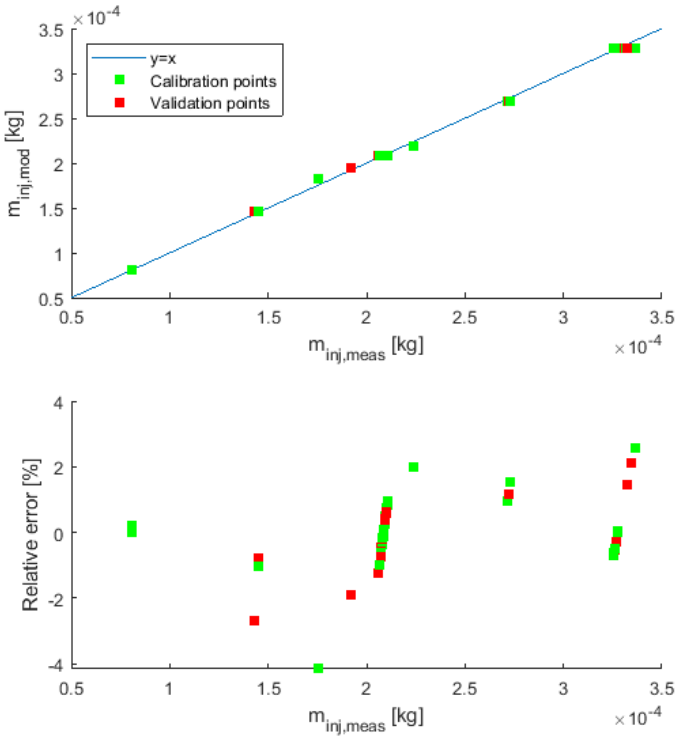

Figure 8: Modelled injected mass compared to the measured injected mass per power stroke. The green points represent the operating conditions used for the calibration of the model, while the red points are the validation data.

An analysis of the error sensitivity to the number of operating conditions used for the calibration is shown in Figure 9. It can be seen, that already with 30% of the data used for the calibration, the mean relative error is around 1%. This analysis is obtained by varying the percentage of measurements used for the calibration from 1% to 100% with steps of 1% and for each percentage, 100 sets of randomly chosen operating conditions were used.

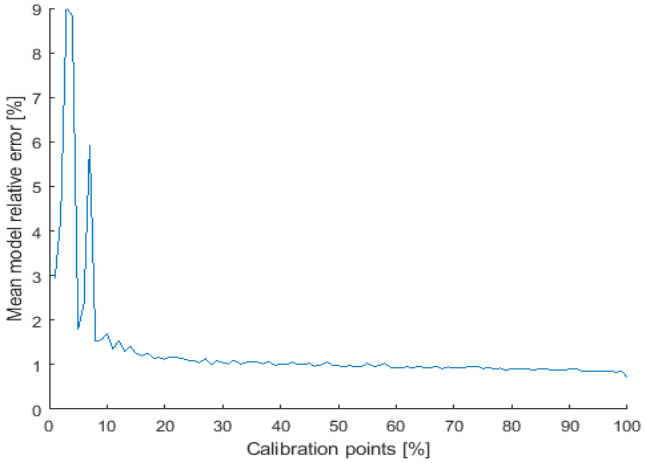

Figure 9: Sensitivity analysis of the injection model relative error to the number of points chosen for the calibration over the total amount of available measurements.

The calibration of the ignition delay model (8) is shown in Figure 10. It is evident that the accuracy of that model is lower than the one of the injection model seen above. Even though in general the main trend is captured, the relative error remains as big as 20% for some operating conditions.

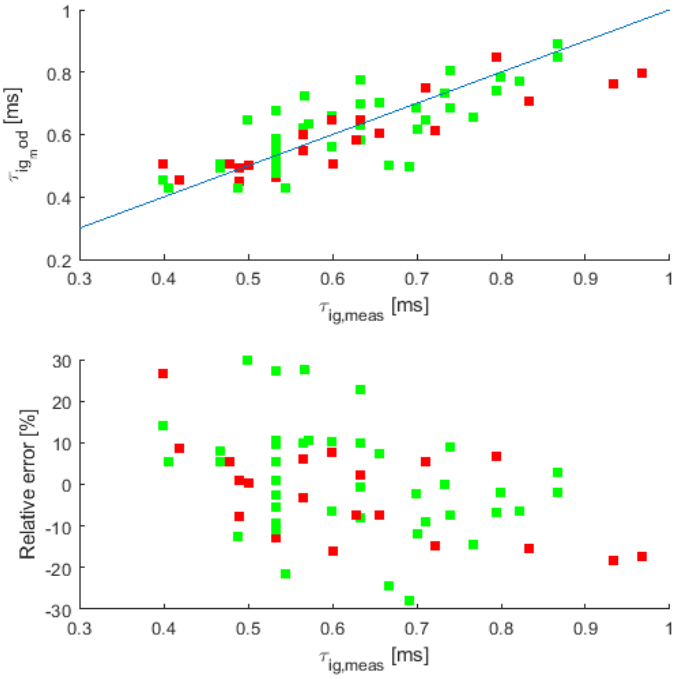

Figure 10: Modelled ignition delay compared to the measured ignition delay. The green points represent the operating conditions used for the calibration of the model, while the red points are the validation data.

However, as Figure 11 shows, also when varying the number of data used for the calibration, the mean relative error does not sink below 10%. This, together with the stochastic distribution of the relative error, suggests that the model has physiological limitations that does not allow it to capture certain dynamics.

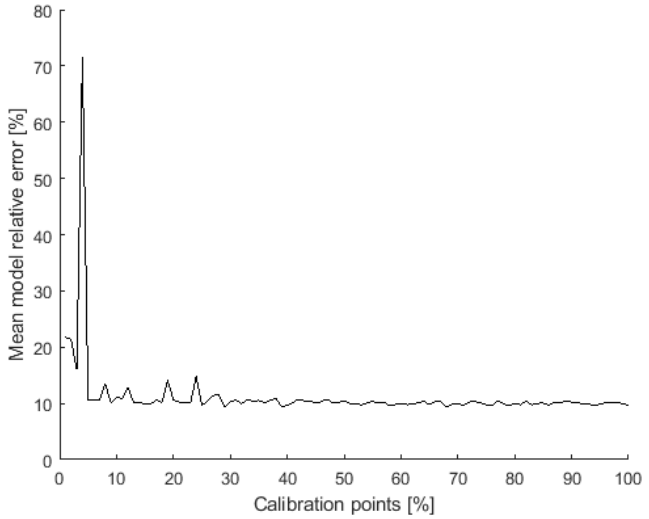

Figure 11: Sensitivity analysis of the ignition delay model relative error to the number of points chosen for the calibration over the total amount of available measurements.

A more detailed insight in the model behaviour is provided by Figure 12. There, the effect of four parameters that are expected to influence the ignition delay are investigated closely. The fuel pressure strongly influences the physical structure of the spray. An increase of the fuel pressure leads to bigger cone angles and a smaller Sauter mean diameter that, in turn, allows a faster evaporation due to the increased surface-to-volume ratio of the spray droplet ensemble. For this reason, it is expected that increasing the fuel pressure would result in a shorter ignition delay. The measurements confirm that expectation and the model demonstrates to be able to capture that dynamic.

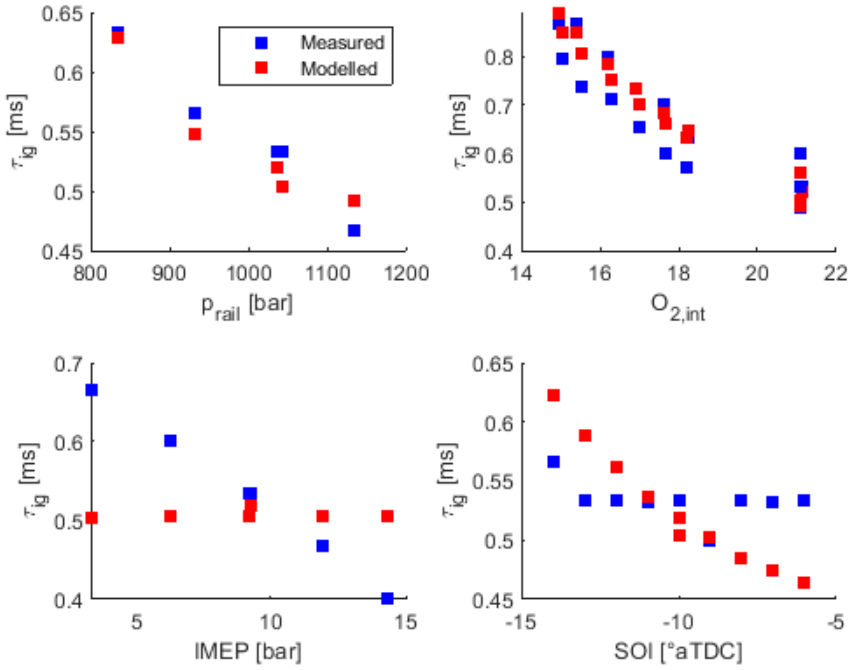

Figure 12: Comparison between modelled (red) and measured (blue) ignition delay and dependency from fuel pressure (top, left), intake oxygen concentration (top, right), load (bottom, left), and injection timing (bottom, right).

Opposite to that, the influence of the oxygen concentration in the cylinder at intake valve closing was already accounted for with a dedicated term in the original equation. Oxygen has two effects on the ignition delay. Regarding the physical part, a higher concentration of oxygen requires less air entrainment to achieve a certain oxygen-to-fuel ratio. On the other hand, the presence of oxygen allows the build-up of that pool of radical that is indispensable for ignition. The results shown in Figure 12 confirm that the model is able to replicate those effects.

The injection timing has an indirect effect on the ignition delay since the choice of the SOI influences the conditions (reads temperature, pressure and density) the fuel finds when it is injected. Accordingly, an injection close to the TDC should result in shorter ignition delays while a very soon injection would occur in colder conditions requiring longer to the fuel to ignite. The model shows exactly this behaviour. However, it tends to overpredict its importance; the measured ignition delays are barely affected by the SOI.

A variation of the engine load, if it is obtained by modifying the injection duration only, should not have any influence of the ignition delay. However, as the measurements show, this is not the case. The higher the engine load, the shorter the fuel takes to start the combustion. That behaviour is a consequence of the higher heat transfer that occurs at higher loads and lead to higher liners, head, and piston temperatures. This heat is partially re-transferred to the charge during the compression stroke leading to higher temperatures close to TDC. The consequence are shorter ignition delays. As shown in Figure 12, this is exactly what happens in reality; however, the model is not able to capture that. Moreover, it

would also be complicated to model such a phenomenon since it is very engine specific since the whole engine geometry and cooling system play a role.
The analysis above shows that there exist some phenomena, which the adopted ignition model is not able to replicate adequately. This leads to the not negligible relative error seen above. The drawback of that inaccuracy on the final result of the exhaust gas temperature model will be investigated later.
As explained above, the effect of the outlet process on the temperature of the exhaust gas is modelled with a simple multiplication parameter (14). This is possible because the pressure in the exhaust manifold is constant for all the operating conditions. In a real application, the exhaust process should be modelled taking into account a variable backpressure caused by the presence of the turbocharger. A comparison between the predicted exhaust gas temperature and the measured one is shown in Figure 13. The model is able to estimate the exhaust gas temperature with a relative error of around 6% at most. The relative error shown in the lower plot suggests that for colder exhaust gas the model minorly under predicts the temperature, while under hotter condition, a small over prediction can be observed.

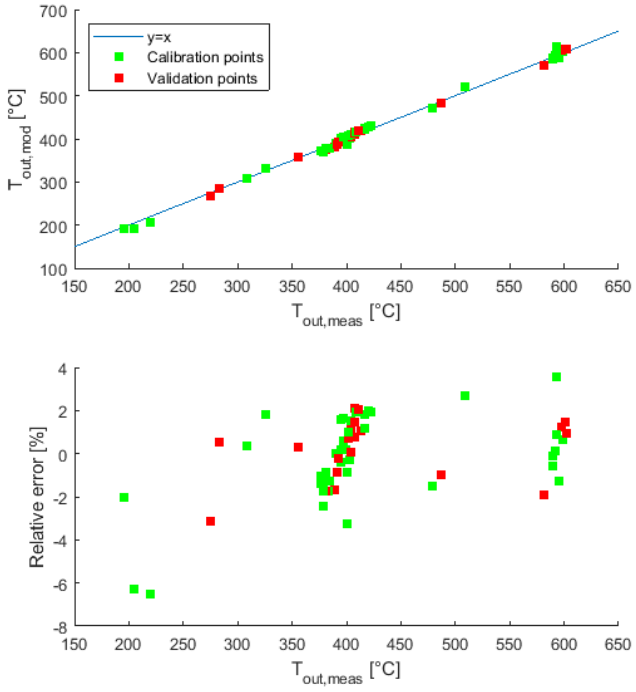

Figure 13: Modelled exhaust gas temperature compared to the measured exhaust gas temperature. The green points represent the operating conditions used for the calibration of the model, while the red points are the validation data.

Since the calibration of this model consists basically in the fitting of one single parameter, the relative error of the model is expected to reach a low, stable value also with few calibration points. The analysis of the sensitivity of the model mean relative error to the number of measurements used for the calibration is shown in Figure 14. The peak of the relative error is lower than 2% and a value of around 1.5% is reached already with around 20% of the total available measurements.

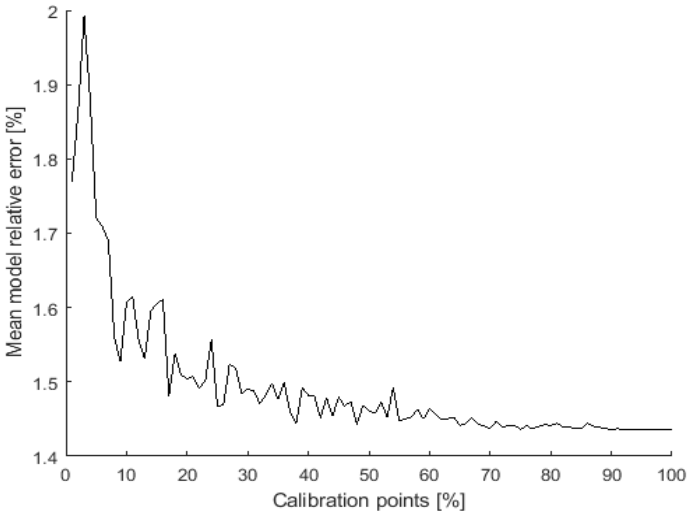

Figure 14: Sensitivity analysis of the exhaust gas temperature model relative error to the number of points chosen for the calibration over the total amount of available measurements.

2.2.6 Sensitivity analysis

As seen above, the sub-models that govern the estimation of the exhaust gas temperature show a certain inaccuracy. In particular, the performances of the ignition delay model were seen to be quite weak compared to the other sub-models, with relative errors up to 30%.
Figure 15 shows how the mean relative error of the model reacts to the variation of the injected mass and of the ignition delay. The importance of a precise estimation of the injected mass is demonstrated by the fact that errors of up to 15% is reached with a deviation of 30% from the calibrated injected model. However, as shown above, the mean relative deviation of that model is as low as 1%, so the uncertainty reflected on the final result of T_{exh} is negligible.

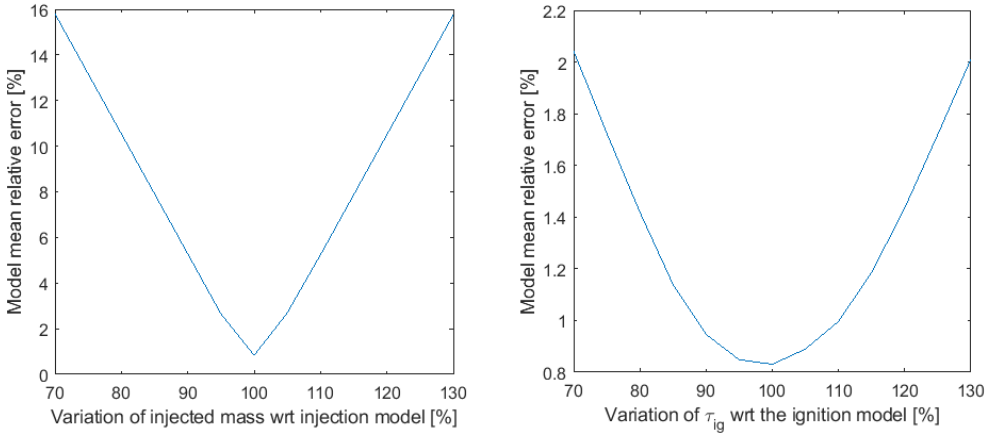

Figure 15: Dependency of the relative error of the model on the injected mass (left) and on the ignition delay (right).

On the other hand, the calibrated model for the ignition delay still had errors of up to 30% compared to the measurements. However, as shown in the right side of Figure 15, this error has a much lower impact than the injected mass on the accuracy of the estimation of exhaust gas temperature. With a value of the ignition delay corresponding to 130% of the one given by the calibrated model, the performances of T_{exh} model get worse by roughly 1.2% only. This limits the accuracy requirements of the ignition delay model and enables the usage of the suggested model even without specific tuning to another engine.

2.2.7 Fuel composition

The fuels investigated in the present work can be seen as a combination of carbon, hydrogen, and oxygen atoms. HVO and GTL, being purely paraffinic compounds have a general structure of the form C_xH_y where the number of hydrogen atoms y must be equal to $2x + 2$. This means that the ratio between hydrogen and carbon atoms remains above 2. As seen in the chemical analysis of the fuels, the molecular chain HVO is minorly longer than the one of GTL. This means, that the value of x is higher for HVO than for GTL. Conventional diesel in turn, contains also a certain amount of aromatics ($22.8 wt\%$, mainly monoaromatics). This lowers the ratio y/x (i.e., hydrogen-to-carbon ratio) to values below 2. Finally, OME is the only compound that has oxygen content. Its general formula is therefore $C_xH_yO_z$. The ratio between the number of carbon atoms and hydrogen atoms is the same as in the case of paraffinic hydrocarbons, that is, $y = 2x + 2$. One of the distinguishing characteristics of OME is the absence of $C - C$ bonds. This is possible because between two carbon atoms there is always an oxygen atom leading to z being equal to $x - 1$. Considering the general equation for combustion in a lean environment already shown in (3), it is to expect that the differences in the composition of the fuels can be seen also in the exhaust species concentration. In particular, the oxygen concentration in the exhaust is influenced by all the elements of the fuel and it can be easily measured with a λ sensor.
The O_2 concentration in the exhaust is given by the number of oxygen moles divided by the total number of moles of which the exhaust gas consists of:

$$x_{O_2} = \frac{\left(x + \frac{y}{4} - \frac{z}{2}\right) \cdot (\lambda - 1)}{x + \frac{y}{2} + \left(x + \frac{y}{4} - \frac{z}{2}\right) \cdot [(\lambda - 1) + \lambda \cdot 3.76]}$$

(15)

In order to characterise a fuel, the ratio between x and y or z are sufficient. Accordingly, the equation (15) can be simplified dividing both the numerator and the denominator by x:

$$x_{O_2} = \frac{\left(1 + \frac{\tilde{y}}{4} - \frac{\tilde{z}}{2}\right) \cdot (\lambda - 1)}{1 + \frac{\tilde{y}}{2} + \left(1 + \frac{\tilde{y}}{4} - \frac{\tilde{z}}{2}\right) \cdot [(\lambda - 1) + \lambda \cdot 3.76]}$$

(16)

with $\tilde{y} = y/x$ and $\tilde{z} = z/x$.
Since the measurement instrumentation used for the present work returns only the dry concentrations of the exhaust gas species, the term accounting for the presence of water must be removed from equation (16) leading to:

$$x_{O_2,dry} = \frac{\left(1 + \frac{\tilde{y}}{4} - \frac{\tilde{z}}{2}\right) \cdot (\lambda - 1)}{1 + \left(1 + \frac{\tilde{y}}{4} - \frac{\tilde{z}}{2}\right) \cdot [(\lambda - 1) + \lambda \cdot 3.76]}$$

(17)

The normalized air-to-fuel ratio λ is calculated as

$$\lambda = \frac{\frac{m_{air}}{m_{inj}}}{AFR_{stoich}}$$

(18)

where AFR_{stoich} is the stoichiometric air-to-fuel ratio, while m_{air} is the trapped mass at intake valve closing and m_{inj} is the injected fuel mass per engine cycle. The trapped air consumption is assumed to be available on-board thank to an air mass flow rate measurement. The model for injection already presented above (7) was adopted to calculate m_{inj}. The general equation for combustion (3) is used

also for the calculation of the stoichiometric air-to-fuel ratio. The AFR_{stoich} is nothing but the ratio between the two terms of the left side of the equation when $\lambda = 1$:

$$AFR_{stoich} = \frac{\left(x + \frac{y}{4} - \frac{z}{2}\right) \cdot \left[M_{O_2} + 3.76 \cdot M_{N_2}\right]}{xM_C + yM_H + zM_O} = \frac{\left(1 + \frac{\tilde{y}}{4} - \frac{\tilde{z}}{2}\right) \cdot \left[M_{O_2} + 3.76 \cdot M_{N_2}\right]}{M_C + \tilde{y}M_H + \tilde{z}M_O}$$

(19)

Substituting equation (19) in equation (18) and finally in (16) an expression for the exhaust oxygen concentration dependent on the fuel composition is obtained. Rearranging the terms of that expression yields

$$\begin{aligned}\tilde{y}\left[8AFR\left(4.76x_{O_2,dry} - 1\right)M_H + \left(2 - 2x_{O_2,dry}\right)\left(2M_O + 3.76M_{N_2}\right)\right] \\ + \tilde{z}\left[8AFR\left(4.76x_{O_2,dry} - 1\right)M_O + 4\left(x_{O_2,dry} - 1\right)\left(2M_O + 3.76M_{N_2}\right)\right] \\ = -8\left[AFR\left(4.76x_{O_2,dry} - 1\right)M_C + \left(2M_O + 3.76M_{N_2}\right)\right]\end{aligned}$$

(20)

where AFR is the actual air-to-fuel ratio. This is an equation with two unknowns and therefore underdetermined. However, it is enough to have two different operating conditions to get a determined system of two equations and two unknowns. With more than two operating conditions, the system becomes overdetermined. Being the system linear, in the case it is overdetermined, ordinary least squares can be applied to find a value for $\tilde{y}_{ls}$ and $\tilde{z}_{ls}$ that minimizes the sum of the squares of the differences between the linear function and the independent variable. Once $\tilde{y}_{ls}$ and $\tilde{z}_{ls}$ are calculated, the stoichiometric air-to-fuel ratio, which is a fuel characteristic parameter can be found using equation (19). Opposite to the model for the exhaust gas temperature presented earlier (modelled T_{exh}) for every operating conditions, the method presented here for the estimation of the stoichiometric air-to-fuel ratio AFR_{stoich} returns one single value that fits the provided set of measurements.
The calculation referring to the exhaust oxygen concentration presented above does not require any calibration apart for the sub-model used for estimating the injected mass. This however has already been calibrated for being used in the model for the exhaust gas temperature. The downside of the fact that this tool does not need calibration is that the measured air mass flow must be extremely precise.

2.2.8 Soot-NOx trade-off

As will be shown later in Figure 38, the emissions of soot and NOx trace a trade-off that is characteristic for each of the tested fuel. If enough measurements were available to characterize the full operating range of the engine, it would be possible to trace a line that at best approximates the resulting soot-NOx trade-off. If that line would be known at least for conventional diesel, it would be possible to calculate the deviation of the on-line recorded pollutant concentrations from that line and use that value as a distinguishing feature of the used fuel.
In order to do that, the raw soot and NOx concentration measured in the exhaust must be transformed into “quasi-specific” emissions by dividing them by the amount of energy injected in form of fuel. The used injection model is the one presented earlier and adopted for the calculation of the stoichiometric air-to-fuel ratio. NOx is measured in ppm. In order to convert it in mass per unit of time, the volumetric flow rate in the exhaust must be known. Assuming a known intake mass flow rate $\dot{m}_{air,in}$ and assuming it to be equal to the exhaust mass flow rate $\dot{m}_{air,exh}$, the volumetric flow rate in the exhaust manifold (upstream of the turbine) is

$$\dot{V}_{air,exh} = \frac{\dot{m}_{air,exh} \cdot T_{out} \cdot \bar{R}}{p_{exh}}$$

(21)

where p_{exh} is the pressure in the exhaust and is assumed to be measurable on board and $\bar{R}$ is the universal gas constant. The volume flow rate of NOx in the exhaust is therefore

$$\dot{m}_{NO_x} = [NO_x] \cdot \dot{V}_{air,exh} \cdot \frac{p_{exh}}{T_{out} \cdot R} \cdot M_{NO_x}$$

(22)

with M_{NO_x} being the mean molar mass of NOx. The quasi-specific NOx emissions are obtained by dividing the mass flow rate by the fuel flow rate multiplied by the lower heating value:

$$\dot{m}_{NO_x,sp} = \frac{\dot{m}_{NO_x}}{m_{inj} \cdot n_e \cdot LHV}$$

(23)

A similar procedure is applied for the soot emissions. The quasi-specific emissions of NOx and soot are further adjusted by a multiplicative parameter that plays the role of a constant engine efficiency and is determined fitting the actual measured specific emissions.
To the so obtained quasi-specific soot-NOx trade-off, a line of the form

$$y = \left(\frac{1}{C_{to,1} \cdot x + C_{to,2}}\right)^{C_{to,3}} + C_{to,4}$$

(24)

can be fitted. $C_{to,1}$ to $C_{to,4}$ are fitting parameters, x is the variable representing the quasi-specific NOx levels calculated with (24) and y is the approximated quasi-specific soot. The quasi-specific trade-off and the fitted line are displayed in Figure 16.

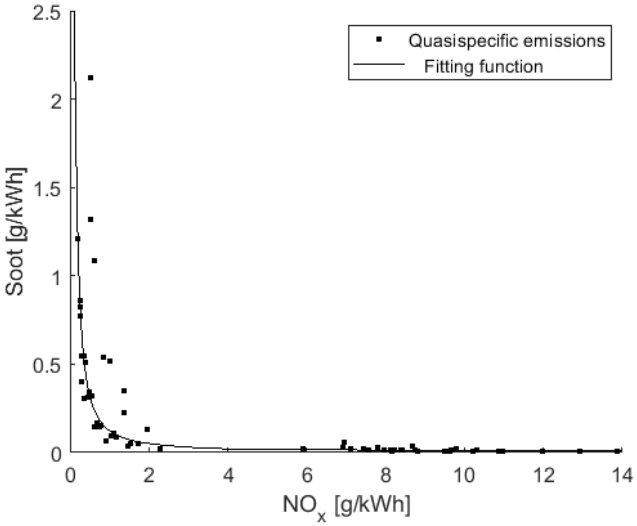

Figure 16: Quasi-specific soot-NOx trade-off of diesel and fitting line.

Since, as seen in the experimental part previously, by varying the engine load, the points identified by ($x = NO_x$, $y = soot$) move perpendicularly to the soot-NOx trade-off line, it was decided to group the operating conditions according to their injection duration and to apply the procedure described above for those groups and then sum up the results. This guarantees that the trade-off dependency on the engine load is taken into account.
Comparing the quasi-specific emission values measured on board with the function (24) already calibrated for conventional diesel fuel, an indication of the deviation of the actual emissions from the reference ones is obtained.
Of course, also the emissions measured with diesel have an error relative to the calibrated fitting line (24) since it is designed to minimize the error, not to reduce it to zero. An example of the evolution of the average of that error when increasing the number of measurements is shown in Figure 17. It can be

seen that the average of the error remains relatively constant independently of the number of measurements used. However, the standard deviation is massive when less than 30 operating conditions are considered.

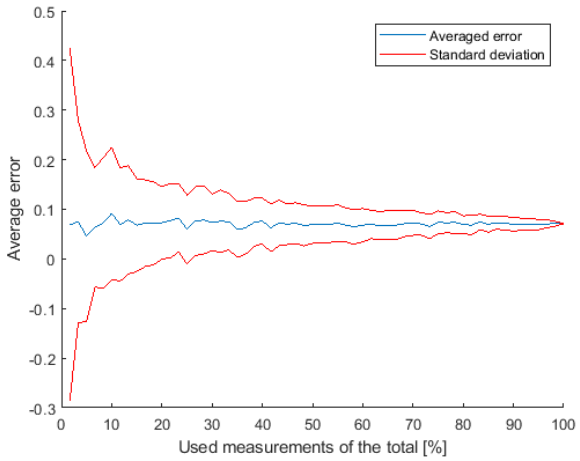

Figure 17: Error between quasi-specific emissions and fitting line for diesel points.

2.3 WP3: Energy requirement of exhaust aftertreatment (Empa)

This section provides a description of the work conducted for the analysis of the energy demand to regenerate DPFs. The needed energy is dependent on the origin of the soot particles, as well as their size and morphological structure. With this, not only the sample preparation, but also the regeneration process itself need to be defined. This chapter describes the sample preparation and regeneration as well as the basics for the computation of the corresponding energy demand. The energy demand is derived using the activation energy evaluated from the measurements.

Particle filter segment preparation and particle size distribution

The previous examinations show a significant reduction of volatile particle compounds by applying a DOC upstream of PF segments during the loading process with diesel soot. This causes the need for higher regeneration temperatures and therefore a better determination of the activation energy of the carbon black. For this reason, all subsequent samples were loaded in this way by the LAV/ETHZ in the exhaust gas partial flow of a diesel engine.
The characteristics of PF (particle filter) samples differ, according to the used fuel and the engine mode. With this, not only the structure and number, but also the particle size, morphology and reactivity are varying. A total of 28 samples were prepared with soot, using diesel, HVO (Hydrogenated Vegetable Oil), and OME 7 (diesel blend with 7% Poly(OxyMethylene) dimethyl Ether) as fuels (Appendix, Table 1). In Addition to the examination of different fuels, a variation of the operation mode of the diesel engine led to differing particle sizes for the PF loading. At least 4 samples were loaded using each engine mode and each fuel type.
The resulting soot particle sizes for filter loading were examined with SMPS measurements of the LAV/ETHZ, which resulted in the fitted number size distributions, shown in
Figure 18.

Figure 18 a) shows the number size distributions of diesel, HVO and OME 7, displaying the mean particle size lies in the range of 133 to 150 nm. The indicated mean particle mobility diameters are the count median diameters (CMD) determined by a log-normal fit.
In Addition, the particle size distribution of the variated operation mode of the diesel engine are shown in
Figure 18 b) and c).

Figure 18 1 b) shows the particle size distributions for the soot samples that were loaded with 5 mass fractions of a normal particle size motor setting (dark blue, CMD 145 nm) and 1 mass fraction with a motor setting of a two-modal particle size mixture with finer particles of 73 nm and normal particles of 135 nm (light blue). The soot particle size distributions shown in
Figure 18 c) were used for the loading of the samples, later referred to as "1n 5f". In this loading mode, the PF was loaded with the normal particles (red, CMD 142 nm) and a combination of both fine particles (orange, CMD 138 and 64.3 nm) in the ratio 1:5.
The CMDs in these figures were determined with a 2-modal fit.

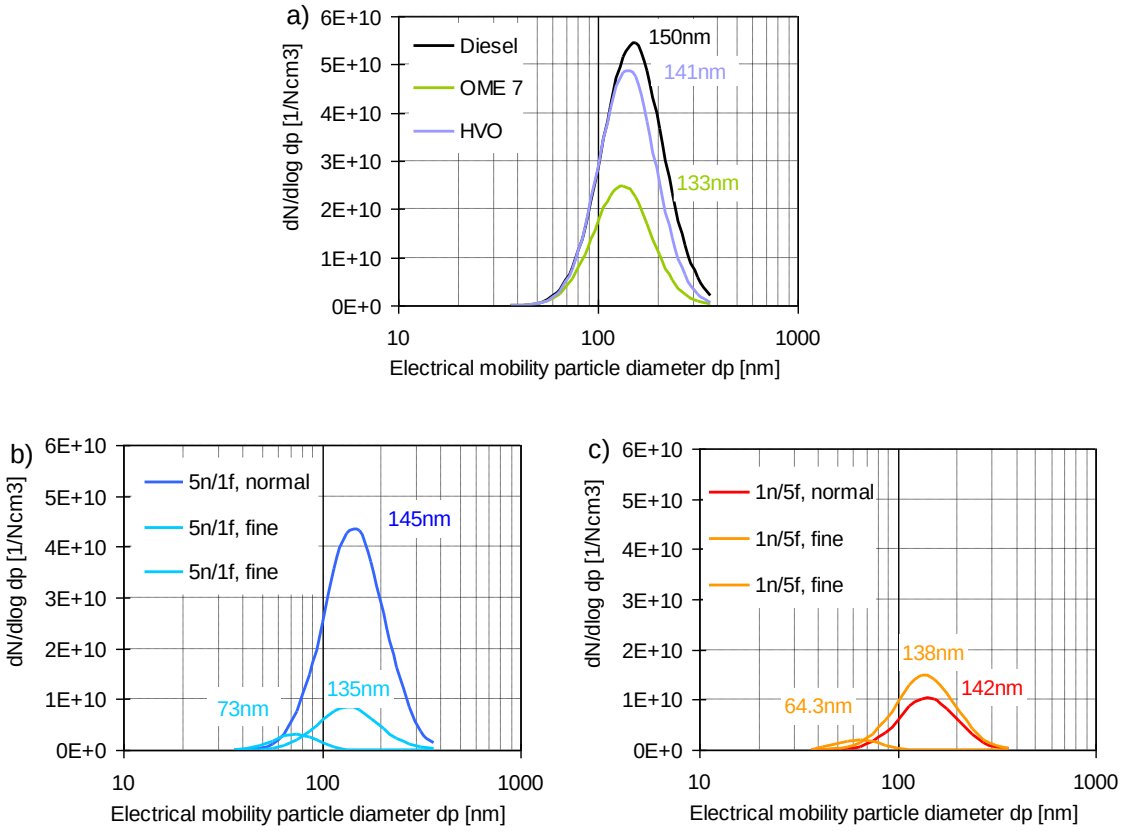

Figure 18: Fitted raw number particle size distributions:, a) Diesel, OME 7 and HVO, b) Diesel and Diesel soot mix with a low amount of smaller particles (73nm), c) Diesel and Diesel soot mix with a higher amount of smaller particles (64nm).

In addition to the particle size distribution, the total particle numbers used for the loading of PF sam-ples are relevant. Figure 19 shows the total cumulated particle numbers of the loading modes and used fuels described above. The resulting samples were named after the fuel type and for the influence of particle size additionally with the loading method. "Diesel 5n 1f" samples were therefore loaded 5 times during the "5n 1f, normal" mode and 1 time using both "5n 1f, fine" modes. The samples "Diesel 1n 5f" were loaded 1 time using the "1n 5f, normal" mode and five times using both "1n 5f, fine" modes. In addition, "Diesel fine" samples were loaded using only "5n 1f, fine" modes.

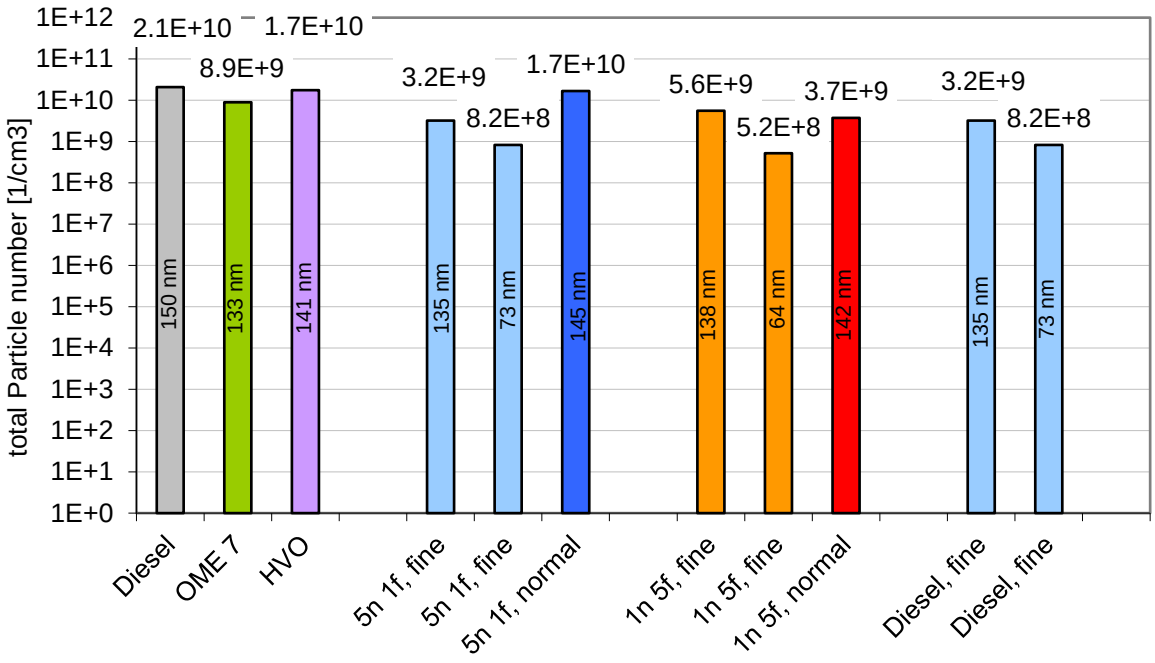

Figure 19: Calculated total particle number of the particle size distributions of Fig 1. The CMD values are indicated in the bars.

To compare the different soot samples, the ratio of the finest particles (73 nm and 64 nm) to the total particle mass of each sample was calculated. The estimated particle number ratios of fine to normal sized particles in the mixture 5normal/1fine were 4.1 % and for 1normal/5 fine 7.2 %. For the sample fine, the proportion of finer particles was 8.6 %.
The ratio of fine to total particle number of the mixtures was estimated. Since the mode of the larger particles, cubic ratio of diameters, is decisive for the mass, and since this mode had a similar distribution in both parts of the mixture, it can be assumed that the average density of the larger particles must be similar and is relevant for the mass in both cases.
The effective ratio of PN-fine to PN-total was therefore extrapolated using the total PN of the normal modes.

2.3.1 Soot sample regeneration and soot mass determination

The PF samples, loaded with the methods that are described above were regenerated by burning the soot off with an air-nitrogen mixture of 8.4 % oxygen content at a flow rate of 0.09 kg/min.
The burnt soot mass was determined by the weight difference before and after regeneration compared with the calculated mass resulting from the measured emitted mass flow of carbon monoxide and carbon dioxide (Figure 20). To achieve a low residual soot mass, which is influencing the computation of the activation energy, the soot was burnt off until only low ppm CO values were measured in the exhaust gas. The soot mass determined by the emission (y-axis) was on average 4.2 % below the mass determined by weighting (x-axis) for the same sample. The results can be approximated with a linear equation, with a standard error of 0.99 g with an R^2 of 0.39. Regarding only the 79 % of measured points with the lowest deviation (below 25 %, red dotted lines) the standard error can be reduced to 0.65 g with a R^2 of 0.76 (considering only the blue points). This indicates a good correlation for the majority of the measured samples.

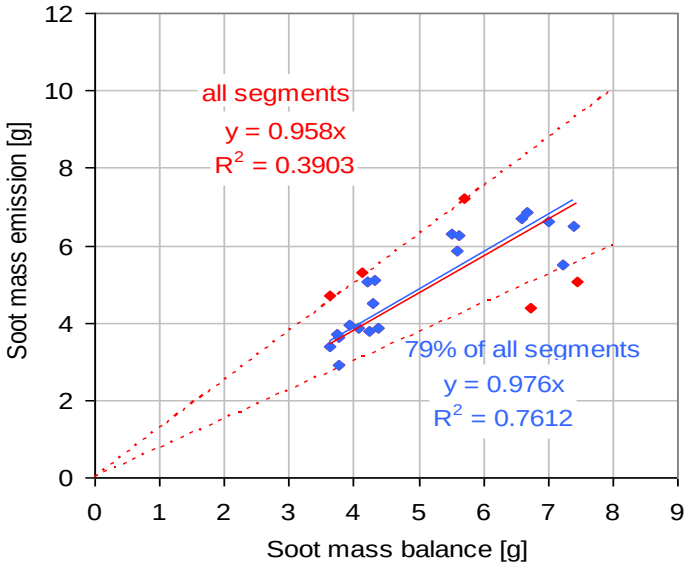

Figure 20: Comparison of the burned soot masses (average 5.1 g) determined by weighing (soot mass balance, x-axis) and by CO- and CO2 emission (soot mass emission, y-axis). The red dots contain the results of all samples (with a R^2 of 0.39) and the blue dots contain only the points where the deviation of the soot masses is below 25% (inside the red dotted lines, with a R^2 of 0.76).

2.3.2 Activation energy computation and heat demand evaluation

To determine the activation energy E_A and the pre-exponential factor A, a simple Arrhenius equation was applied, as it proved to be the most reliable method after extensive evaluations:

$$\frac{dm_s}{m_{s_{red}} dt} = \frac{\dot{m}_s}{m_{s_{red}}} = k_m = p_{O_2}^n \cdot A \cdot e^{-\frac{E_A}{RT_r}} \quad (25)$$

The coefficient of the burn rate $\dot{m}_s$ and the residual soot mass $m_{s_{red}}$ is defined as k_m. The activation energy and the pre-exponential factor are in correlation to the logarithm of the regression values of the burn rate $\dot{m}_s$,which is the time dependent differential of the soot mass m_s, normalized with the oxygen content $p_{O_2}^n$ and the residual soot mass $m_{s_{red}}$ and also the reciprocal value of the corresponding burn up temperature T_r:

$$E_A \sim ln\left(\frac{\dot{m}_s}{m_{s_{red}} \cdot p_{O_2}^n}\right) \text{ and } \frac{1}{T_r} \quad (26)$$

Several simultaneous value groups of temperature, burn up rate, current residual soot mass and oxygen content were determined per sample. Using these values of all samples with the same soot loading, the activation energy and the pre-exponential factor were determined by regression.
For the evaluation of a real world heat demand, the results of the experiments were applied, using the following assumptions. The energy required for regeneration is supplied by an additional heating of the exhaust gas. For the computation of the regeneration energies and times of total DPFs, depending on the regeneration temperature, the exhaust gas flow of the truck of 1000 kg/h and an exhaust gas temperature of 200 °C during normal operation are assumed. The heat capacity is calculated with an average oxygen content of 8 % and the average temperature from regeneration and normal operating temperature.
With the given operation Temperature T_n, the regeneration temperature T_r and the exhaust mass flow $\dot{m_{exh}}$, as well as the heat capacity of the filter with the soot $\bar{c_p}$, the heat demand for the regeneration of the PF Q_r can be determined.

$$Q_r = (T_r - T_n) \cdot \bar{c_p} \cdot \left(- \frac{ln\left(\frac{m_s}{m_{s_{red}}}\right)}{k_m} \right) \cdot \dot{m_{exh}}$$

(27)

2.4 WP4: Platform for Virtual Sensors (Vir2sense)

This section provides a description of the work conducted for the development of the fast models for combustion and emission formation. The section is divided in three sub-sections; the first sub-section describes the process for the systematic determination of different combustion characteristics of the fuels tested, which was later used for the combustion model developement. The second sub-section presents the process of the fast combustion model development, starting from a model describing the mixing rate and leading to the development of the fast heat release rate model. The final sub-section describes the development of the NOx and soot emission models. Results from the models compared to experiments can be found in the results section of this report.

2.4.1 Investigation of combustion characteristics

Following the measurements conducted within WP1 and the analysis perfromed within WP1 and WP2, the combustion characteristics and in particular the analysis of the mixing rate has been automised in order to accelerate the analysis and avoid human bias in the investigation of the results. The results of this analysis are subsequently used for the development of the fast HRR model.
The automation of the analysis of the mixing rate was achieved using a simplified characteristic mixing rate curve, which was fitted to the measured one. The simplified curve uses points derived from the measured one in order to determine the shape of the mixing curve and thus the difference in apparent air-fuel mixing between the different operating conditions and fuels investigated. The points used in the final analysis were taken as the first points around the maximum which had a value of 95% of the maximum value. The simplified mixing rate curve was then constructed using the characteristic points determined from the measurement. These points were the start of diffusion combustion (P1), the end of rise of f_{mix} (P2) and the end of constant f_{mix} (P3). Figure 21 exemplarily shows a measured HRR and resulting mixing rate curve (blue), along with the fitted simplified mixing rate curve (right, green).
The analysis of the combustion characteristics was initiated by an analysis of the sensitivity of calculation assumptions on the resulting observations. This is followed by a study of the locations of the points of characteristic mixing rate curves for different fuels, in order to determine changes in the combustion characteristics, and enable the development of the fast HRR model. The abovementioned analysis results are included in sections 3.4.1 and 3.4.2 respectively.

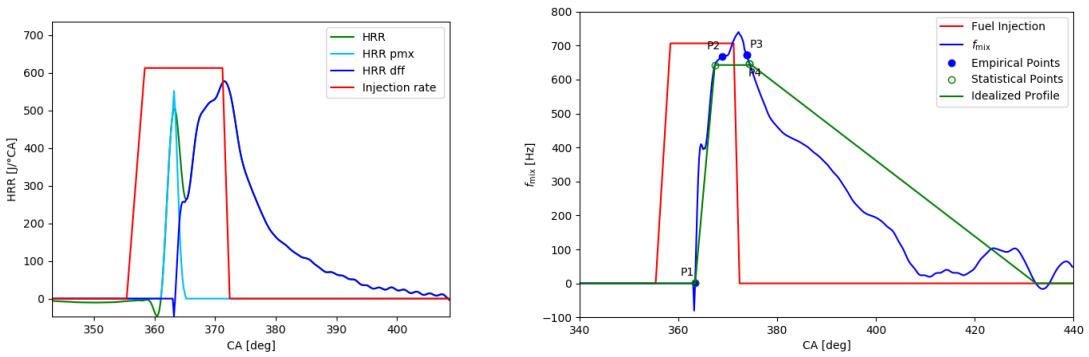

Figure 21: Injection rate and measured heat release rate, differentiating between premixed and diffusion combustion (left), and the resulting characteristic mixing rate curve (f_{mix})

2.4.2 Modelling of combustion

Following the development of the automatic HRR processing tool and its use for the analysis of the combustion characteristics of the different fuels, the analysis results were used for the model development. For the HRR model, the characteristic mixing rate results were used to tune the fast combustion model, which is composed of sub-models for the estimation of ignition delay, premixed combustion, as well as early and late diffusion combustion.
The model tuning was started by tuning the individual sub-model parameters in order to fit the model to the measurements with diesel fuel, for this particular engine configuration. Following this, key parameters of each sub-model which reflect the changes observed in the combustion analysis were tuned to reflect the observed changes in combustion when employing the different fuels. Following the observations from the analysis, the fuels were divided into groups, which reflected the fuel composition and the resulting effect on ignition and combustion. This split ultimately allowed also the fit of the relevant model parameters using an algebraic relationship to the fuel composition, finally allowing the simulation of any combination of fuel characteristics.
The major observations of effect of fuel composition on the fuel ignition and combustion are presented in the list below, for each fuel group:

- Neat paraffinic fuels (HVO, GTL):
    - Ignition delay chemistry was accelerated, while a lower dependency of ignition delay on charge oxygen content (lower variation of ID with EGR) was implemented
    - A higher relative proportion of premixed combustion was used
    - The early diffusion combustion limit (ie the characteristic mixing rate) was increased, and its dependency on EGR was reduced
    - The dependency of the duration of the late diffusion combustion (mixing after end of injection) on EGR and fuel amount were increased
- Paraffinic fuels blended with diesel (HVO20, GTL20):
    - Ignition delay chemistry was accelerated, while a lower dependency of ignition delay on charge oxygen content (lower variation of ID with EGR) was implemented
    - The early diffusion combustion limit (ie the characteristic mixing rate) was increased, and its dependency on EGR was reduced
    - The dependency of the duration of the late diffusion combustion (mixing after end of injection) on EGR and fuel amount were increased
- Oxygenated fuels blended with diesel (OME7, OME15):
    - Ignition delay chemistry was accelerated
    - The proportion of fuel in the premixed combustion was increased
    - The proportion of fuel allocated in the early diffusion combustion was increased, while the early diffusion combustion limit (ie the characteristic mixing rate) was increased, and its dependency on EGR was reduced
- Fully renewable fuel, paraffinic & oxygenated (R100):
    - Ignition delay chemistry was accelerated
    - The proportion of fuel in the premixed combustion was increased
    - The proportion of fuel allocated in the early diffusion combustion was increased, while the early diffusion combustion limit (i.e. the characteristic mixing rate) was increased, and its dependency on EGR was reduced

2.4.3 Modelling of NOx and soot emissions

The process for the NOx and soot model development followed closely that of the combustion model. At first, the models were adapted to fit the modelling framework, and were tuned using the measurements with diesel fuel in order to capture all the variations in emissions caused by the changes in operating conditions. The models were then tested using the data from different fuels in order to identify changes in emissions caused just by the fuel; i.e. the difference observed in emissions when running the models with parameters tuned for diesel compared to the measurements with different fuels

indicated the actual difference in emissions under the same conditions, indicating the model parameters needed to be adjusted for each fuel type. The relevant model parameters were then fitted for each fuel, in order to provide accurate emission predictions for all fuels and under all tested operating conditions. The major observations for each of the emission models for each group of fuels are included in the list below:

- NOx model
  - General observation: the effect of fuel composition on the NOx emissions is not very significant
  - All fuels:
    - Differences in combustion phasing, captured directly in the HRR model, was the major contributor in the NOx emissions; i.e. fuels which show a faster burn rate also result in higher NOx emissions under constant conditions
  - Oxygenated fuels:
    - Fuel-bound oxygen contributes to NOx formation proportionally to its concentration; this is inherently included in the model by including the fuel-bound oxygen in the NOx formation rate calculation
- Soot model:
  - General observation: fuel composition alters the soot emissions significantly
  - All fuels:
    - Lower aromatic content (higher paraffinic or oxygenated content) reduces engine-out soot emissions. Through automatic tuning of model parameters it was observed that lower aromatic content results in lower soot production, as expected by theory
    - Higher oxygenated content also results in lower engine-out soot emissions. Automatic model parameter tuning indicated increased soot oxidation with oxygenated fuels, in particular under operating conditions with high engine-out soot (high EGR/low intake oxygen levels)

All model results are presented in detail in the results section.

2.5 WP5: Virtual Sensors in GT-Power (Combustion and Flow Solutions)

2.5.1 Objective of the work package

Work package 5 consists of coupling the developed model from WP4 with GT-Power in order to optimize parameters and investigate the influences of engine operating conditions on model prediction and application potential to multi cylinder engines.
After development and validation of the basic test bench model (described in WP1) in GT-Power, the coupling is implemented, connecting the 1-D simulation through an interface with the developed platform in WP4. The application of an efficient optimizing tool allows for fast optimization of the combined model and its parameters over a wide range of operating conditions and engine parameters. Finally, the coupled model is employed on a multi-cylinder engine model to define optimal engine operation.

2.5.2 MTU base model

The single cylinder engine test bench (described in WP1) is modelled in the commercial 1D engine simulation package GT-Power.
In a first step, a simplified engine setup is employed to determine important model parameters such as compression ratio, heat loss coefficients, valve lashes etc. and to obtain heat release rates. Transient pressure and temperature boundary conditions from measurements are applied in the “backward” computation (also called Three Pressure Analysis, TPA). Figure 22 depicts the simplified engine setup

using wall temperature calculation and optimizer blocks for multi objective optimization within the GT-Power environment.

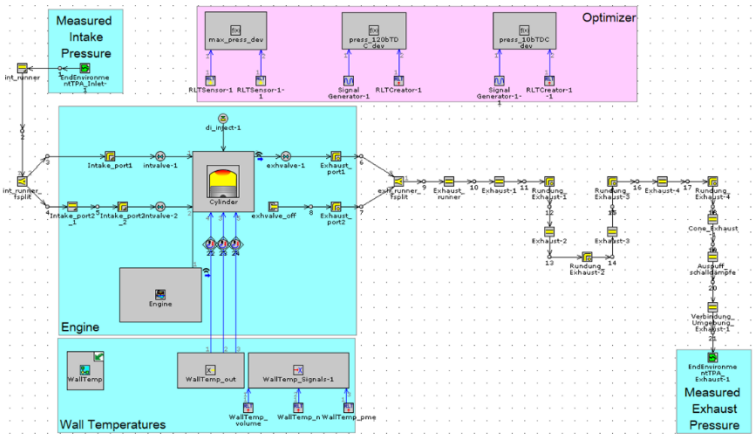

Figure 22: Simplified engine model in GT-Power for three pressure analysis, TPA

The obtained heat release rates through TPA for every operating condition can then be used as input for the full engine model, allowing the validation of all involved components with experimental data.
After optimization of relevant parameters and generation of heat release rates, a “forward” calculation is performed with a full engine model shown in Figure 23. This allows for validation of all involved components with experimental data over a wide range of operating conditions.

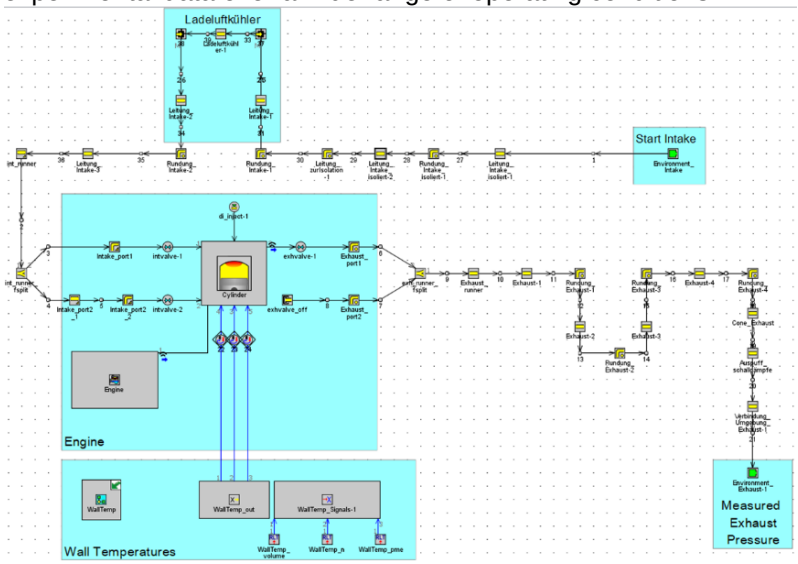

Figure 23: Full engine model in GT-Power with all relevant components

2.5.3 MTU Fast Running Model

The full engine model described in the previous chapter was subsequently reduced in the development of a fast running model (FRM). Fast running models provide immense reduction in computational time through an increase in temporal discretization while a high level of accuracy can be retained, thus enabling faster optimization procedures compared to detailed full engine models. Multiple flow volumes of the respective fluid paths are combined in a simplified geometry while an optimization is run in each combination step to assure accurate representation of the physical processes over all operating points.

No linearization is applied and the cylinder module is retained (Figure 24) to allow for predictive combustion simulations.

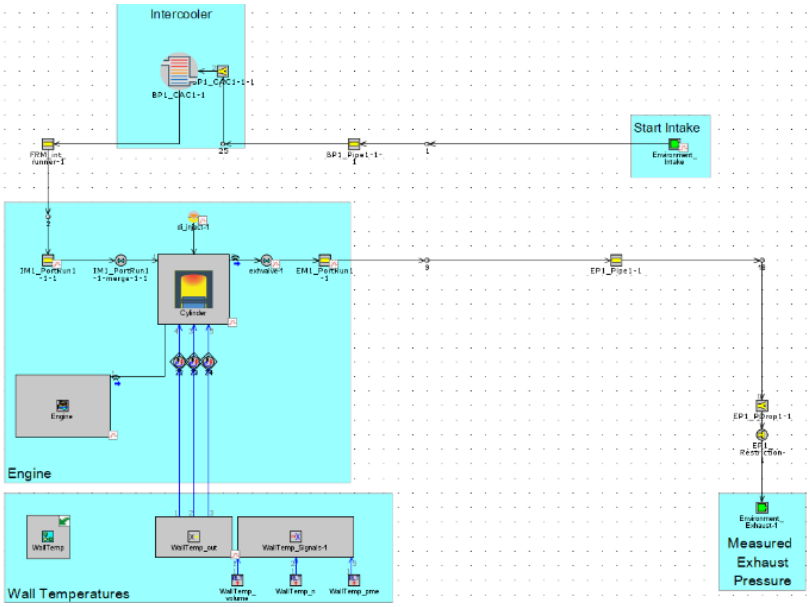

Figure 24: fast running GT-Power model (FRM) of the MTU test bench engine

2.5.4 MTU FRM with Python

The python code developed in WP4 was then applied to the fast running MTU model. GT-Power provides an interface between the codes and contains its own python 3.7 installation in GT-Suite. A python model block can be placed in the model map and inputs and outputs are passed to and from the python model. The placement and respective connections are shown in Figure 25.

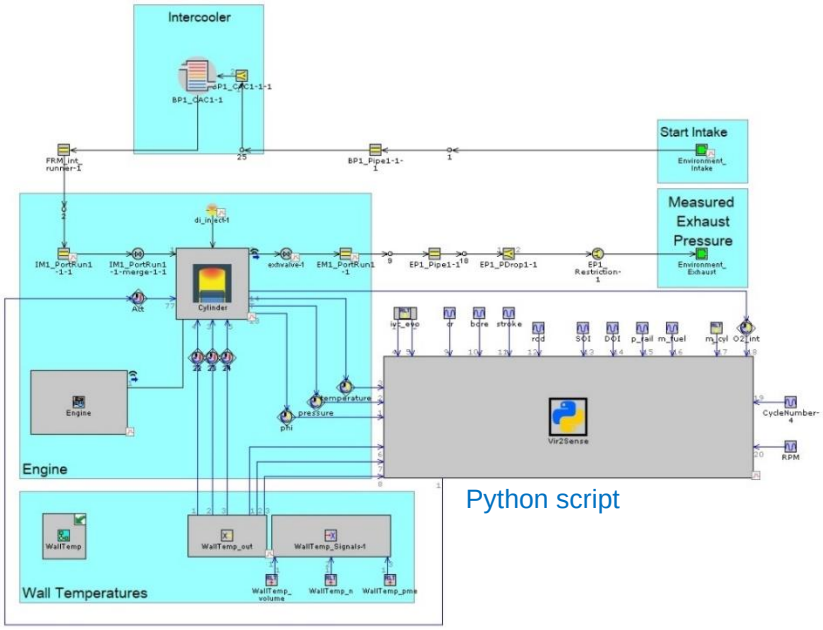

Figure 25: fast running GT-Power model with integrated python script

Inputs can be extracted from different parts of the engine model and are handled at runtime. When the crank angle in the cylinder module reaches start of injection (SOI), the temperature and pressure are used by the script to predict injection, ignition delay, heat release rate and emissions. These arrays are stored within the python implementation to access the values through interpolation in every subsequent timestep and feed them back into the GT model to actuate model blocks.

2.5.5 Multi cylinder engine model

In order to investigate the model capabilities on a realistic engine configuration, the python implementation was applied on a GT-model of a Mercedes 6-cylinder heavy duty diesel engine. Detailed information about the engine, test bench data and GT base model development can be found in [11]. The original model is quite comprehensive and detailed in order to represent the engine on the testbench at FHNW as exactly as possible, while prescribed heat release rates are employed for the combustion simulation in analogy to the approach employed in the development of the MTU396 model described in previous chapters. For a planned optimization with the python model integration however, the model was first reduced by combining flow volumes and valves wherever possible in analogy to the approach outlined earlier for the MTU single cylinder engine.
A speedup of a factor 10 (202 s full engine model vs. 19 s non-predictive FRM) and a speedup of a factor 5 (41 s predictive FRM with python and all added systems in place) was achieved through the step wise model reduction process.
The python script used on the MTU model and its implementation plus the handling of inputs, outputs and controls were adapted to the OM501 fast running model and its 6 cylinders as depicted in Figure 26.

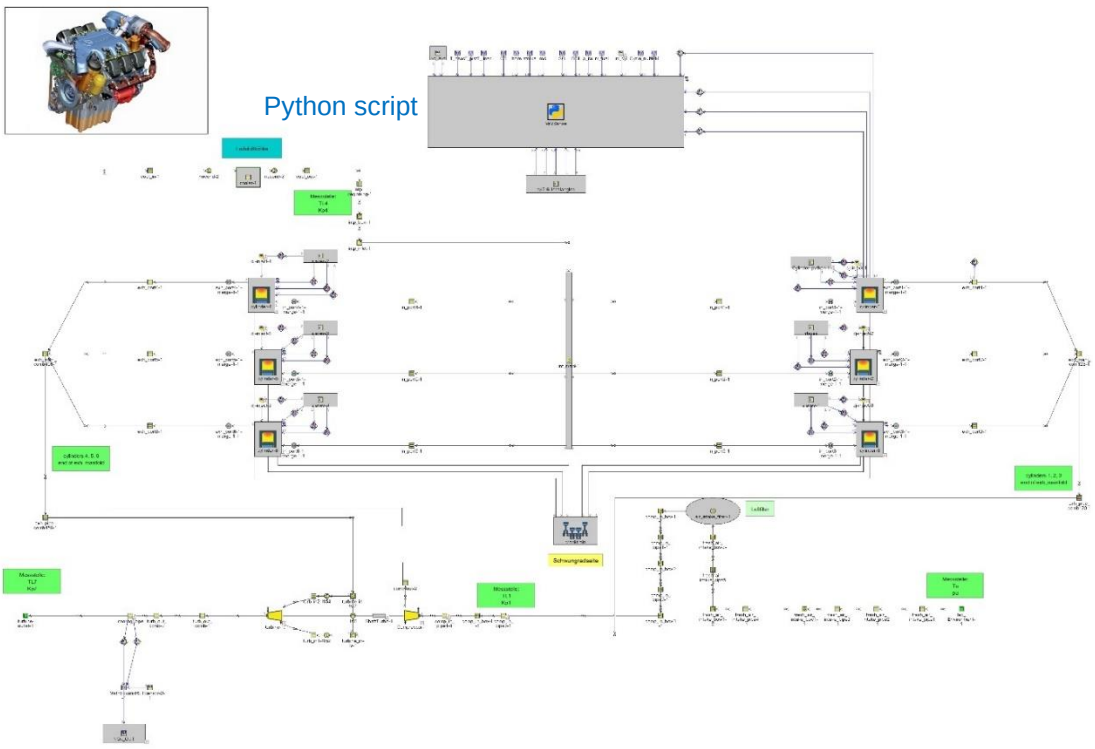

Figure 26: fast running GT-Power OM501 model with integrated python script (baseline, no exhaust aftertreatment and EGR)

As the original engine on the testbench adheres to EURO IV emission standards, a few modifications to the engine model were needed. The addition of common rail injection and exhaust gas aftertreatment

demonstrates not only how modern heavy duty Diesel engines but also retrofit Diesel engines can reach EURO VI emission legislations for alternative.
The pump injector unit in the model was replaced by a common rail system which was parametrized to reach equal power output and maximum cylinder pressures at different engine loads. This model then served as the representation of the baseline case in terms of BSFC, emissions and performance for the comparison with optimized cases. The injection was modelled with a 7-hole injector (170 µm diameter) and a maximum rail pressure of 2000 bar (full load operating condition).
The DPF was implemented using a separate python routine with the data extracted from the results outlined in WP3. As the system represents a steady state, a constant backpressure due to filter loading (50 mbar at full load) and a continuous regeneration of the soot was assumed and modelled by an orifice. The required fuel to regenerate the DPF is computed in each loop depending on soot mass fraction in the exhaust and added to the BSFC which in turn is minimized in the optimization routine. The SCR system is represented by a DOC block generating additional backpressure and its size was chosen big enough to reach a maximum space velocity of 25'00 1/s at full load operation. The conversion efficiency for the NOx reduction is calculated in each time-step depending on space velocity at standard conditions and temperature in the SCR system. The calculated NOx emissions after the SCR system are then used for the optimization. Figure 27 shows the final Gt-Power model used in the optimization, while Table 3: overview of model additions to the original OM501 model gives an overview of model parameters and Table 4 operating conditions and chosen optimization strategy shows the operating points and chosen optimization parameters and targets.

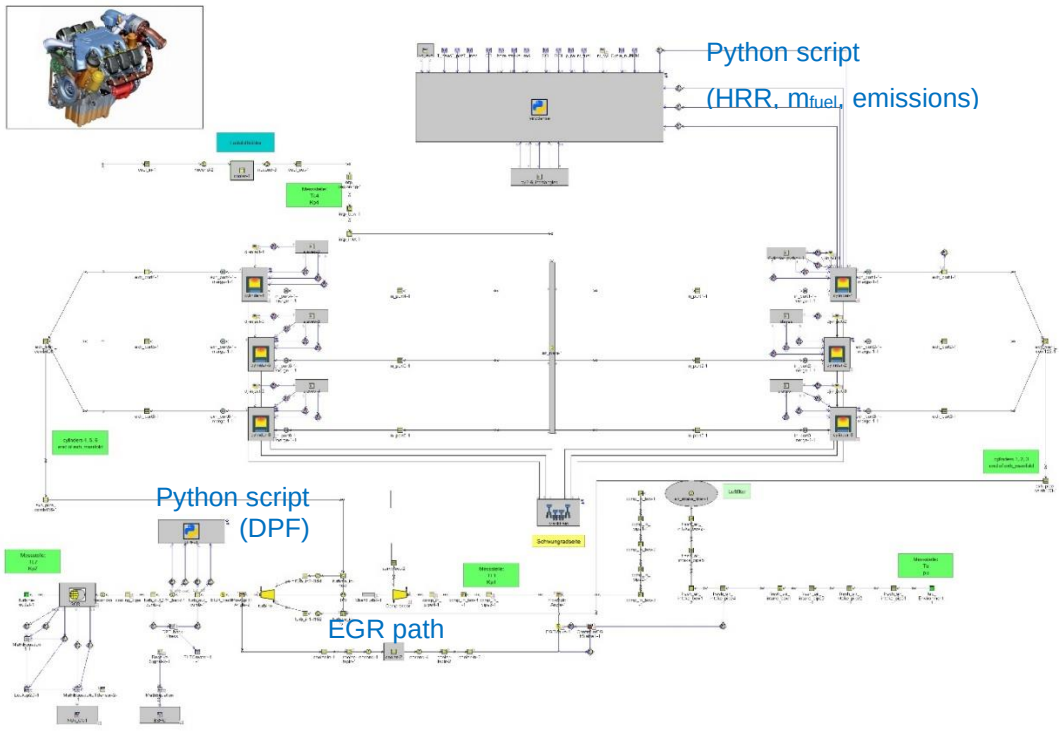

Figure 27: fast running GT-Power OM501 model with python scripts for combustion characteristics and particle filtration (including aftertreatment & EGR)

Table 3: overview of model additions to the original OM501 model

Exhaust gas recirculation (EGR)	Low pressure exhaust gas recirculation with 2 EGR throttles & controllers
Injection system	Common rail, 200 bar p_{max} 7-hole nozzle tip, D_{nozzle}=170 µm
Diesel particulate filter (DPF)	Continuous regeneration at constant Δp=50 mbar BSFC penalty due to regeneration energy calculated by separate model
Selective catalytic reduction (SCR) system	NOx reduction efficiency depending on temperature and space velocity

Table 4 operating conditions and chosen optimization strategy

Operating points engine load	25%, 50%, 75%, 100%
Fuels per operating point	Diesel, HVO, HVO20, OME7, R100
Optimization target	0.4 g/kWh NOx @ minimal BSFC (Stage V emission standard for heavy duty Diesel engines)
Parameters to optimize	Start of injection (SOI), duration of injection (DOI), rail pressure, EGR rate

3 Results and discussion

3.1 WP1: Engine measurements (LAV)

In this section the results obtained from the postprocessing of the raw data collected at the engine testbench are presented.

3.1.1 Combustion

The heat release rates of the eight test fuels are shown in Figure 28. As expected, the effect of the higher cetane number of GTL is clearly related to a decrease of the ignition delay. The effect is more pronounced in the case of neat GTL. Accordingly, the peak of premixed combustion is smaller in the case of GTL and GTL20 since the shorter ignition delay reduces the time available for the injected fuel to pre-mix with air before the combustion begins. In addition, the fact that the density of GTL is smaller than the one of diesel and the LHVs are almost identical suggests that the chemical injection rate is smaller when using GTL or GTL20. After the premixed combustion peak, the curves of the HRR rise again. In that phase, GTL is in advance compared to diesel. GTL20 and diesel in turn, do not differ in an appreciable manner. This phenomenon could be explained by the smaller density of GTL that enhances the entrainment of air as confirmed by the Naber and Siebers model for injection sprays [12]. Despite the smaller lower heating value of GTL, both GTL and GTL20 have a diffusion combustion peak similar to the one of diesel. Together with the weaker late phase combustion, this observation suggests that the mixing of GTL proceeds faster than the one of diesel and compensates for the smaller LHV. This aspect will be further investigated below.

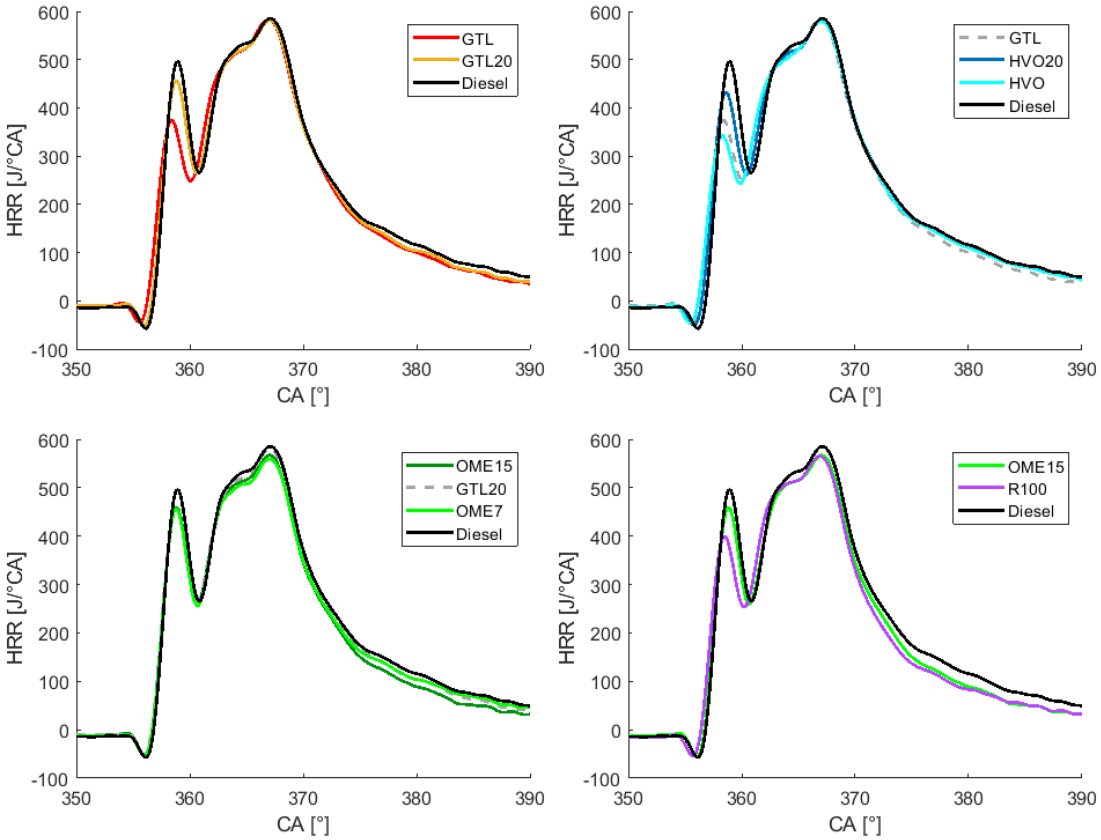

Figure 28: Heat release rates at reference condition.

In general, the differences observed between diesel and GTL apply also with HVO but in the latter they are more pronounced. It can be observed that the premixed combustion peak of HVO20 is even smaller than the one of GTL20 and the same is true for neat HVO compared to neat GTL. Responsible for the smaller premixed peaks are the shorter ignition delay of HVO due to the different evaporation characteristics. These are shown in Figure 29 and reveal that compared to GTL, HVO has a more homogeneous composition regarding the molecules length. This can be deduced from its distillation curve that is flatter compared to the other two fuels. Therefore, the absence of a fraction difficult to evaporate could be the explanation of the shorter ignition delay of HVO. Here it is important to note that the cetane number test procedure includes the evaporation properties of the fuel, but under different environment than in a direct injected diesel engine. Therefore, the comparison of the cetane number only is not conclusive for ignition and combustion characteristics. Looking at the diffusion combustion, analogously to what happen with GTL, in presence of HVO its onset arises sooner. The peak of diffusion combustion is barely affected by HVO despite the lower density compared to diesel. After the injector closure, according to the smaller mass of fuel burned in premixed mode and with the lower density, the magnitude of the late phase combustion of HVO and HVO20 lies between the one of GTL/GTL20 and diesel.

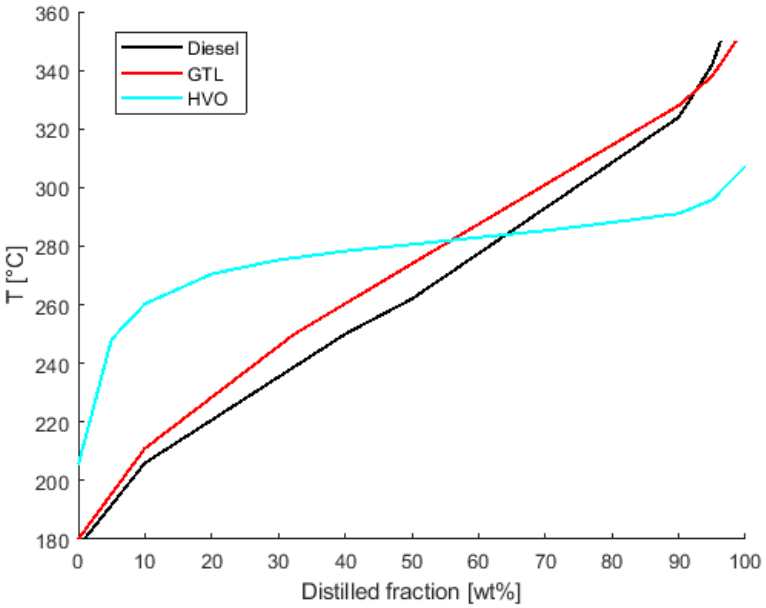

Figure 29: Distillation curves of diesel, GTL, and HVO.

OME was not tested neat. Despite having a higher cetane number than diesel, the ignition delay is not changed appreciably by the presence of OME. On the magnitude of the premixed peak, two counteracting effects play a role. On the one hand, the fact that OME has a smaller lower heating value, turns into a lower amount of energy ready to be released (reads flammable fuel) at the start of combustion. On the other hand, the presence of oxygen in the molecules of OME lowers the stoichiometric air-to-fuel ratio of the blend. This means that the blend needs less air entrainment to dilute to a flammable mixture and therefore at the instant of the start of combustion more fuel could be prepared to burn. The HRR of OME7 and OME15 suggest that in the case of the first blend the first factor (reduced LHV) could be more important and the fact that by increasing the blending ratio to 15% the peak does not diminish could indicate that the second effect (less oxygen entrainment needed) could be dominant for OME15. During the onset of the mixing limited combustion, the heat release rate develops analogously for all the fuels. Differences are to find later when a stable combustion regime sets in. There it can be observed as, due to the smaller LHV of OME, the blend OME7 shows a clearly reduced combustion rate compared to diesel while the trend is reversed by the blend OME15 that, despite having an even smaller LHV is again closer to the diesel line. At end of injection, that fuel is burned in late phase combustion. As expected, OME15 shows the weakest late phase combustion. In turn, OME7 shows a stronger heat release rate later after EOI.

R100 is a blend whose composition was explicitly chosen to be compliant with the EN590 standard regarding density and viscosity. Moreover, being a mixture of HVO and OME with 5% 2-Ethyl-1-hexanol as a stabilizer, this blend is fully renewable. The percentage of OME in R100 (18*vol*%) is comparable with presence of OME in OME15. The presence of a relevant amount of HVO (77*vol*%) in R100 is responsible for a remarkable reduction of the ignition delay relative to diesel. This, combined with the smaller lower heating value of R100, leads to a weaker premixed combustion as to diesel. Similarly to what was observed with neat HVO, the onset of diffusion combustion arises sooner with R100 than with diesel. Once the mixing limited combustion has reached a stable reaction rate, R100 shows a heat release rate similar to the one of OME15 and therefore lower than diesel. At the end of injection, the reaction rate of R100 sinks faster than all the other.

In order to investigate the mixing of the fuels the so called characteristic mixing rate is used. This is defined as:

$$\nu_{mix} = \frac{1}{\tau_{mix}} = \frac{HRR_{dff}}{Q_{avail}} = \frac{HRR_{dff}}{\int_{SOI}^{t}(\dot{q}_{inj} - HRR)dt}$$

(28)

and is a measure of how fast the injected fuel finds the necessary oxygen to burn. The mixing rate is a characteristic parameter of the diffusion combustion process and allows to describe it independently of the ignition delay and the premixed combustion.
Figure 30 shows the curve of the characteristic mixing rates in diffusion combustion for all the test fuels at reference condition. Considering the top-left plot, GTL shows the highest frequency while GTL20 lies between the two neat fuels. The mathematical explanation of why the mixing frequency of GTL is higher than the one of diesel can be understood by looking at the terms of equation
(28). Since the heat release rate peak of diffusion combustion is similar for all the fuels, the numerator of
(28) is therefore unchanged. The difference lies in the denominator. The density as well as the premixed portion of GTL are lower resulting in a net lower denominator. Physically, the reason why GTL has a higher mixing frequency than diesel can be explained considering the factors that influence ν_{mix}. τ_{mix}, which is the reciprocal of ν_{mix}, can be seen as

$$\tau_{mix} = \tau_{diff} + \tau_{evap} + \tau_{ign}$$

(29)

where the three terms on the right side of the equation refer to the time needed by the injection spray to entrain the necessary oxygen to reach a flammable composition (τ_{diff}), to the time it takes to evaporate the fuel (τ_{evap}), and to the ignition time (τ_{ign}). During diffusion combustion and the resultingly high temperature the evaporation and ignition are reasonably fast that the diffusion part remains dominant. However, to detect minor differences the analysis of the other two factors are of interest as well. For example, GTL and HVO show a shorter ignition delay (in particular due to the different molecular composition) in comparison to diesel and diesel and GTL show different boiling curves (Figure 29), in comparison to HVO. Therefore, GTL is assumed to have a relatively short τ_{evap} and τ_{ign} while Diesel is assumed to have only a relatively short τ_{evap} and HVO is assumed to have a relatively short τ_{ign} only. The diffusive part of the mixing time τ_{diff} is influenced by the spray structure and the oxygen demand. The latter is increased with increasing H/C ratio of the fuel which is higher for paraffinic compounds. The distillation curve already seen in Figure 29 suggests that the mean molecule size of HVO is bigger than the one of GTL, leading to different H/C ratios of 2.05 and 2.27, respectively, leading to stoichiometric air-to-fuel ratios of 14.78 and 15.08

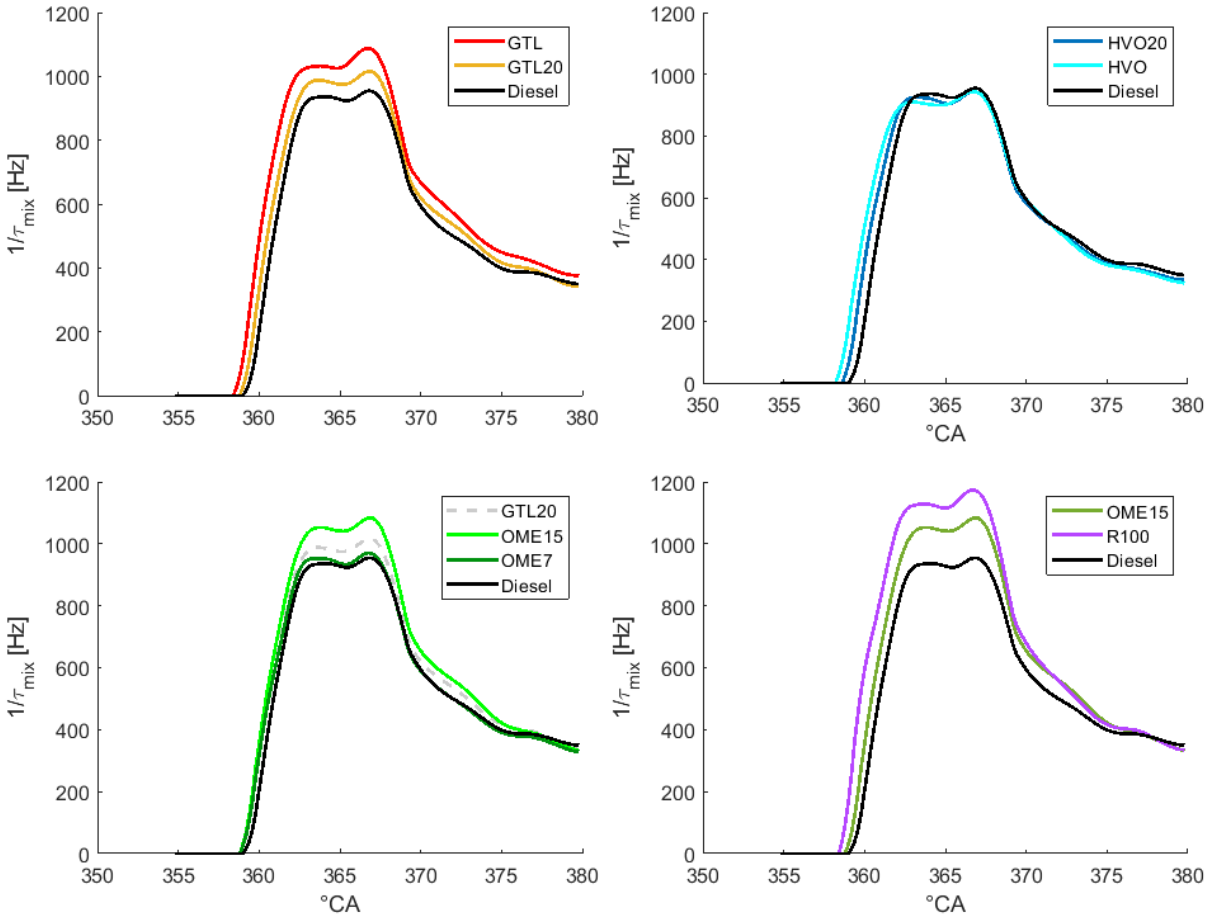

Figure 30: Characteristic mixing rate of the test fuels at reference condition.

The characteristic mixing rate helps understanding the opposite behaviour of OME7 and OME15. This reveals that the differences between diesel and OME7 are very weak while a remarkable increase of the characteristic mixing rate is observed when looking at OME15. The reason of the so high burning rate of OME15 is attributed to the fact that, due to the presence of oxygen content that reduces the oxygen demand, OME15 dilutes faster to a flammable composition, in other words, the flame sits closer to the nozzle, where the turbulences are stronger than in the periphery of the spray. In the case of OME15, this effect is dominant on the influence of the reduced LHV.
R100 shows a similar behaviour compared to OME15. Due to the high presence of HVO, the ignition delay of R100 is shorter and due to the lower stoichiometric air-to-fuel ratio, the mixing frequency is higher. This leads to the rapid decrease of the HRR after the end of injection observed in Figure 28.

3.1.2 Combustion metrics

The fact that in the future more than one fuel for compression ignition engines could be available will imply the need for a strategy to recognize the fuel being used or at least its emissions and combustion characteristics in order to optimize the operating strategy. Of course, the fuel recognition must be performed on-board, meaning that the engine must be equipped with all the necessary sensors to accomplish that task.
The goal of the present study is to characterize combustion and emission metrics of the individual fuel compounds. In order to do so, the emissions and combustion futures analyzed above for few selected operating conditions will be investigated closer.

a. Ignition delay

As seen in above in the analysis of the heat release rates of the various fuels, the paraffinic compounds show a better ignitability compared to the others.
That observation is confirmed by Figure 31, where the ignition delay of diesel, the paraffinic fuels, and the corresponding blends for a variation of EGR and fuel pressure around the reference condition is shown. All the fuels react as expected to the applied variations. A decrease of the intake oxygen concentration leads to an increase of the ignition delay and the same holds true when the fuel pressure sinks. Under all the displayed conditions, diesel shows the longest ignition delays, while HVO the shortest. The ignition delay of GTL and HVO are similar. The blends HVO20 and GTL20 are similar and between diesel and the corresponding neat paraffinic fuels. However, the reduction in ignition delay of the blends compared to diesel is depending on the operating condition and does not represent the blending ratio.

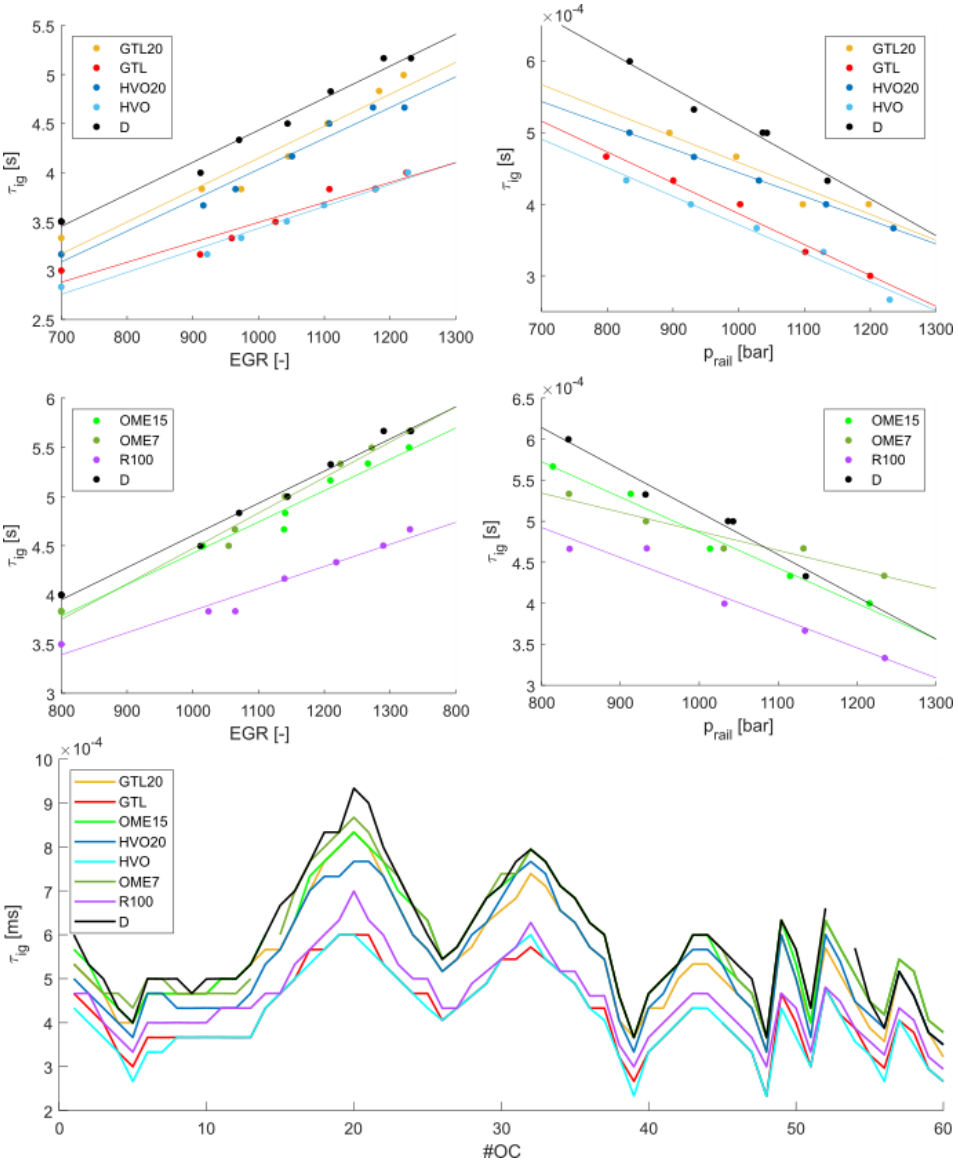

Figure 31: Ignition delay of diesel, the paraffinic fuels, the corresponding blends (top), and diesel, OME7, OME15, and R100 (centre) for a variation of EGR (left) and fuel pressure (right). Below, the ignition delay for all the operating conditions and all the tested fuels can be seen.

The ignition delays of OME7 and OME15 are in the same range compared to diesel. The stated high cetane number of OME is not the most decisive factor for the duration of τ_{ig}. The ignition delays of OME15 and R100 are very different from each other even though the percentage of OME is very similar. The reason of the very good ignitability of R100 is therefore due to the high presence of HVO.
When looking at the evolution of the ignition delay over the entire measurement matrix, it can be seen that the trends described for the EGR and fuel pressure variations are consistent all over the investigated operating range.

b. Premixed combustion

The fraction of fuel burning in premixed combustion is calculated as

$$pmx = \frac{m_{pmx}}{m_{inj}} \quad (30)$$

where m_{pmx}: mass burned in premixed combustion
m_{inj}: total injected mass

The premixed combustion is strongly coupled to the ignition delay. As it can be seen in Figure 32, paraffinic fuels, having a better ignitability, tend to show a smaller fraction of premixed burning fuel. Moreover, the premixed fraction of HVO and HVO20 is smaller than the one of GTL and GTL20, respectively. This trend is confirmed also for a variation of fuel pressure.
Despite having ignition delays shorter than the ones of diesel, the fraction of the blends OME7 and OME15 burning in premixed mode are not always smaller than the ones of diesel. This may be due to the fact that OME, having a lower stoichiometric air-to-fuel ratio needs less oxygen entrainment. This means that at the start of combustion, for identical ignition delays and identical mass of air entrained, the flammable fuel mass in the case of OME is higher. This advantage of OME becomes particularly evident at high EGR rates. R100, due to the large presence of HVO and according to its good ignitability, shows very small fractions of premixed burning fuel. In general, the EGR variation highlights the differences between the fuels relative to the premixed fraction better than a fuel pressure variation.
Despite the evolution of pmx in both the variations (EGR and fuel pressure) is quite consistent, when looking at the entire set of measurements, it appears clear that the operating condition has a much stronger influence on the premixed combustion than the choice of the fuel. Especially when performing a load variation by changing the duration of injection (last 10 points to the right), the parameter pmx, varies very strongly due to the change of m_{inj}.

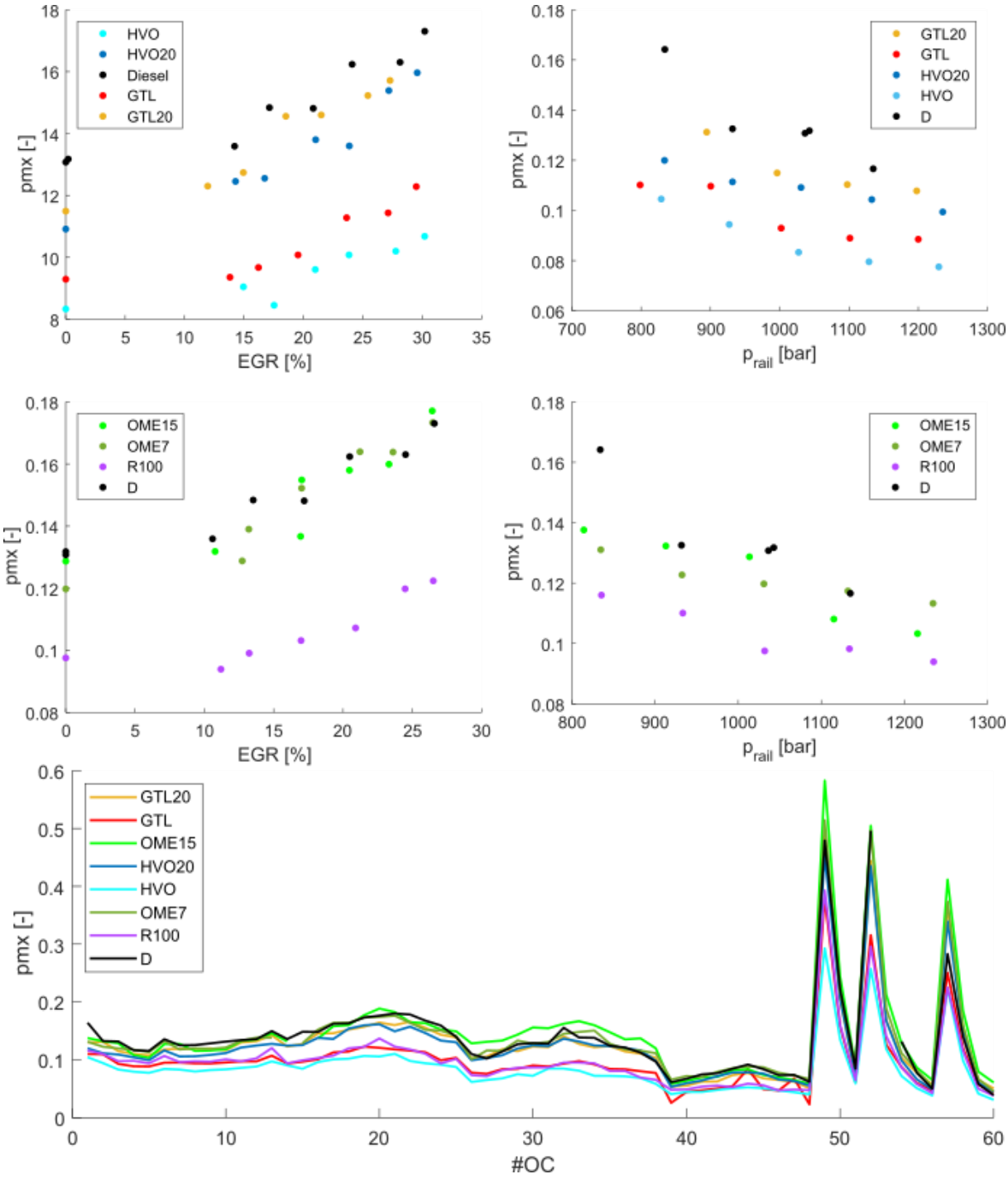

Figure 32: Fraction of fuel burning premixed (pmx) of diesel, the paraffinic fuels, the corresponding blends (top), and diesel, OME7, OME15, and R100 (centre) for a variation of EGR (left) and fuel pressure (right). Below, the pmx for all the operating conditions and all the tested fuels can be seen.

c. Characteristic mixing rate

The characteristic mixing rate is a distinguishing feature of the diffusion combustion process. For this reason, the maximum attained mixing rate is investigated as mark for the diffusion combustion of different fuels. The composition of the fuel plays a decisive role regarding the resulting characteristic

mixing rate. For example, a higher stoichiometric air-to-fuel ratio shifts the flame downstream in the mixing space where the turbulence and therefore the mixing are weaker.
Figure 33 shows the peak of ν_{mix} for diesel, HVO, GTL, and the corresponding blends. GTL has a maximum attainable mixing rate higher than the one of diesel and this is true for different EGR rates and different fuel pressures. HVO in turn confirms that it does not increase the mixing rate compared to diesel. It appears, even in low magnitude, that the blend of diesel and HVO shows a lower mixing rate than the corresponding neat fuels. The reason for this is in adverse effects of the individual components of the mixing rate (i.e. evaporation, diffusion and ignition, as previously describe).

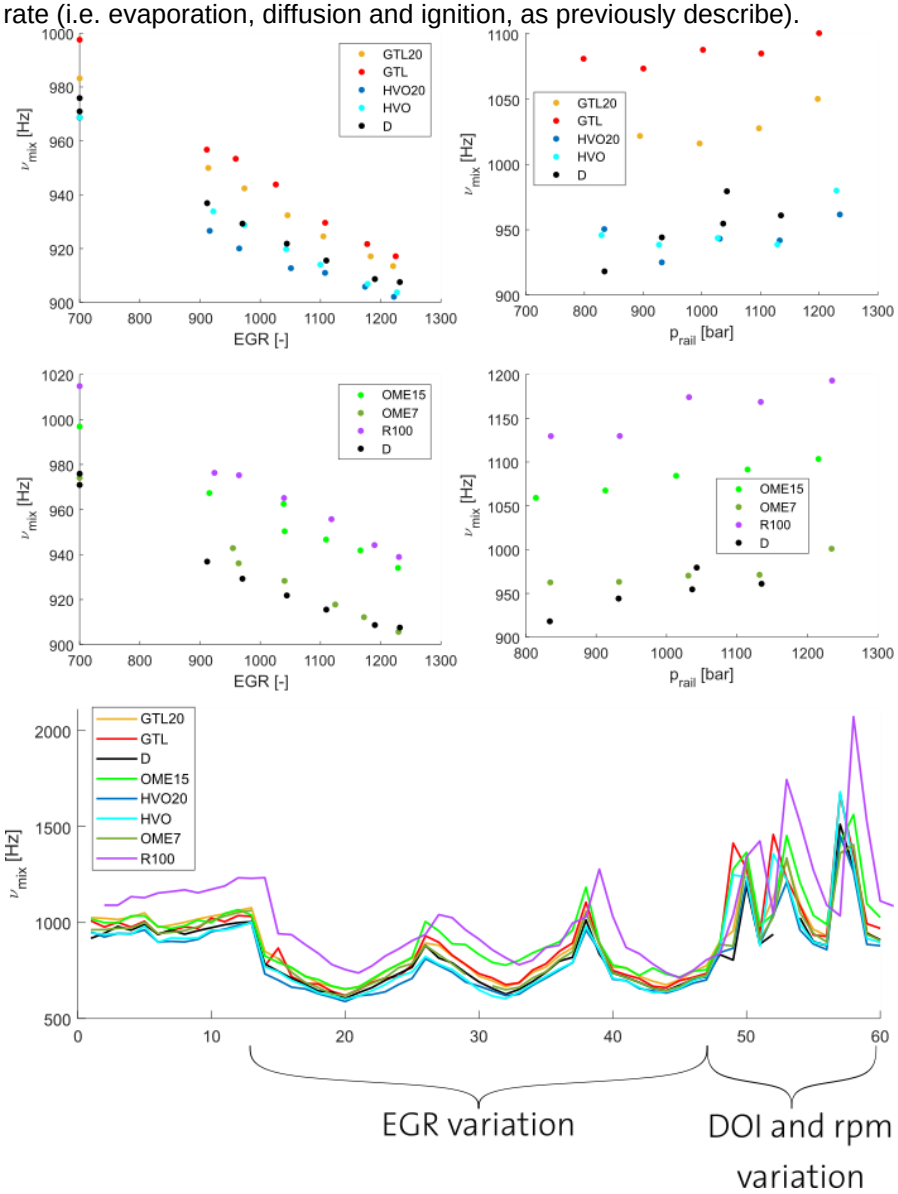

Figure 33: Characteristic mixing rate of diesel, the paraffinic fuels, the corresponding blends (top), and diesel, OME7, OME15, and R100 (centre) for a variation of EGR (left) and fuel pressure (right). Below, the characteristic mixing rate for all the operating conditions and all the tested fuels.

Furthermore, the maximum attainable mixing rate decreases linearly whit the intake oxygen concentration since if the oxygen availability sinks, more air must be entrained to reach a certain equivalence ratio. This means that the flame will set in at more peripheral locations, where the turbulences are lower. For this reason, the mixing rate becomes weaker. On the other hand, to an increase of the fuel pressure, a corresponding increase of ν_{mix} could be expected due to the increase

of injection velocity and therefore of turbulence. However, it must be considered that also the mass flow rate becomes larger with bigger fuel pressures and this increases the denominator of equation (28). A detailed analysis of the injected kinetic energy can be found in [13].
Blends containing OME show the same behaviour of the other fuels. An increase of the recirculated exhaust gas corresponds to a decrease of the maximum attainable mixing rate. The variation of the fuel pressure demonstrates that rising fuel pressures make the mixing rate higher but the effect is not as strong as the one obtained by varying the intake oxygen concentration. The fully renewable blend, due to the large portion of OME, shows the larger maximum ν_{mix} while an addition of only 7*vol*% of OME to diesel does not lead to noticeable increases of the mixing rate.
The maximum attainable mixing frequency should be dependent, apart on the fuel, on the turbulence level in the flame region. The evolution of ν_{mix} over the entire measurement matrix shows that the effect of the EGR rate is important. However, the strongest oscillations are observed when the DOI (and therefore the load) is changed. In particular, the shortest injections (1ms) show the highest peaks. The reason for that behaviour is that with so short injections the available energy and even more the heat release rate in that (very short) diffusion combustion is difficult to detect.

d. Exhaust temperature

Fuels with different lower heating values and different combustion behaviour are supposed to show different exhaust temperatures. The evolution of the exhaust temperature for a variation of EGR and fuel pressure around the reference condition is shown in Figure 34.

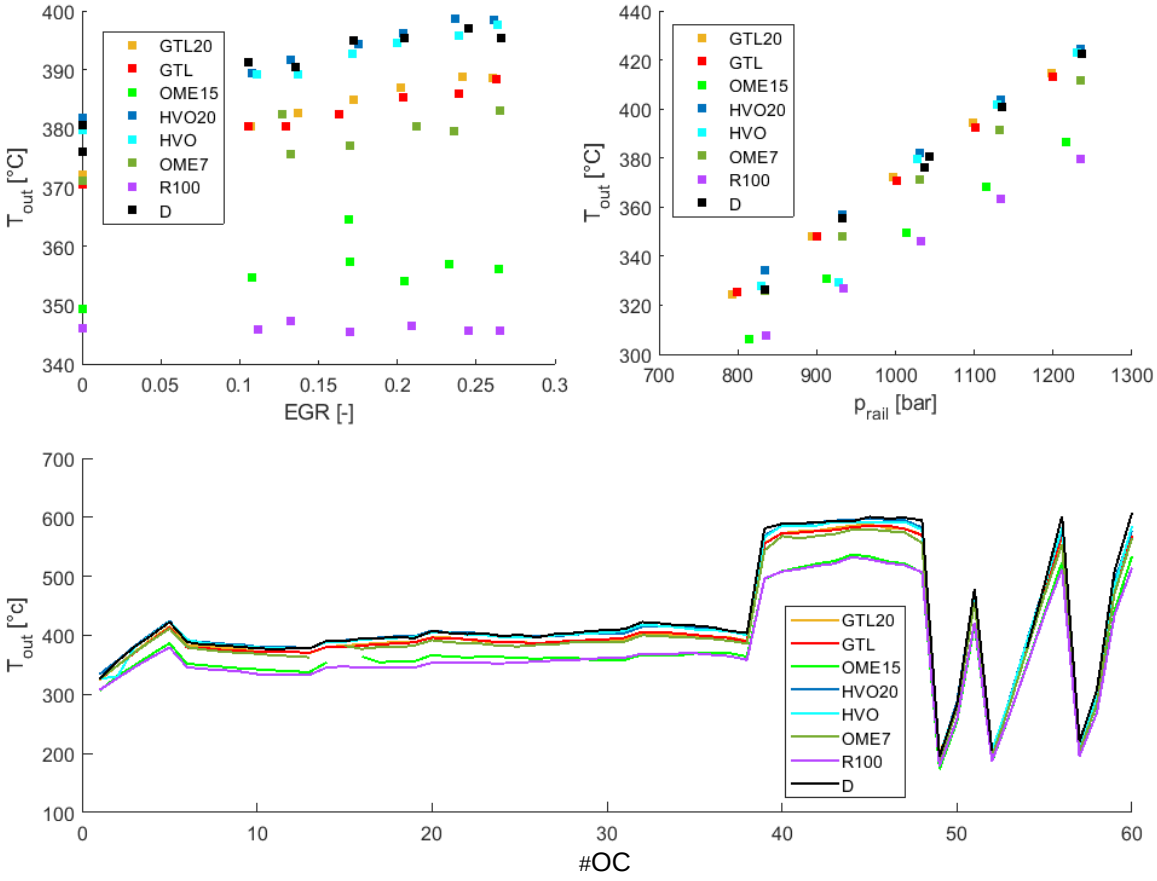

Figure 34: Exhaust temperature of the tested fuels for an EGR variation (top left) and a fuel pressure variation (top right) around the reference condition. The exhaust temperature of the complete measurement matrix is shown below.

As expected, the increase of the fuel pressure leads to an increase of the exhaust temperature according to the increase of injected mass. This behaviour is common to all the tested fuels. R100 shows the

lowest temperatures consequently to the smallest LHV among the test fuels. A similar trend is also shown by OME15. Neat GTL, due to the higher mixing frequency, can also be distinguished from diesel by a lower exhaust temperature. All the rest four fuels (diesel, HVO, HVO20 and GTL20), have higher and very similar exhaust temperatures.
The variation of fuel pressure causes exhaust temperature oscillations of up to 20%. The oscillation due to the EGR variation are much smaller. This allows seeing also the differences between the non-oxygenated fuels and reveals that GTL and GTL20 lower the exhaust temperature, probably due to the higher mixing frequency seen in Figure 33 that advances the centre of combustion. Opposite to that, HVO and HVO20 behave identically to diesel and this result is in good agreement with the mixing rates. The large presence of oxygen content in OME15 and R100 allows the two fuels to be less sensitive to the EGR rate. This can be seen as the increase of exhaust temperature when decreasing the intake oxygen concentration is almost invisible compared to the evolution of the other fuels.
In Figure 34 also the exhaust temperature for all the recorded operating conditions of the measurement matrix for all the test fuels is shown. The differences between the fuels, apart for OME15 and R100, are small. The operating condition itself has a much stronger influence on the exhaust temperature than the fuel used.

e. Indicated specific energy consumption

The eight test fuels show different combustion behaviour. Different rates of heat release lead to different engine thermal efficiencies and, therefore, to different indicated specific energy consumptions. Since with the experimental setup used for the present work, the low-pressure cycle could even perform work on the piston, the ISEC is computed as follows:

$$ISEC = \frac{\dot{m}_{fuel} \cdot LHV}{IMEP_{HP} \cdot V_d \cdot n_e \cdot 1/4} \cdot 3600 \left[\frac{kJ}{kWh}\right] \quad (31)$$

where: $\dot{m}_{fuel}$: Fuel mass flow rate $[kg/s]$
LHV: Lower heating value of the fuel $\left[\frac{kJ}{kg}\right]$
$IMEP_{HP}$: Indicated mean effective pressure of the high pressure cycle $[Pa]$
V_d: Displacement volume $[m^3]$
n_e: Engine speed $[Hz]$
A high ISEC corresponds to a low thermal efficiency of the engine. The energy consumption over a variation of EGR rate and fuel pressure around the reference condition are displayed in Figure 35.

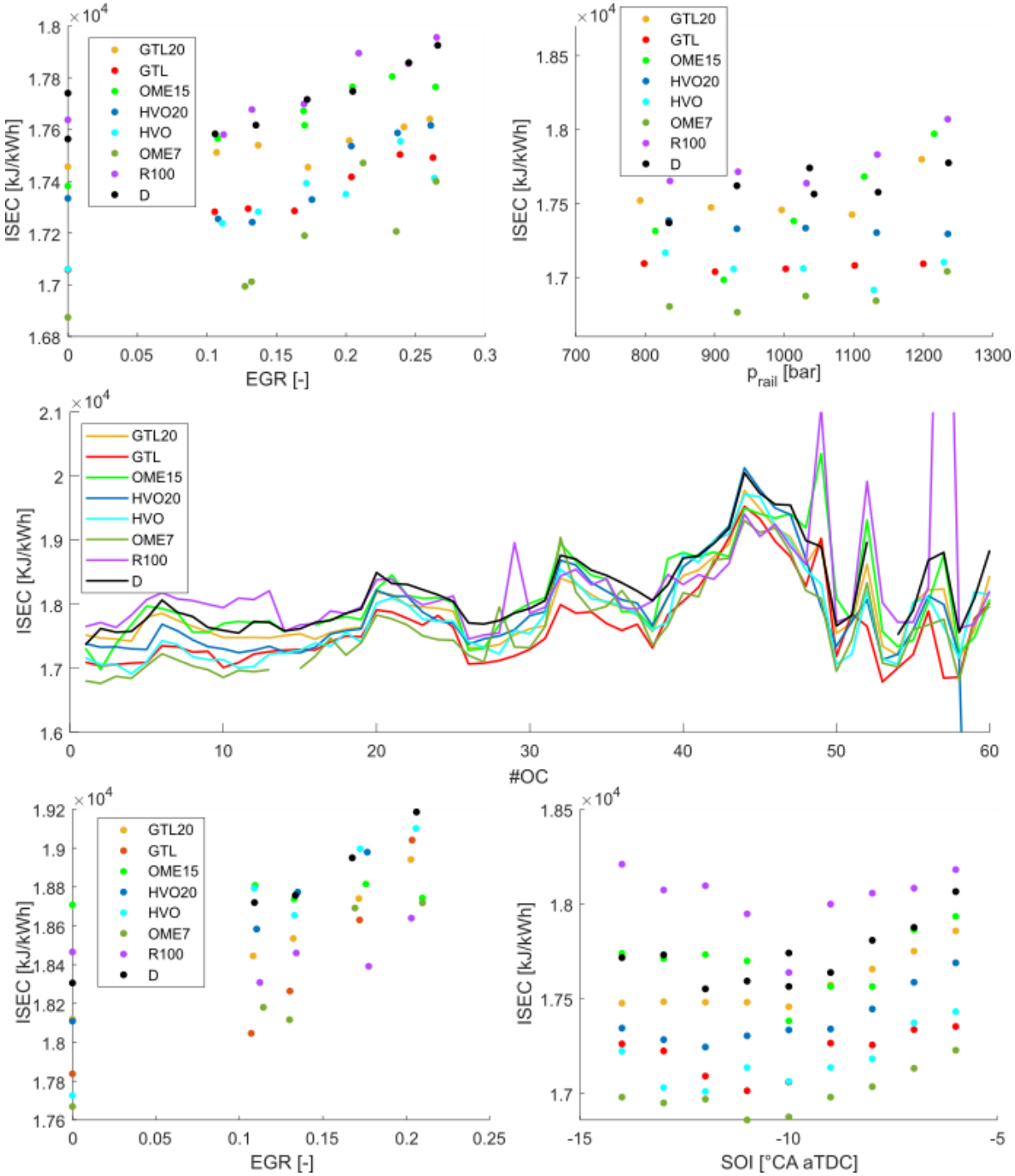

Figure 35: Top: ISEC for all the fuels for a EGR variation (left) and a fuel pressure variation (right) around the reference condition. Middle: ISEC for all the fuels and all the operating conditions. Bottom: ISEC for a EGR variation and a duration of injection of 3ms (left) and a SOI variation (right) around the reference condition.

In both cases, OME7 is the fuel showing the lowest indicated specific energy consumption. When increasing the recirculation rate, also the energy consumption increases since the centre of combustion is shifted towards unfavourable crank angle positions. The variation of fuel pressure does not correspond to a remarkable variation of the engine efficiency. Apart from OME7, also neat GTL and neat HVO show lower ISEC compared to diesel. In the case of the EGR variation, also GTL20 behaves

similarly to the two neat paraffinic fuels. The highly oxygenated fuels (OME15 and R100) have an energy consumption similar to the one of diesel. The fact that OME7 shows the lowest ISEC while OME15 has one of the highest can be explained by considering two counteracting phenomena. On the one hand, the presence of OME increases the reaction speed leading to a higher efficiency. On the other, it is also responsible for a lower amount of injected fuel energy, leading to a lower load and, therefore, lower combustion temperatures that could turn in a lower thermal efficiency. In the case of OME7, the first effect could be dominant, while in the case of R100 and OME15 the latter could play a more important role.

In addition, Figure 35 shows the indicated specific energy consumption for all the operating conditions of the measurement matrix for all the test fuels. The various fuels do not have distinguishing behaviours but it can be observed that R100 shows under certain conditions the worst ISEC (e.g., OC from 1 to 13) and in certain other cases one of the best (OC from 38 to 45). In order to investigate furhter that behaviour, the indicated specific energy consumption over a variation of SOI and a variation of EGR with prolonged DOI ($3ms$) is showed in the bottom part of the same figure.

It can be observed that in the case of the SOI variation around the reference point ($DOI = 2ms$), the ISEC of R100 reaches a minimum for a start of injection at 10° CA before TDC. Its entire trend however remains higher than the other fuels. The heat release rate of R100 (Figure 28) is characterized by a small premixed combustion resulting from the short ingition delay. This means that the pressure and temperature increases due to premixed combustion are smaller in the case of R100 with respect to the other fuels. Having in mind the T-s-diagram of a diesel cycle, it is easy to understand that if the diffusion combustion takes place at lower pressures, the efficiency of the cycle sinks, explaining the high ISEC values of R100.

On the other hand, when the injeciton duration is prologed to 3ms, the value of the efficiency of the cycle fueled with R100 improves compared to the rest of the test fuels. The reason can again be explained by means of the T-s-diagram. The characteristic mixing rate of R100 is very high. This means that the shape of the diffusion combustion curve in the T-s-diagram would shift closer to a isochoric heat transfer compared to what happen with the other compounds. This effect, however, becomes dominant only when the diffusion combustion is prolonged and has the consequence of increasing the engine efficiency lowering ISEC.

Since 77*vol*% of R100 is HVO, these two fuels are expected to behave similarly. However, as it can be observed in the bottom row of Figure 35, the opposite is true. In order to look more into details this difference, the heat release rate of diesel, HVO, and R100 for two different injection duration and two different EGR levels are shown in Figure 36. From those curves it is evident that the oxygen content present in R100 shows its effects at best when the diffusion combustion lasts longer. There, the higher mixing rate keeps the heat release rate almost as high as the one of diesel even with a DOI of 3ms and despite a difference of more than 11% in lower heating value. HVO, in turn, achieves combustion rates comparable to the ones of diesel only with a DOI of 2ms. When the injection duration is increased to 3ms, the lower density of HVO shows its effect reducing the heat release rate in diffusion combustion regime. Summing up, R100, despite having a smaller LHV compared to diesel, manages to achieve the same heat release rate as the one of diesel for both injection durations. On the other hand, HVO is 5% lighter than diesel and this results in the lowered HRR when the DOI is prolonged. This could explain the oppostie behaviour of HVO and R100.

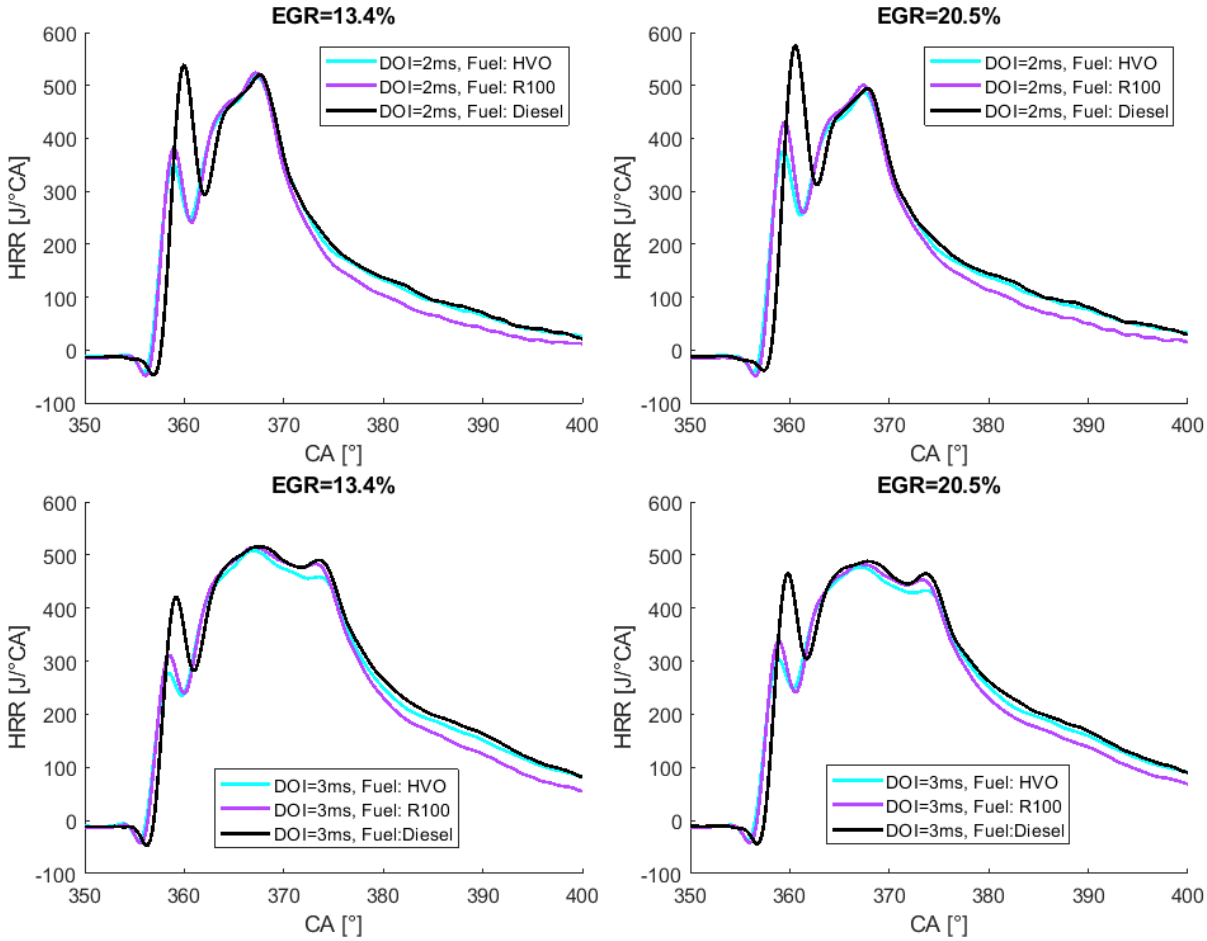

Figure 36: Heat release rate of diesel, HVO, and R100 with an injection duration of 2ms and an EGR rate of 13.4% (top left) and 20.5% (top right). Heat release rate of diesel, HVO, and R100 with an injection duration of 3ms and an EGR rate of 13.4% (bottom left) and 20.5% (bottom right).

3.1.3 Emissions

The emissions of compression ignition engines are characterized by the well-known NOx-soot trade-off. For this reason, in the following the focus will be on those two species.

In order to better spot the differences, if any, regarding emission performances of between GTL and HVO, first HVO20 and GTL20 are compared to diesel in Figure 37. It is observed that GTL20 emits less soot than diesel but minorly more NOx at comparable EGR rates. Opposite to that, HVO20 shows its soot reduction potential only at very high EGR rates while, when the intake oxygen concentration is not excessively low, the soot emitted by HVO20 is similar compared to the concentration measured with diesel. On the other hand, the NOx concentration is lowered by the presence of 20% HVO. These results are in good agreement with the observations made when analysing the combustion of the two blends. It was observed that GTL20 compared to HVO20 has a more pronounced premixed combustion phase. In turn, the mixing controlled phase of HVO20 is more important than it is for GTL20. It is well known that the diffusion combustion plays a predominant role for the soot emissions, while the increase of temperature due to the heat released during the premixed combustion is determining among others for the NOx formation phase.

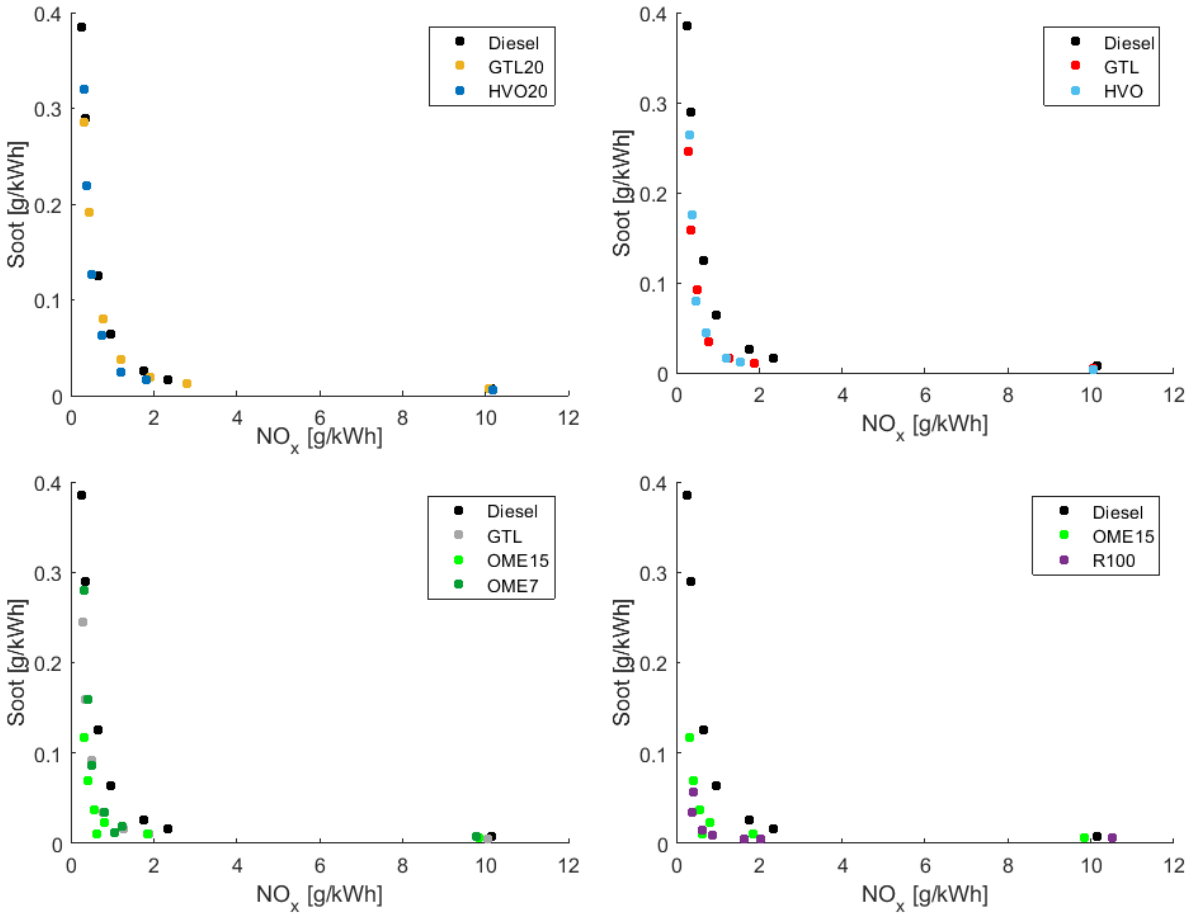

Figure 37: Specific soot-NOx trade-off of diesel compared with GTL20 and HVO20 (top left), neat HVO and neat GTL (top right), OME7 and OME15 (bottom left), and OME15 and R100 (bottom right).

The same comparison is shown between pure GTL and pure HVO. It can be seen that the improvement of the trade-off due to the alternative fuels is remarkable. However, the tendencies observed with HVO20 and GTL20 are confirmed. Neat HVO, despite strongly reducing the soot emissions compared to diesel, still shows a higher soot concentration in the exhaust with respect to GTL. NOx is also reduced when using the two paraffinic compounds, with HVO being the most effective. The two paraffinic fuels appear similar on the trade-off line but with the ECU settings used, HVO shows generally more soot and less NOx. The difference to diesel is attributed to the missing aromatics of the paraffinic fuels.
Regarding NOx, this is formed under high temperature conditions. In a compression ignition combustion as the one of the reference condition of the present study, the premixed combustion is responsible for a large part of the increase of cylinder pressure and temperature. As it will be shown later in Figure 32, diesel releases up to 18% of the energy with a premixed combustion while the fraction of fuel burning in a flame propagation regime is much smaller with GTL and HVO. This means that with the latter fuels the temperatures during diffusion combustion remains lower and accordingly the formation of NOx proceeds slower. In addition, a shorter residence time (proportional to the mixing time) decrease the NOx formation rate. However, this mechanism is in trade-off with the higher combustion temperature resulting from the fast mixing. An additional difference could result from the different adiabatic flame temperature of the neat fuels.
The presence of oxygen in the molecules of OME have a large influence on the specific soot emissions of the blends OME7 and OME15. The comparison with the emission values of neat GTL allows understanding that already 7% in volume of OME in diesel offsets the advantage of GTL on diesel. Indeed, the emission levels of OME7 are very similar to the one of the neat paraffinic fuel. The effect of OME on particulate matter has already been investigated extensively in the literature [14], [15], [16], [13]

and therefore it will not be explained in detail here. It is worth however to note that the reduction of PM is more than proportional to the content of OME in the blend. Already with 7*vol*% OME the soot level can be reduced by up to 57% while the blend OME15 reaches soot values that are up to 78% lower than the ones of diesel. The soot reduction of R100 compared to the reference diesel is large, up to 90%. This is due to the combined effect of the presence of oxygen content in OME and the lack of aromatics of HVO. R100, at similar EGR rates, shows also smaller specific emissions of NOx compared to the reference diesel.

a. Soot-NOx trade-off

The paraffinic fuels improve the soot-NOx trade-off due to the lack of soot precursors. The oxygen available in the OME molecular structure allows a further reduction of the soot emissions. For these reasons, the trade-off between soot and NOx are different from fuel to fuel. In order to characterise the shape of those trade-off, the specific soot emissions of soot are approximated with the following function:

$$Soot_{fit} = \frac{1}{(C_1 \cdot NOx + C_2)^{C_3}} + C_4 \quad (32)$$

where C_{1-4} are fitting parameters.

The fitted functions for the different fuels are displayed in Figure 38. However, as seen in above, there is a distribution perpendicularly to a hypothetical fitting curve. The parameter causing that deviation was found to be the DOI. When increasing the injection duration, the soot emission increase without showing a corresponding NOx reduction. The result is a steeper curve when approaching the soot axis from the right side.

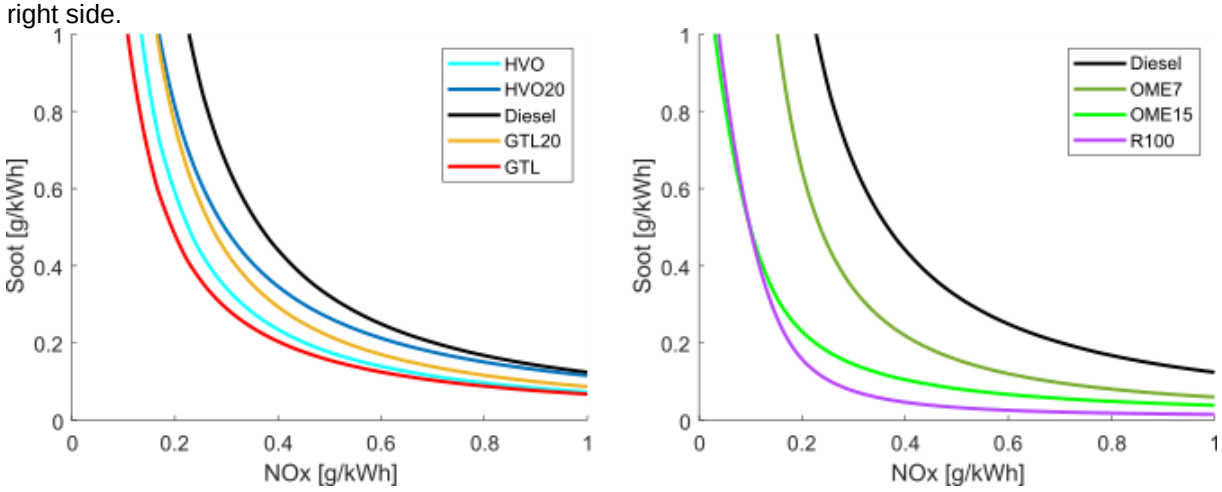

Figure 38: Fitted soot-NOx trade-off line for diesel and the paraffinic fuels (left), and diesel and the OME based blends (right).

This means that the values of the fitting coefficients C_{1-4} are dependent on the measurement matrix. If more high-load points were measured, the fitting line would be shifted to the right. In order to characterize the entire range of measurements, a procedure based on different weightings of the errors was applied.

The error that must be minimized by the fitting line is given by

$$err = (1 - w) \cdot |err_{<0}| + w \cdot err_{>0} \quad (33)$$

$err_{<0}$ is the sum of the negative errors and $err_{<0}$ is the sum of the positive errors. w is a weighting parameter.

By varying the weighting factor w from 0 to 1, a fitting closer to the less soot intensive data is found. Superimposing a series of fitting curves found by weighting differently the error (33), a representation of the most probable soot value for a given NOx concentration for each fuel can be found. For a given measurement matrix, that plot is characteristic of the used fuel.

In order to visualize how the alternative fuels behave compared to the reference diesel, the values referring to diesel are subtracted to the soot probability values of the alternative fuel and the results are shown in Figure 39 and Figure 40. Areas with negative values means that diesel is more likely to emit soot with that concentration than the alternative fuel. The differences are of course more evident when comparing diesel and the neat paraffinic fuels. A zone showing positive values between 2 and 5.5 g/kWh NOx can be observed while a negative area that follows the soot-NOx trade-off starting at soot values of around 0.1g/kWh and raises for NOx values lower than 2g/kWh is present. This means that in the case of GTL and HVO, the trade-off is shifted towards lower soot values.

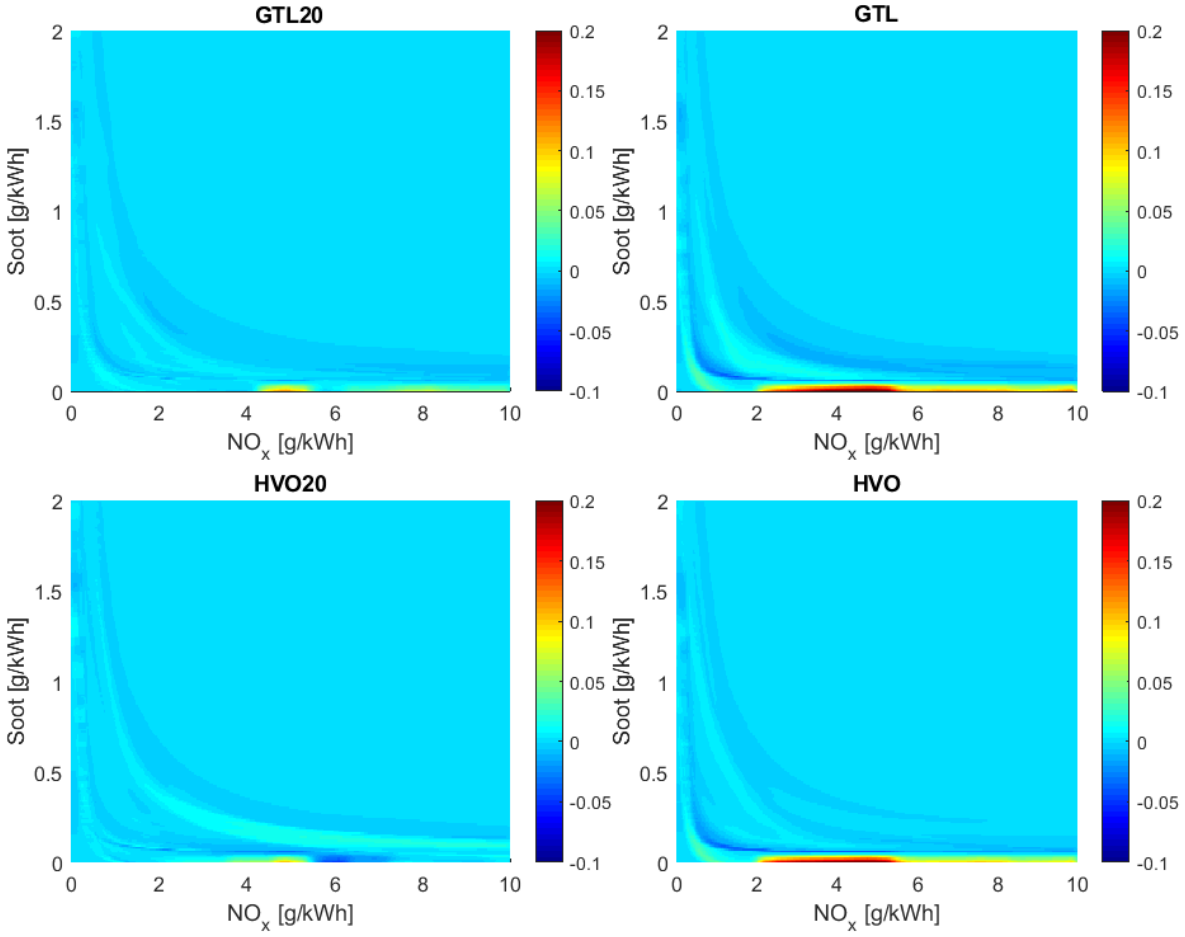

Figure 39: Most probable soot values for given NOx emissions of diesel subtracted to the values for GTL20, GTL, HVO20, and HVO.

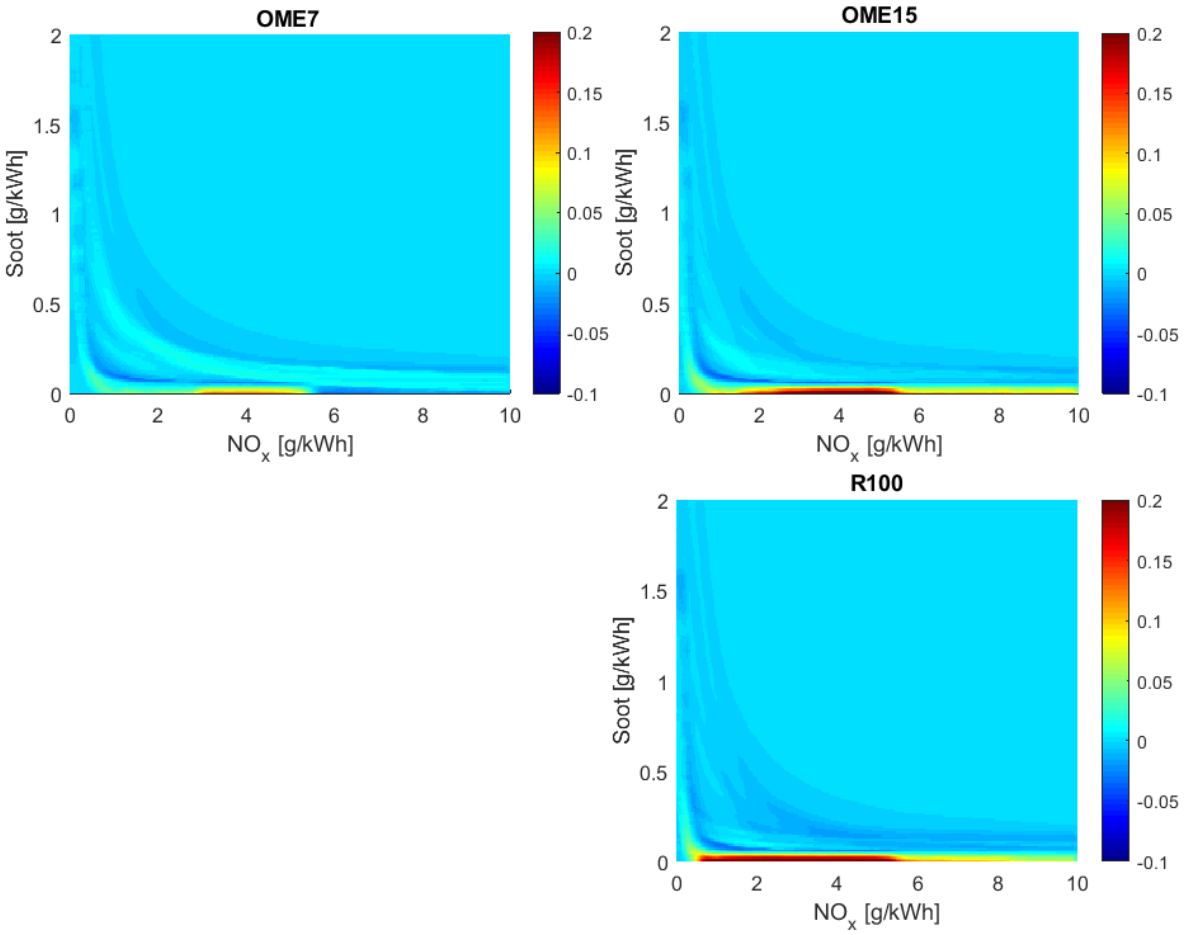

Figure 40: Most probable soot values for given NOx emissions of diesel subtracted to the values for OME7, OME15, and R100.

The soot reduction when switching from diesel to the oxygenated blends is evident, especially at intermediate EGR values, that is between 2 and 5.5 g/kWh. The effectiveness of R100 in reducing the particulate mass is clearly higher than the one of OME15. The positive area of R100 extends from 0.5 g/kWh NOx up to 5.5, while the one of OME15 is more limited. In general, however, all the OME based blends show a certain improvement of the trade-off (reads, either less soot or less NOx). This becomes more evident the higher the fraction of OME in the blend.
From the images, it is difficult to spot the differences between GTL and HVO or GTL20 and HVO20. For this reason, the same pictures as the ones in Figure 39 are shown again in Figure 41 but this time subtracting the values for GTL and GTL20 to the ones of HVO and HVO20, respectively. Positive values indicate zones where the soot-NOx emissions of HVO/HVO20 are more likely to be found compared to the ones of GTL/GTL20. Especially the comparison between HVO20 and GTL20 on the left side of the picture shows that the GTL20 has a better trade-off (reads lower combined soot-NOx emissions) compared to HVO20. The same observation can be done also for the comparison HVO/GTL but there the differences are not so pronounced.

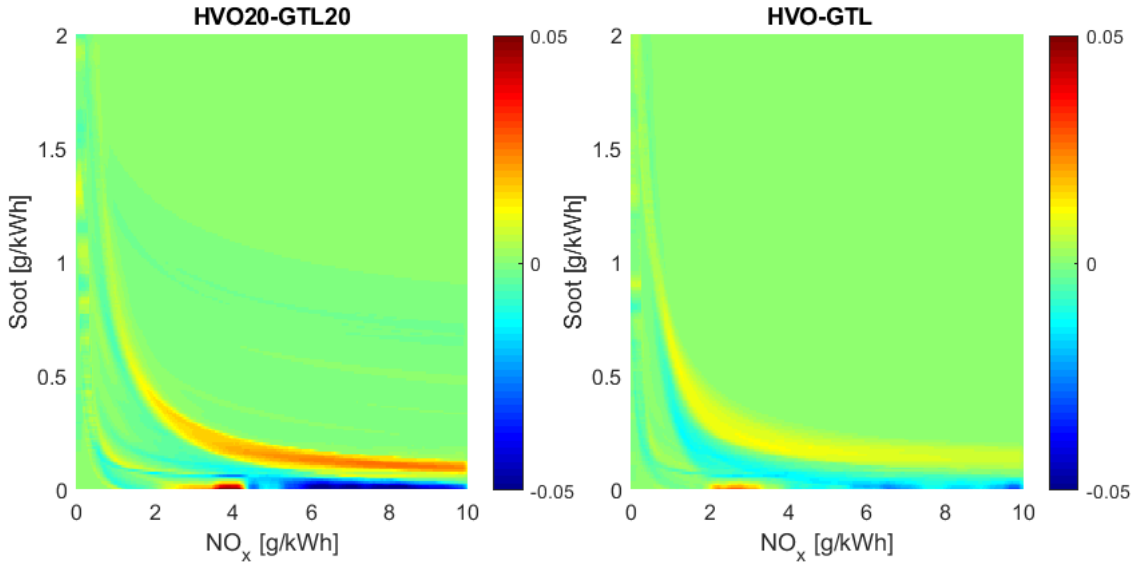

Figure 41: Most probable soot values for given NOx emissions of GTL20 subtracted to the values for HVO20 (left), and GTL subtracted to HVO (right).

b. Exhaust oxygen concentration

The concentration of oxygen in the exhaust is also a fuel dependent parameter. Not only different stoichiometric air-to-fuel ratios can lead to different rest oxygen, but also a different fuel density.
Of course, also the intake oxygen concentration modifies the amount of oxygen that can still be found in the exhaust, as Figure 42 shows. At constant load, the oxygen consumption remains unchanged; therefore, the decreasing O_2 concentration in the exhaust is a consequence of its dilution through the recirculation of exhaust gas. Diesel, HVO, HVO20, and GTL show the lowest exhaust oxygen concentrations. This observation agrees with the stoichiometric air-to-fuel ratio of the fuels. Adding oxygen content to the fuel leads to a reduction of the oxygen needed to oxidize the injected mass. This is what happens with OME7, OME15, and R100. The effect, however, is only visible for OME15 and R100. The behaviour of GTL20 is hard to explain but may be due to the fact that the changes due to the EGR are so important that the differences between fuels appear small.

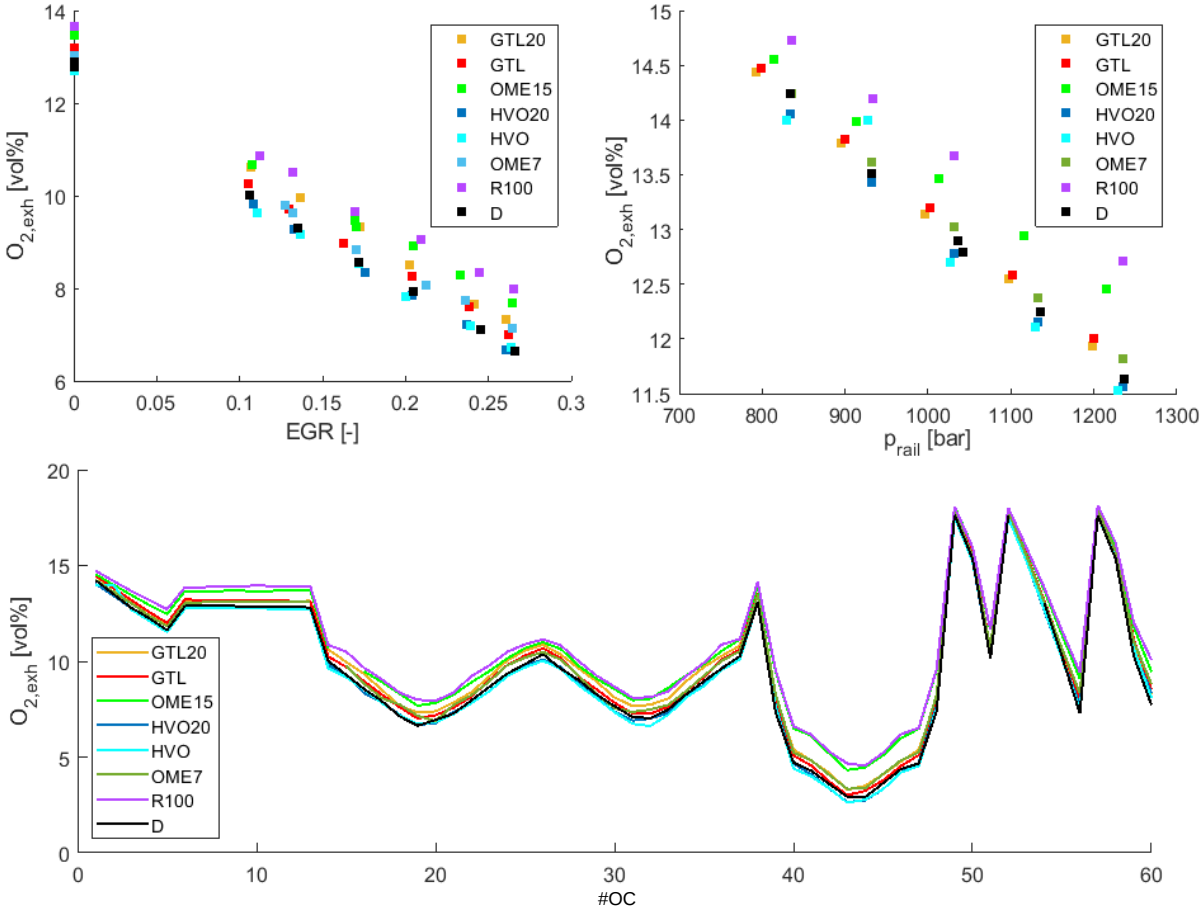

Figure 42: Exhaust oxygen concentration in the exhaust for all the fuel for a variation of EGR (top left) and fuel pressure (top right) around the reference condition. The exhaust oxygen concentration of the complete measurement matrix is shown below.

Looking at fuel pressure variation it can be seen that the statements made for the EGR variation hold true also in the case of a fuel pressure variation. The oxygenated blends show the highest oxygen concentration in the exhaust while the paraffinic fuels, diesel, and the blends between them consume more oxygen and reduce its concentration accordingly. The increase of the fuel pressure at constant DOI, corresponds to an increase of injected mass and therefore of the oxygen need. This can be seen in the exhaust oxygen concentration that sinks with increasing injection pressure.
The trends observed above hold true also for the rest of the measurement matrix.

3.2 WP2: Fuel identification/“fingerprint” (LAV)

Both the model for the exhaust gas temperature and the system of equation for the stoichiometric air-to-fuel ratio are calibrated or tailored for conventional diesel. This means that the output of the models for other fuels must not necessarily be physically meaningful but be instead an indication of existing differences between diesel and the alternative compounds. Therefore, the goal of the tools presented before is to compare the prediction based on the diesel characteristics with the measurements and, depending on the differences between these two values, try to extrapolate information about the fuel being used.
For the reason explained above, in Figure 43 the relative deviation of the modelled exhaust gas temperatures from the measured ones are reported. Being calculated as

$$dT_{out} = \frac{T_{out,mod} - T_{out,meas}}{T_{out,meas}}$$

(34)

a positive deviation indicates that the model over predicts the exhaust gas temperature. As expected, in the case of oxygenated blends the values given for the model are clearly higher than the actual ones. This is due to the smaller LHV of those blends compared to diesel. Moreover, the oxygen content, by reducing the stoichiometric air-to-fuel ratio, increases the mixing rate leading to a sooner consumption of the injected fuel. This turns in lower temperatures at exhaust valve opening. Over the whole measurement matrix, the model over estimates the exhaust gas temperatures of OME7 by 3.9% on the average, the ones of OME15 by 10.3%, and by 13.0% the ones of R100.

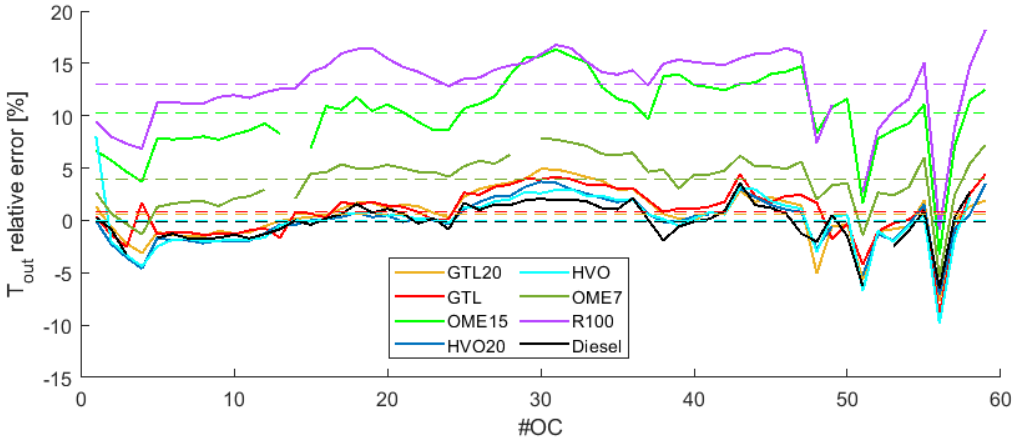

Figure 43: Solid lines: Relative deviation of the model predicted exhaust gas temperature from the measured one for all the fuels and all the operating conditions. Dashed lines: Mean of the solid lines.

The deviations of the values predicted for the paraffinic fuels and corresponding blends with respect to the measured exhaust gas temperatures are less pronounced. This finding was expected since, even though the density of HVO and GTL is smaller than the one of conventional diesel, the LHV is even minorly higher. Nevertheless, as seen in previously, there is a clear difference between the mixing rate of GTL and the one of diesel and HVO. The presence of GTL increases ν_{mix} compared to diesel, while HVO has almost no influence. Those characteristics can be seen also in the modelled exhaust gas temperatures. The model predictions are accurate for diesel, HVO20, and HVO, while they are too high for GTL and GTL20, with an over prediction of 0.88% and 0.65%, respectively. About the model, it is interesting to see that when load variations are performed via a variation of the injection duration (last 10 operating conditions to the right) the predictions become less precise.
Applying the calculation for the stoichiometric air-to-fuel ratio also to the fuels other than conventional diesel leads to the results displayed in Figure 44. It is worth reminding that for the calculation, the injected mass is estimated with a model calibrated for conventional diesel. For this reason, the obtained values for the stoichiometric air-to-fuel ratio of fuels other than diesel are not expected to be physically correct.

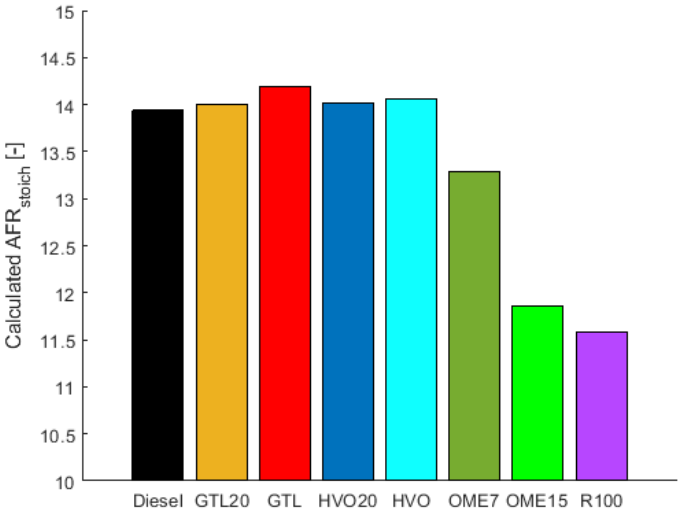

Figure 44: Stoichiometric air-to-fuel ratio (AFR) resulting from the back-calculation of the fuel composition starting from the intake and exhaust composition.

For diesel, a value of 13.94 is obtained. For GTL, due to the higher hydrogen-to-carbon ratio, a higher calculated AFR_{stoich} is expected. Indeed, for both GTL20 and neat GTL an increase of the calculated value can be observed. The results regarding HVO20 and neat HVO are analogous to the values obtained for the GTL. However, in the case of HVO the increase of calculated stoichiometric air-to-fuel ratio is smaller. This is due to the lower H/C ratio of HVO that lowers also the actual AFR_{stoich} compared to GTL. The presence of OME in OME7 and OME15 lowers the need of oxygen entrainment. This results in higher oxygen concentration in the exhaust and in turn in lower calculated stoichiometric air-to-fuel ratios. Compared to OME15, R100 has a minorly higher OME content and a definitely lower density because of the substitution of diesel with HVO. This explains the lower value of calculated AFR_{stoich} obtained.

As explained above, equation (20) is solved by using more than two measurements and obtaining an overdetermined system. In principle, as long as the measurements chosen do not refer to identical operating conditions, the system has one solution. However, if very similar operating conditions are used, e.g., a variation of SOI around a reference point, where the air mass flow rate and the injected fuel mass do not change the solution could suffer from strong uncertainties. The reason is that the uncertainty of the measurements of the air consumption could be (and usually is) bigger than the relative change in the exhaust oxygen concentration. Because of this, the measurements chosen for solving the system of equations should preferably be chosen so that they display an engine load/speed variation or an EGR rate change.

Another useful information from the exhaust species concentration can be gained looking at the nitrogen oxides and soot mass emitted by the engine and comparing them with a reference line fitting the soot-NOx trade-off of quasi-specific values referring to conventional diesel, as explained earlier. Different fuels have demonstrated to have differently shaped soot-NOx trade-offs.

Figure 45 shows the averaged difference between the quasi-specific NOx and soot emissions of the different fuels and the line fitting the soot-NOx trade-off of diesel at best. As reported previously, the alternative fuels tested lower the engine out soot levels compared to diesel. This behaviour is reflected in the value of the averaged difference between measured emissions and diesel fitting line; the fuels show deviations that are smaller than the one of diesel. In this context, a smaller deviation means that the points in the soot-NOx trade-off lie either closer to or below the fitting line. As expected, the fuels that can be recognized most easily are the one with a remarkable OME contend: OME15 and R100. The oxygenated compound reduces strongly the levels of particulate matter in the exhaust leading to big differences when compared to the behaviour of conventional diesel. Also neat HVO shows a distinguishing behaviour in the soot-NOx trade-off, the average difference with the diesel one is

remarkable. OME7, GTL show a similar shift with respect to the diesel fitting line. GTL20 and HVO20 manage to reduce its emissions mostly below the diesel levels.

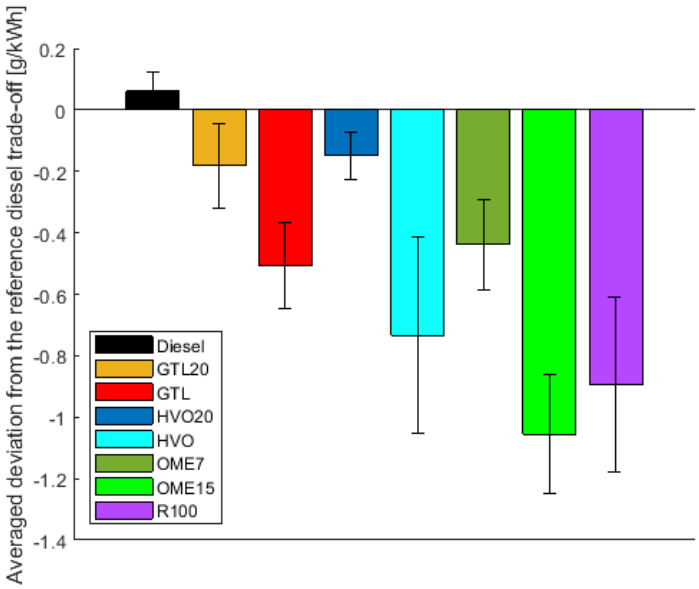

Figure 45: Averaged absolute distance between quasi-specific soot emission of the test fuels and the fitted trade-off line for diesel. The error bars refer to the standard deviation when only 50% of the operating conditions are randomly chosen 100 times.

The error bars reported in the graph show the standard deviation of the result in the case only the half of the available measurements is used. Those 30 operating conditions were chosen randomly 100 times. It is clear that with so few operating conditions this procedure could suffer from uncertainties. This does not mean that the method itself is weak rather than a bigger number of measurements would be necessary to yield a statistically reliable result.

Alone, the results shown above for the tools presented in earlier are not sufficient to recognize to which fuels the measurements refer. It can be seen that all the three indicators used (exhaust gas temperature, stoichiometric air-to-fuel ratio, and soot-NOx trade-off) are not conclusive regarding the differences between HVO and GTL and the corresponding blends since the direction of their reaction to the presence of paraffinic fuel is the same, only the magnitude of that reaction is different. This does not mean that the indicators are not usable for the purpose of fuel recognition but that a well-calibrated algorithm that is able to combine and interpret al the three of them is necessary. This could be a trained decision tree but the development of such a method goes beyond the goals of the present work. Nevertheless, some qualitative statements about the values assumed by the three tools presented above for the different fuels tested can be made.

According to its lowest energy content and the high mixing frequency, the fully renewable R100 shows the lowest exhaust gas temperature and therefore the highest error compared to the exhaust gas temperature model among the test fuels. OME15 behaves similarly but the calculation of the stoichiometric air-to-fuel ratio yields lower values for R100 than for OME15, making possible to distinguish the two fuels. In addition, also the soot-NOx trade-off of the two fuels differ minorly. The calculated AFR_{stoich} of OME7 is lower than the one of non-oxygenated fuels. Moreover, also the soot-NOx trade off and the exhaust gas temperature, reveal the presence of OME. HVO can be distinguished from HVO 20 mainly based on the differences in the soot-NOx trade-off. In turn, it is not possible to distinguish the exhaust gas temperature of HVO20 from the one of HVO and diesel. HVO20 compared to GTL20 shows a smaller deviation of the measured exhaust gas temperature from the modelled one due to the different mixing frequency. Moreover, also the soot-NOx trade-off of HVO20 is minorly improved compared to GTL20. The calculated stoichiometric air-to-fuel ratio do not show remarkable differences between the two fuels. GTL compared to diesel has minorly lower exhaust gas temperatures but the differences are small. In turn, the soot and NOx emissions are able to reveal the presence of

GTL. The method used to calculate the stoichiometric air-to-fuel ratio from the exhaust oxygen concentration is able to capture the increased hydrogen-to-carbon ratio of GTL but again the differences with respect to the values calculated for diesel are small.
Figure 46 sums up all these observations in a spider plot displaying a fingerprint of each fuel. The fingerprint of diesel is superimposed to the one of the alternative compounds for comparison.

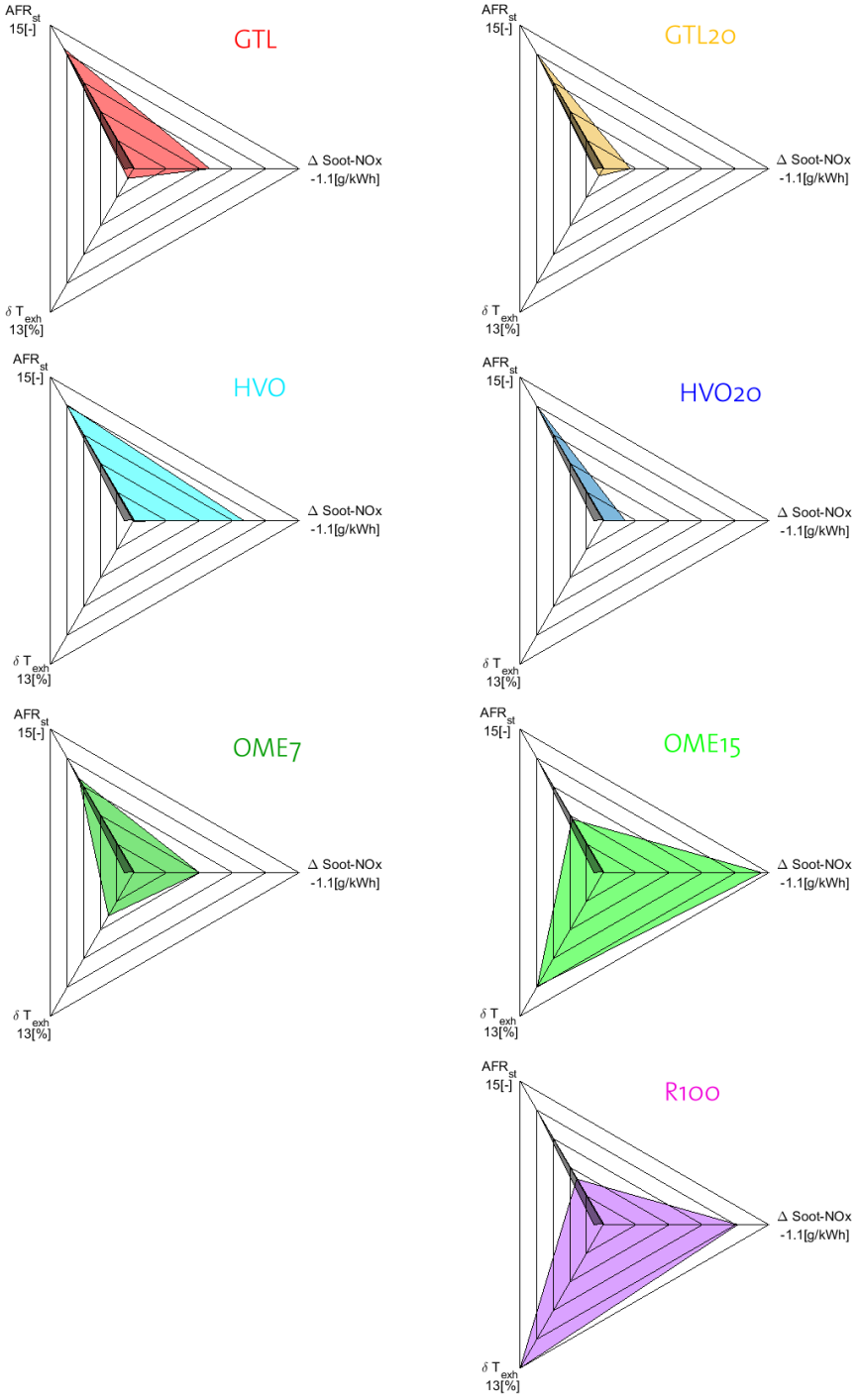

Figure 46: Graphical representation of the fingerprint obtained with the tools presented above for the six alternative fuels compared to the one of diesel (in grey).

3.3 WP3: Energy requirement of exhaust aftertreatment (EMPA)

This section presents the analysis and results of WP3, for the analysis of the heat demand needed for proper regeneration of particle filters. In the following 5 sub-sections, the influence of the soot origin, to specify the used fuel, on the regeneration energy is elaborated. Sub-section two focuses on the influence of the soot particle size on the activation energy, by concentrating on diesel fuel. In addition, an overview on the activation time, influenced by the regeneration temperature is given for diesel soot particles. The heat demand for the real-world regeneration of DPFs is evaluated afterwards. With results from literature, concerning the activation energy of soot from different fuels, the current findings can be classified. At last, a found correlation between the activation energy and pre-exponential factor is shown.

3.3.1 Activation energy related to the soot origin and particle size

The energy demand for the regeneration of PFs can be described by the activation energy. To evaluate the influence of origin and particle size of the soot separately, the experiments and results can be divided into two groups. The first group consists of samples with diesel soot, soot from HVO, and OME 7 fuel. The samples were loaded with a mean particle size in the range of 133 to 150 nm. The second sample group was loaded using diesel fuel with different particle size modes (Diesel fine, Diesel 5n/1f, Diesel 1n/5f) having a dominant mode with a mean particle size of 135 to 145 nm and a mode with a varying proportion of finer particles from 64 to 73 nm (mean).
Figure 47 shows the pre-exponential factor A and the activation Energy E_A for regeneration of PF samples with different fuels and loading modes. The respective coefficient of determination (R^2) is indicated above the blue bars, while the absolute numbers are included in the bars. The comparison of the activation energy of the first group with larger particles shows the highest value for OME 7 with 152 kJ/mol, followed by diesel (137 kJ/mol) and a much lower activation energy for HVO (85 kJ/mol). The samples of the second group using diesel fuel and different particle forming modes, that result in a smaller mean particle size, have also low activation energies, in the range of 83 to 103 kJ/mol (Diesel fine: 103 kJ/mol, Diesel 5n/1f: 83 kJ/mol, and Diesel 1n/5f: 95 kJ/mol).

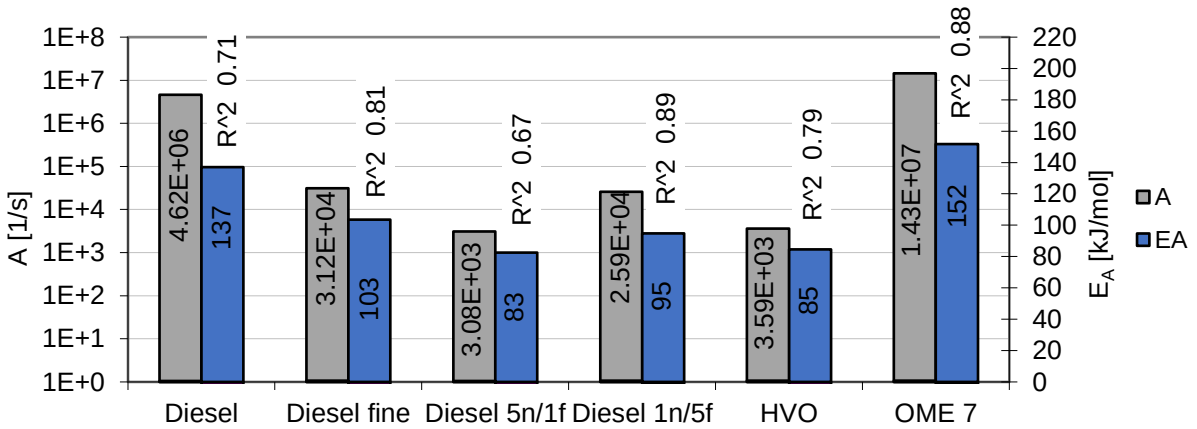

Figure 47: Activation energy in kJ/mol (blue bars) and the pre-exponential factor in 1/s (purple bars) of the measured soot types. In addition, the coefficient of determination R^2 is given for each data pair.

The correlating factor A has the same behavior, regarding soot origin and particle size. The influence of the particle size is shown in detail in Figure 48. The activation energy has a positive dependence on the amount of finer diesel soot particles. With this, the samples with a higher share of small particles had the highest activation energy of the fine diesel soot samples. The mixture with the lowest content of finer particles has a similarly low activation energy value as the soot particles formed by HVO.

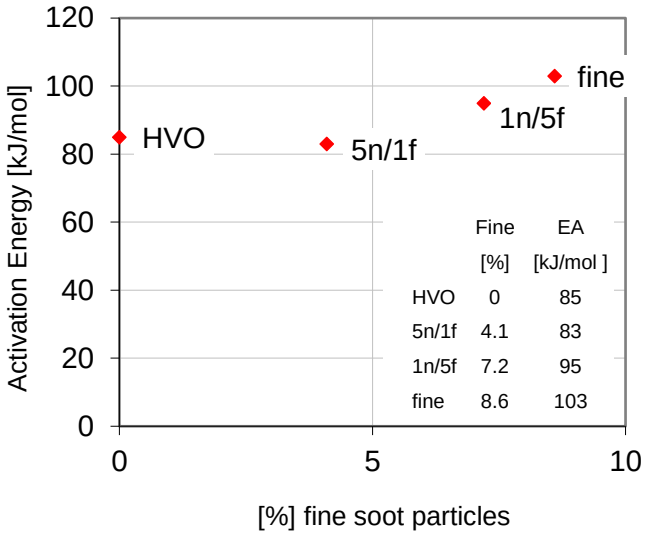

Figure 48: Activation energies of diesel soot mixtures with different contents of finer soot particles in comparison to HVO soot particles.

3.3.2 DPF regeneration temperature and time in relation to the used fuel

The activation energies and pre-exponential factors of different fuels were determined with a pure Arrhenius model, which is also suitable to estimate the regeneration time and the energies required for the complete regeneration of a truck DPF.
Figure 49 shows the burn up time dependent residual soot mass in the filter for different regeneration temperatures for diesel soot. A higher regeneration temperature shortens the regeneration time considerably as the burn up rate is inversely correlated to the regeneration temperature. Figure 50 shows the residual soot of samples loaded with different diesel particle size modes in respect to the regeneration time at 600 °C.

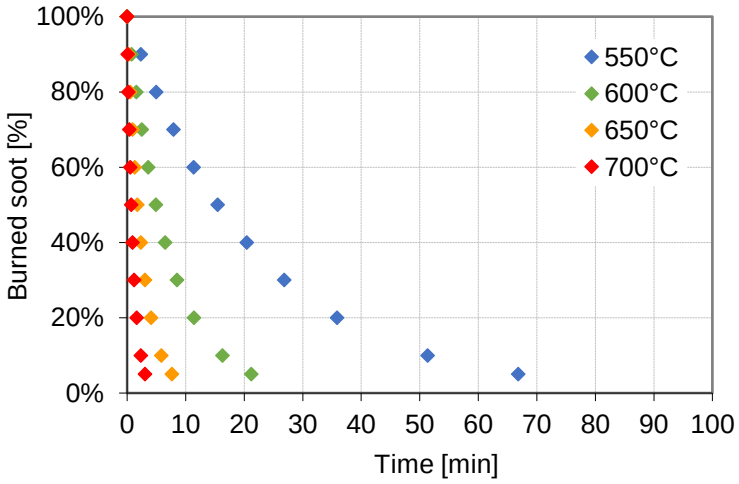

Figure 49: Residual soot mass in the filter, dependent on the burn up time for different regeneration temperatures.

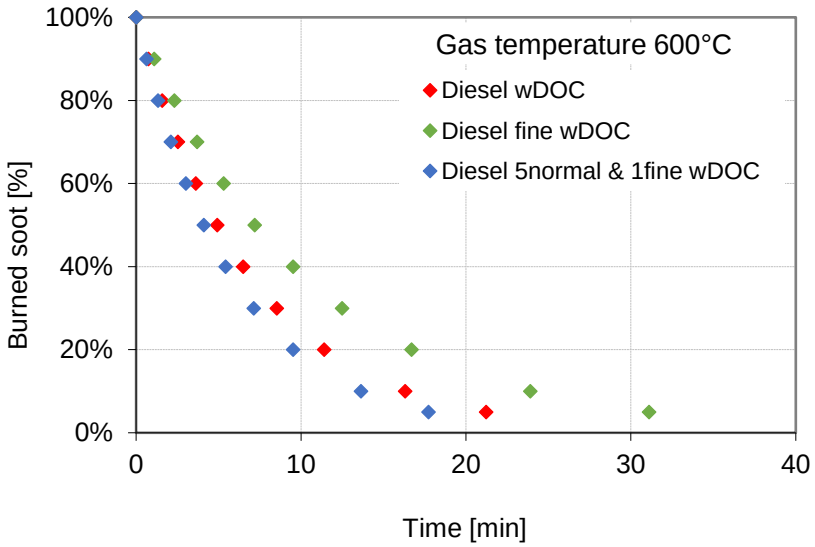

Figure 50: Residual soot mass in the filter, dependent on the burn up time at 600 °C for different diesel particle size loading modes.

The regeneration of different diesel PF, burning off soot, that was formed with different particle size mixtures, shows a slightly shorter regeneration time for diesel soot mixed with a small amount of fine diesel soot particles than for normal diesel soot. In contrast, the sample with a larger share of fine soot particles requires a significantly longer regeneration time.

3.3.3 Operational energy demand for active regeneration

The activation energies of the samples lead to an evaluation of the total energy demand for a real world PF regeneration, relying on the given equations in chapter 2.3.2. Figure 51 shows the calculated regeneration energy needed for PFs, loaded under different conditions, with an exhaust gas temperature of 600 °C. The expected regeneration time is given in addition.

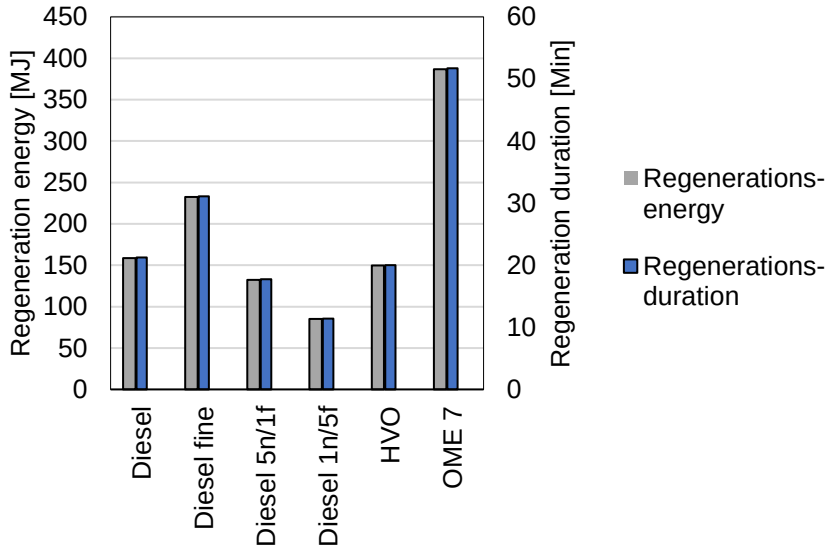

Figure 51: Real-world regeneration energy demand and regeneration time of PFs using different fuels and different engine set-points, with a regeneration temperature of 600 °C.

3.3.4 Literature comparison on activation energy

The resulting values for the activation energy for different fuel types can be compared to other literature. Figure 52 shows the activation energy for soot originating from different fuel types and engine modes found in this study and results of Bhardwaj et al. and Karin et al., also including RME and palm-olein as fuels [17-19]. For the particle size evaluation, there are no directly comparable results in literature. In addition, OME 7 is not mentioned as a fuel in current literature regarding the regeneration of PFs. For Diesel, the found values are in the same range as presented in this study. The activation energy for HVO soot differs. The lack of results concerning this topic, shows the need for further investigations with a broad palette of fuels.

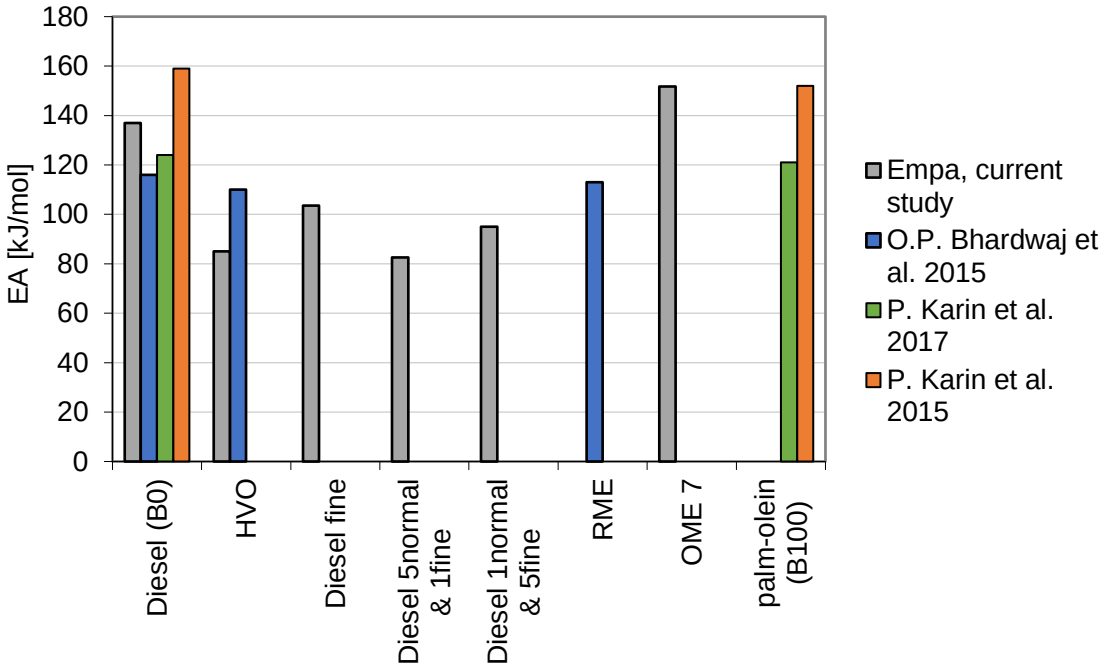

Figure 52: Activation energy for soot origination from different fuels and operation modes of the current study in comparison with other literature concerning this topic [17-19].

3.3.5 Correlation between activation energy and pre-exponential factor

Interestingly, the activation energy and the pre-exponential factor A have a correlation, which could be examined using the gathered data. Figure 53 shows the dependence of the pre-exponential factor on the activation energy of all tested soot types. A is therefore correlated to the activation energy with:

$$A = 0.0462 \cdot e^{0.1329} \cdot E_A \quad (35)$$

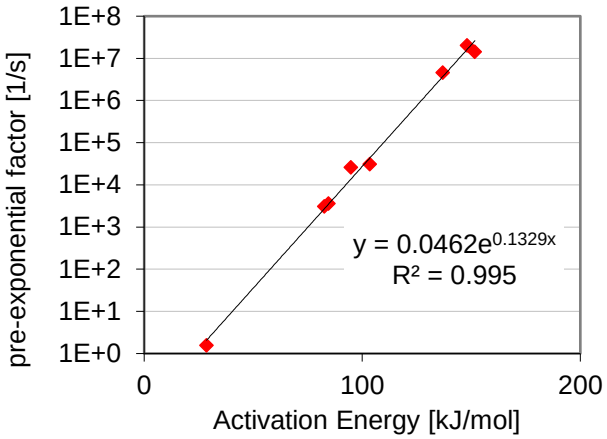

Figure 53: Pre-exponential factors correlating to the corresponding activation energies of the tested soot types.

3.4 WP4: Platform for Virtual Sensors (Vir2sense)

This section presents the consolidated results from WP4, on the development of fast predictive combustion and emission models using different fuels. The section is divided into 5 sub-sections, containing the results of the senstitivity analysis of the automatic HRR analysis code, the observed changes in HRR based on the automatic analysis, the results of the HRR modelling and finally the results of the NOx and soot emission models for the different fuels.

3.4.1 Sensitivity of assumptions for mixing rate analysis

As a first part of the investigation into different combustion characteristics of the different fuels tested, a sensitivity analysis of the effects of assumptions for the measurement evaluation on the analysis results was conducted. This sensitivity analysis focused on the effect of injection rate modelling assumptions on the resulting assessment of characteristic mixing rate. In detail, three assumption groups were distinguished:

c. Distinction between premixed and diffusion portions

The distribution of fuel between premixed and diffusion combustion is important for the computation of the characteristic mixing rate due to its effect on the start of the increase of mixing rate, which coincides with the start of diffusion combustion. This distribution was determined using a modeled availability of fuel for combustion at the point of ignition. Assumptions concerning the mixing and evaporation of the fuel were used to estimate the amount of fuel available for combustion at the point of ignition, and the premixed fuel amount was fitted into the measured HRR curve. The resulting amount of premixed combustion is shown exemplarily for a high load operating point in Figure 54. Without the information of the fuel availability at ignition, the automatic premixed combustion curve fitting results in an overestimation of the premixed combustion amount (left plot, yellow curve), and thus a very late start of diffusion combustion (light blue curve); the premixed combustion amount in this erroneous case is 596% of the fuel available at ignition. When the fuel availability is taken into account (right plot), then the premixed combustion amount is below the fuel injected amount at ignition.

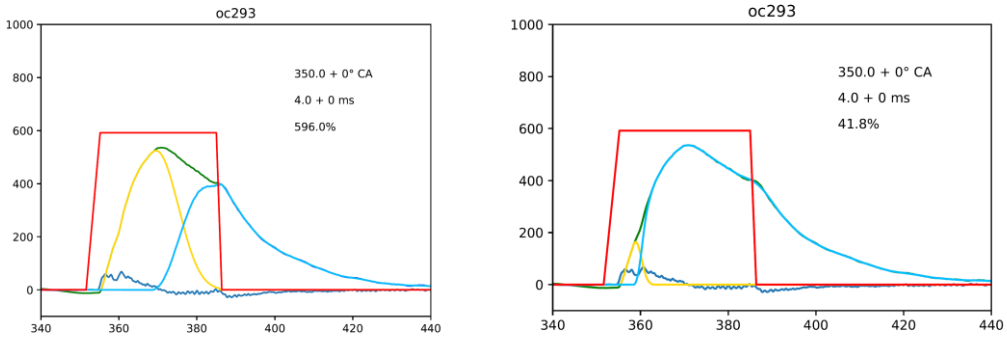

Figure 54: Fit of estimated premixed combustion curve (yellow) into the measured HRR (green) without (left) and with (right) taking into account the fuel availability at ignition

d. Fuel combustion completeness

Due to the nature of the mixing rate calculation, which relates the fuel availability to the instantaneous combustion rate, the mixing rate is sensitive to the final proportion of combusted fuel. For higher combusted proportions, the fuel availability at the latter stages of combustion becomes low, resulting in high calculated mixing rates. This variation is depicted in the left plot of Figure 55, which shows the calculated mixing rate curves for increasing fuel combustion portions. The relative change of the calculated maximum mixing rate is depicted in the right plot of Figure 55 for different combustion proportions. A combustion proportion of 95% was used throughout this investigation, to allow direct comparison of the different operating conditions and fuels used.

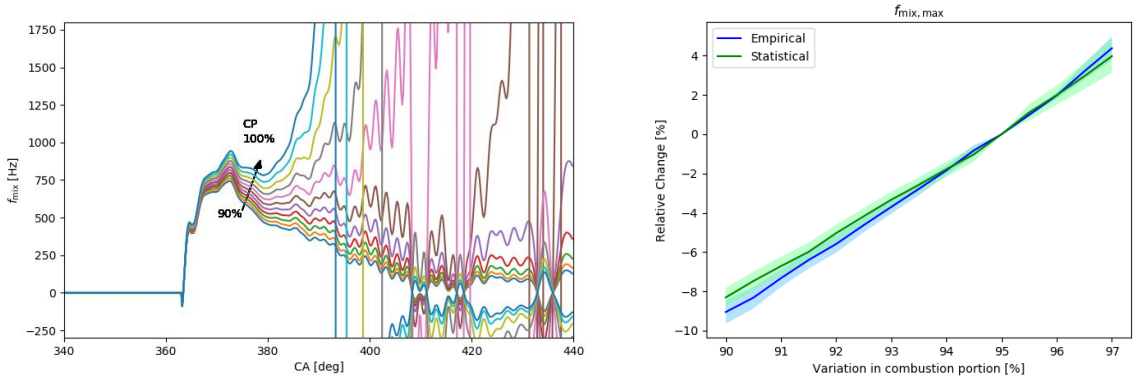

Figure 55: Calculated characteristic mixing rate with varying proportion of fuel combusted (left) and sensitivity of maximum characteristic mixing rate from the assumed combusted proportion (right).

e. Injection parameters

Two injection parameter factors affect the calculated characteristic mixing rate:

i. Sensitivity on estimated Start of Injection (SOI)

The estimated SOI is significant for the calculation of the mixing rate due to its effect on the fuel availability; delayed SOI results in lower fuel availability, resulting in higher f_{mix}. Figure 56 shows the variation of maximum f_{mix} as a result of a variation SOI. The assumed accuracy of estimated SOI is ±0.5CA, with any error being systematic and applicable to all points.

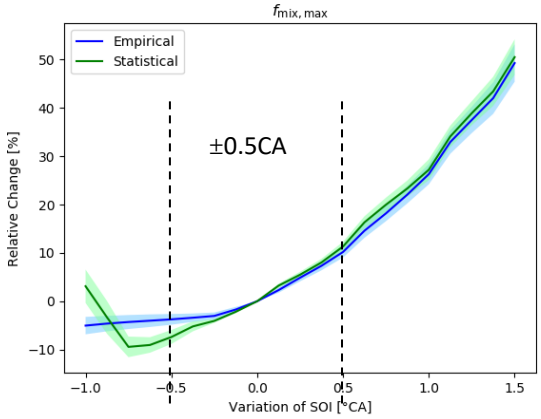

Figure 56: Sensitivity of maximum characteristic mixing rate from the variation of estimated start of injection.

ii. Sensitivity on estimated Duration of Injection (DOI)

Finally, the estimated DOI is also important for the calculation of the characteristic mixing rate. In the modelled injection rate, the DOI was estimated from the measured fuel injected mass, the injector tip characteristics and the injection pressure. Figure 57 shows the variation of maximum f_{mix} as a result of a variation DOI. Despite the strong dependency of the f_{mix} on large errors of DOI (>10%), the error of DOI estimation is expected to be <5%.

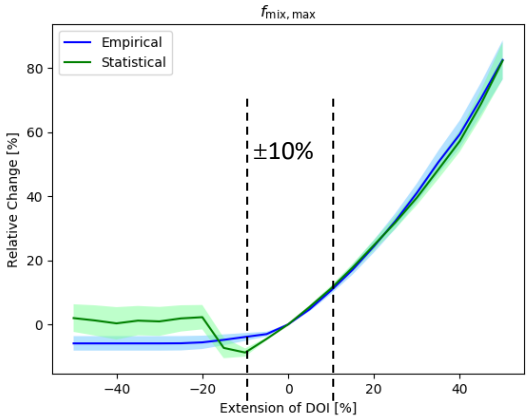

Figure 57: Sensitivity of maximum characteristic mixing rate from the variation of estimated duration of injection.

3.4.2 Changes in mixing rate locations with different fuels

The automatic HRR analysis tool was used in order to identify differences in combustion characteristics between the fuels tested within WP1. The comparison enabled the identification of characteristics of combustion which are subsequently used for the model development. The alternative fuels were compared to diesel for identical engine operating conditions, which allowed the direct comparison of the combustion characteristics. The comparison included both the level of maximum characteristic mixing rate, as well as the locations in time of the characteristic mixing rate points deduced from the analysis (shown in Figure 21).

Figure 58 shows the comparison for the maximum characteristic mixing rate (top, left), as well as the location of P1 (top, right), P2 (bottom, left) and P3 (bottom, right), for 36 different operating points with identical operating conditions for all fuels tested. The 45% line (quantity equal to diesel) is shown for reference in all plots. Only 3 fuels are presented in the analysis for conciseness; for reference, it was observed that neat HVO behaves similarly to GTL, 20% HVO behaves similarly to 20% GTL and OME

7% behaves similarly to OME15%, with less pronounced difference to diesel owing to the lower concentration of oxygenate.
From the plots it is clear that all fuels tested have a higher maximum characteristic mixing rate than diesel. Even a small addition of GTL to diesel (20%) leads to a higher $f_{mix,max}$ than diesel, while further addition of GTL does not seem to increase $f_{mix,max}$ significantly. The highest increase of $f_{mix,max}$ was observed for the mixture of 15% OME to diesel, with the highest proportional increases observed at low mixing rates. This indicates that the highest increase in mixing rates are at conditions where mixing or oxygen availability are low. This is the case when injection pressure is relatively low, and at high EGR rates; in both cases the alternative fuels and in particular the addition of an oxygenated fuel (OME) show a significant advantage in comparison to diesel.
Regarding the locations of the characteristic mixing rate points, the differences between fuels are not as clear. The location of P1 (start of diffusion combustion) closely follows the trend of ignition delay for the fuels, with OME being similar to diesel and higher proportions of GTL (which has a high cetane number) leading to earlier locations of P1. The location of P2 is most advanced for neat GTL, with an almost constant offset to diesel independent of location. OME15 does not show a difference to diesel, while GTL20 is slightly earlier than diesel. The location of P3 is the most varied, with no clear trend. P3 is most advanced for OME15, but this is only true for longer injection duration (where P3 is late in the cycle). This indicates that the advantage of OME15 in terms of combustion duration is mostly apparent when fuel amounts are high and correspondingly oxygen around the spray is limited.

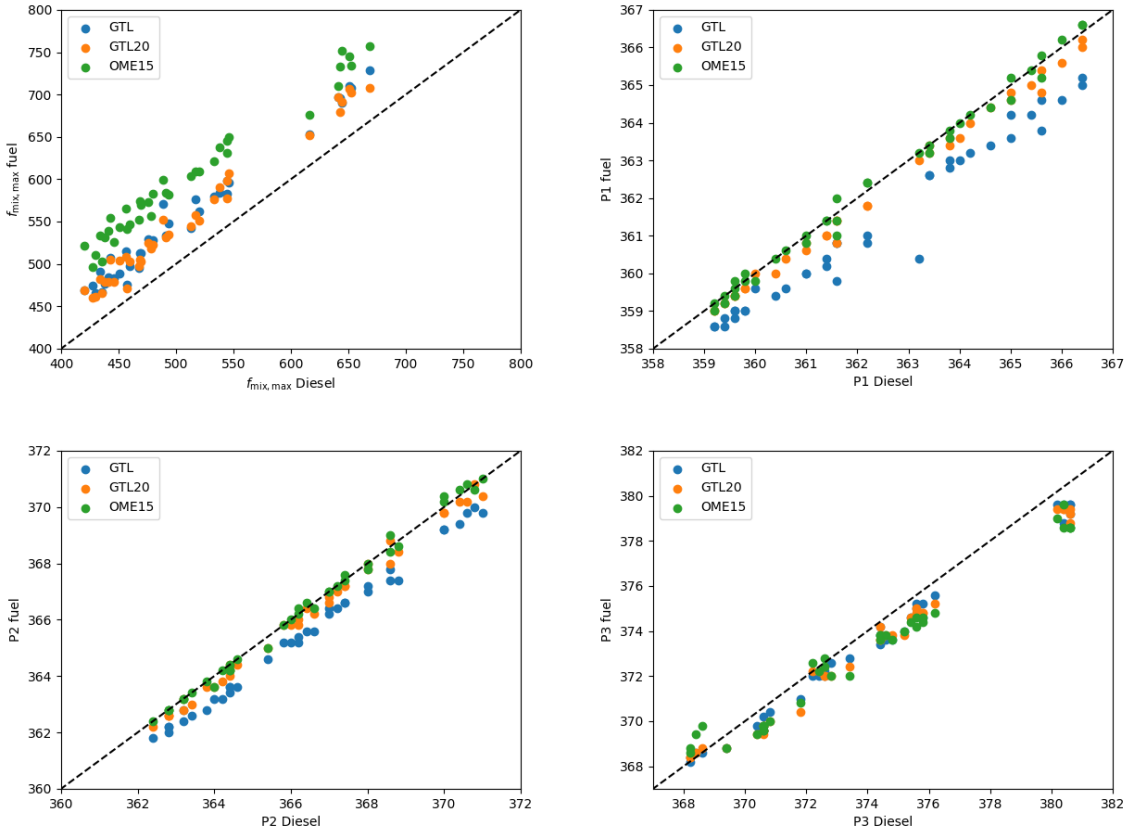

Figure 58: Comparison of maximum characteristic mixing rate and the location of characteristic mixing rate points for various fuels vs. diesel under identical engine operating conditions.

3.4.3 Results for HRR modelling for different fuels

As mentioned in section 2.4.2, the HRR models were tuned individually for the different fuels based on the combustion analysis, in order to reflect the combustion characteristics observed for each fuel. Following the calibration, each combustion model was tested using >60 operating points per fuel, including variations in engine speed (1000…1200rpm), duration of injection (1…3.3ms), start of injection (-14…-6 CA), injection pressure (800…1200bar) and charge oxygen content (EGR) (15…21%).
The observations arising from the measurement analysis presented above were used to identify the most important model parameter changes for different fuels. These model parameters were automatically fitted for each fuel, with the resulting fitted values used to decude the relationship between fuel composition (aromatic/paraffinic/oxygenate content) with the individual model parameters. In total it was identified that for the ID model 2 parameters changed significantly with different fuel characteristics, whereas 10 parameters were adapted for the HRR model. For each adapted parameter a linear or quadratic relationship was fitted to the results in order to capture the change parameter value as a function of any change in composition. The general observations which were depicted in the HRR model are the following:

- Increase in fuel reactivity for shorter ID when cetane number increases
- Adaptation of premixed portion to reflect fuel mixing/evaporation prior to ignition and LHV
- Adaptation of initial diffusion HRR increase based on mixing/stoichiometry
- Adaptation of late phase combustion

Three parameter fits for varying paraffinic (GTL or HVO) and oxygenate (OME) content are presented exemplarily in Figure 59.

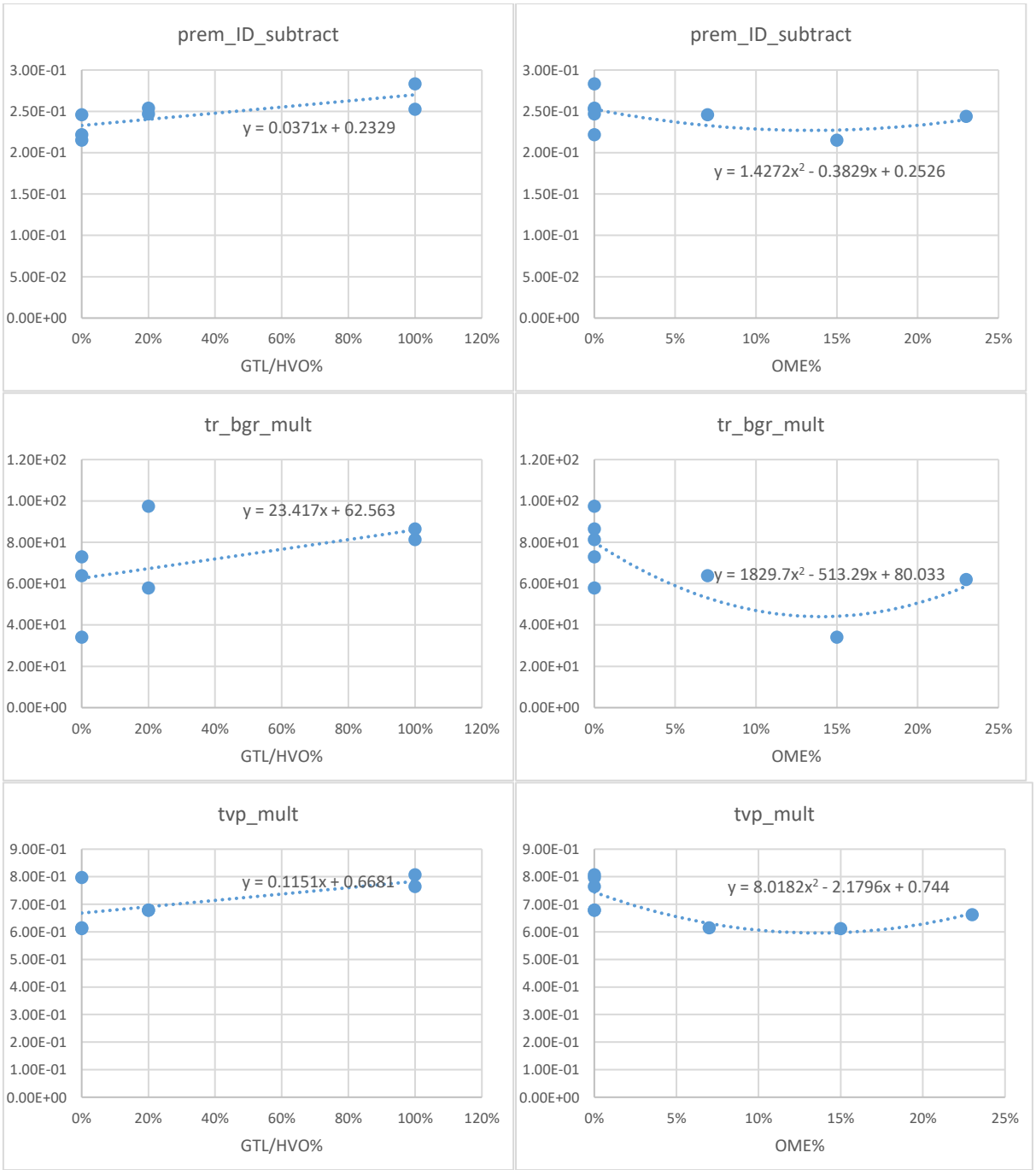

Figure 59: Variation of HRR model parameters with changing paraffinic (GTL or HVO) and oxygenate (OME) content, including fitted equations

Figure 60 shows the measured and simulated HRR and fraction of fuel burned for a specific operating condition for different fuels. The plots depict the small differences between the fuels which have been discussed previously, and show that the models using the fitted parameters capture all the combustion characteristics very well.

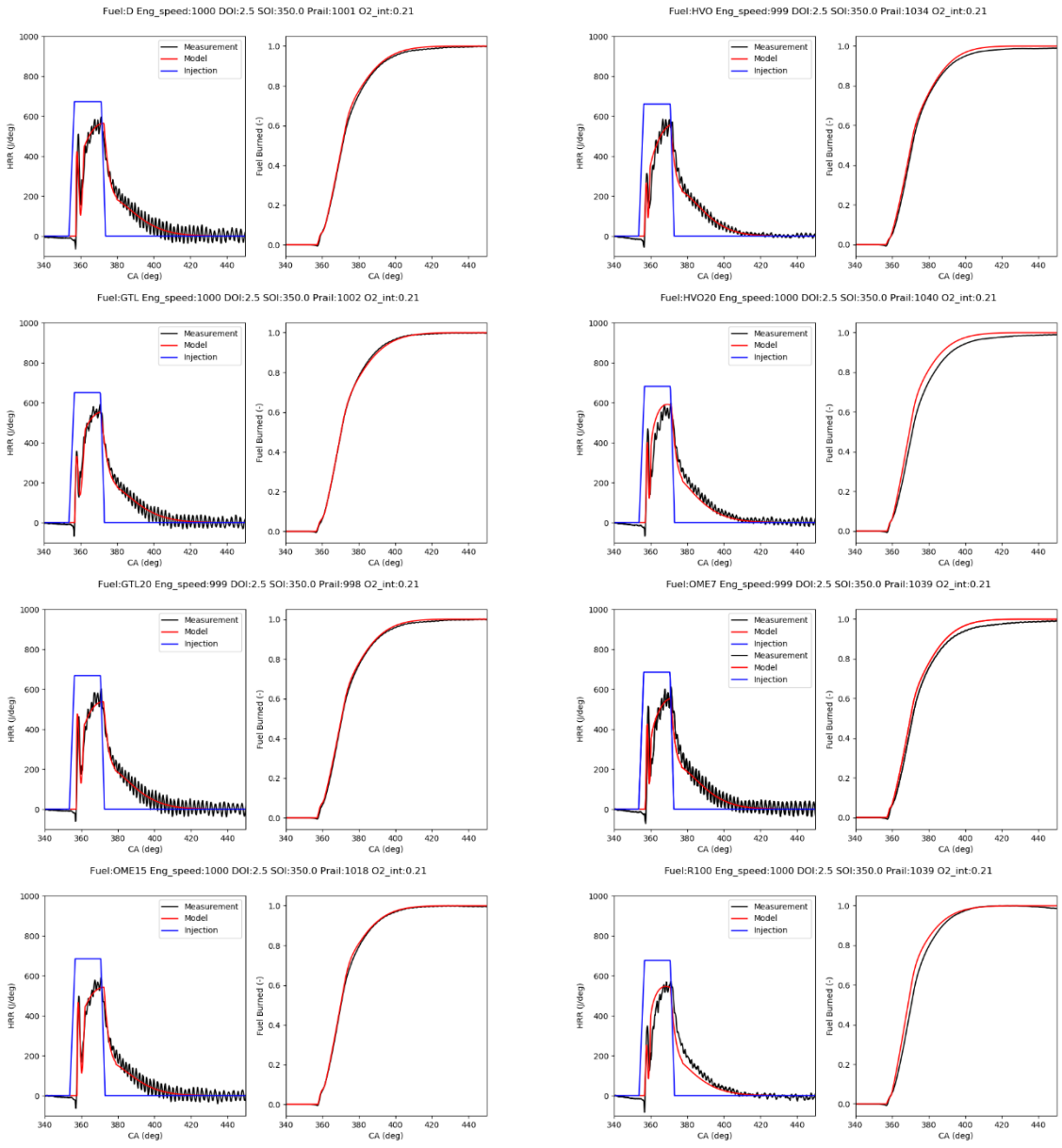

Figure 60: Measured and simulated HRR (left) and fraction of fuel burned (right) for 1000rpm, DOI=2.5ms, SOI=-10CA, P_{inj}=1000bar, $O_{2,int}$=21%, for Diesel, HVO, GTL, HVO20, GTL20, OME7, OME15 and R100

In order to compare all measured operating points simultaneously, it is useful to use the locations where a specific burned fuel fraction is achieved. Figure 61 shows the location of 5% (CA05), 10% (CA10), 50% (CA50) and 75% (CA75) of the fuel burned for diesel (blue), GTL (yellow), GTL20 (green) and OME15 (red). Equivalently, Figure 62 shows the same points for diesel (blue), OME7 (yellow), HVO (green), HVO20 (red) and R100 (purple).It is clear that, despite small differences in some points, the burned fuel locations are captured very accurately for all fuels. Larger errors are encountered in the CA05, due to high sensitivity on ID and small errors in its estimation for the very wide range of operating conditions tested. In addition, small errors are observed in CA 50 when at early locations, i.e. when injection duration is very short; this discrepancy can be partially attributed to the large uncertainties in fuel injection rates when injection durations are short. Finally discrepancies are observed in CA75 especially for HVO20. Nevertheless, the performance of the model considering the wide range of operating conditions and fuels used is considered exceptional.

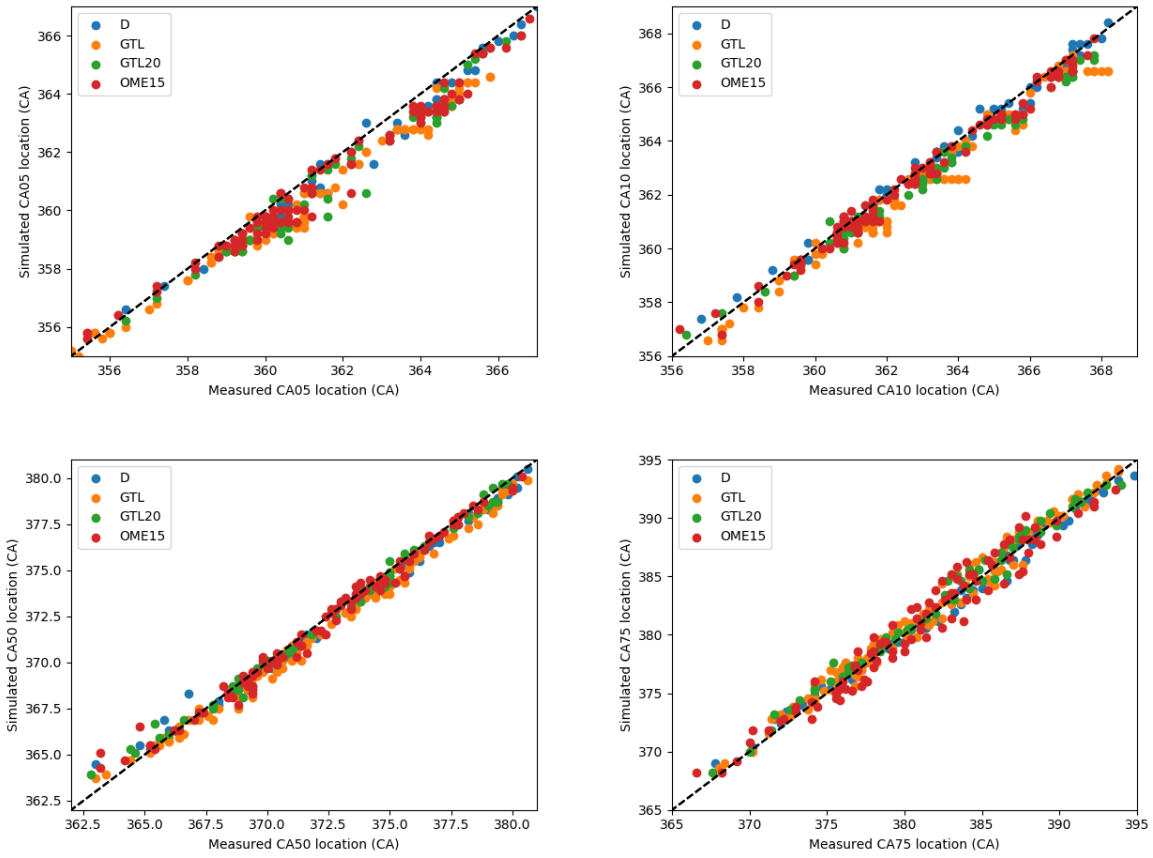

Figure 61: Simulated vs measured CA05 (top, left), CA10 (top, right), CA50 (bottom, left) and CA75 (bottom, right) for >60 operating points using diesel (blue), GTL (yellow), GTL20 (green) and OME15 (red)

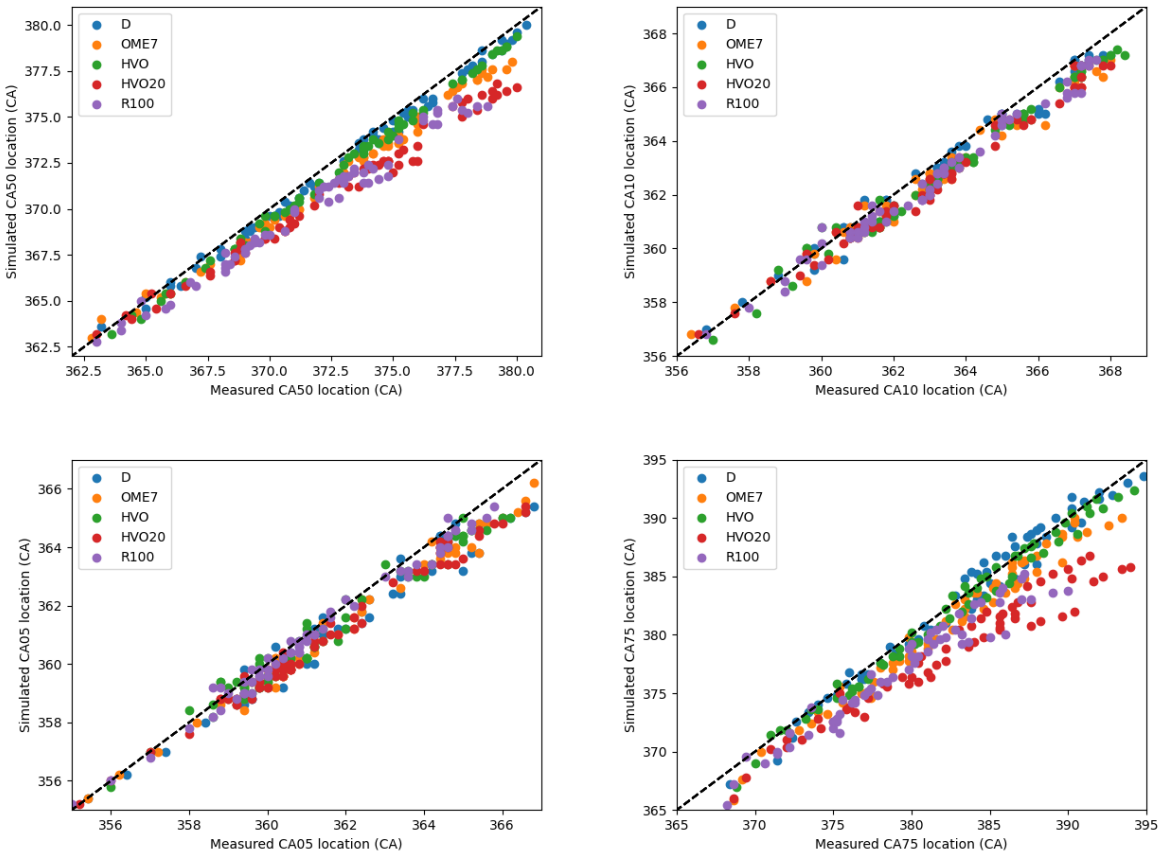

Figure 62: Simulated vs measured CA05 (top, left), CA10 (top, right), CA50 (bottom, left) and CA75 (bottom, right) for >60 operating points using diesel (blue), GTL (yellow), GTL20 (green) and OME15 (red)

3.4.4 Results for NOx emission modelling for different fuels

As described in section 2.4.3, the NOx model fitting process was conducted starting with diesel fuel, and then the model was tested on other fuels. The model fit for diesel fuel only compared to measured NOx concentration in the exhaust is shown in Figure 63.

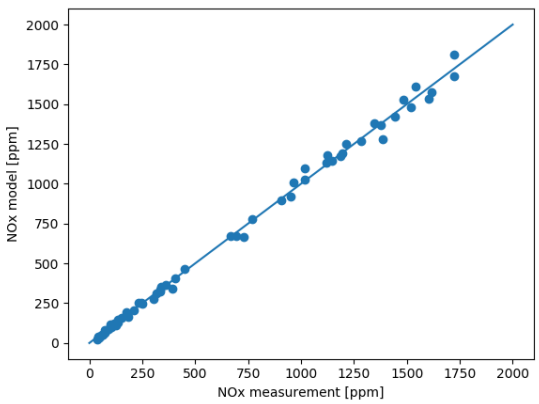

Figure 63: Fit of NOx model vs measured concentration for diesel fuel for varying operating conditions

The performance of the model with constant parameters for different fuels was also very good. This is attributed to the fact that only combustion phasing, which is inherently included in the combustion model, has an effect in the NOx emissions. In addition, the oxygen content of the fuel in the case of oxygenated fuels is included in the model by design. The result of the NOx prediction for different fuels is shown in

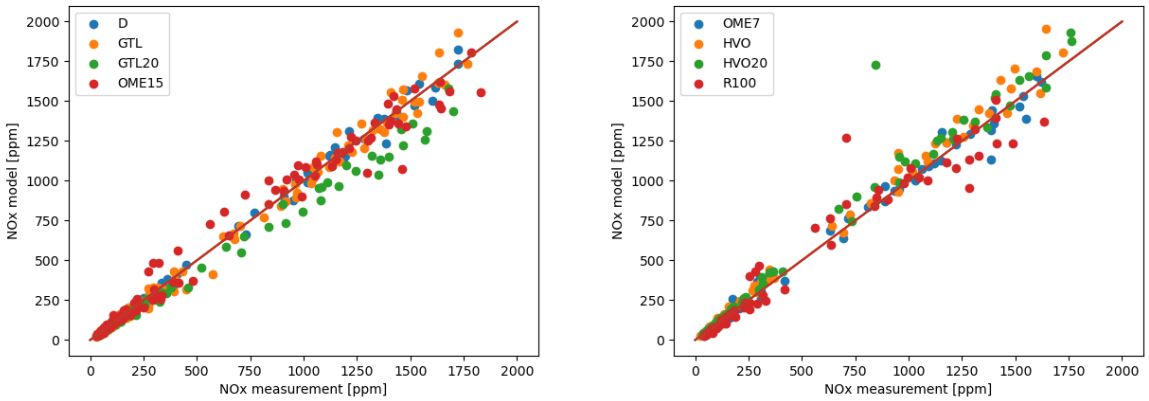

Figure 64: Fit of NOx model vs measured concentration for varying operating conditions for diesel, HVO, HVO20, R100, GTL, GTL20, OME7 and OME15

3.4.5 Results for soot emission modelling for different fuels

Contrary to NOx emissions, the performance of the soot model for different with constant model parameters tuned for diesel was not satisfactory. Nevertheless the emission predictions made with the model tuned for diesel do help to illustrate some differences in soot emissions between the fuels tested.

Figure 65 shows the correlation between measurement and model prediction for different fuels, split between increasing paraffinic (reduced aromatic) content (Diesel, HVO/GTL20, HVO/GTL) and increasing oxygenate content (Diesel, OME7, OM15, R100). From the plots it is shown that both increasing paraffinic and oxygenate content reduces the emissions for constant operating conditions, since the soot predicted by the model tuned with diesel fuel is significantly higher than with the other fuels.

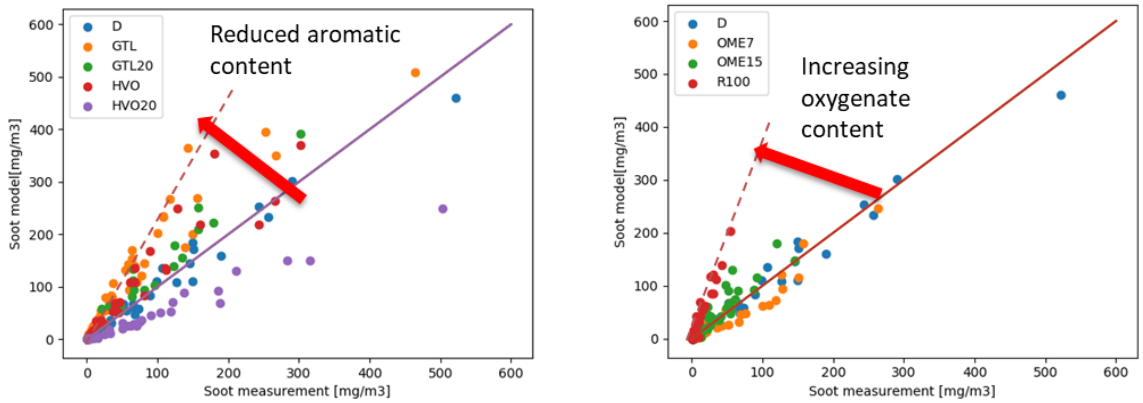

Figure 65: Correlation of predicted and measured soot concentration using the soot model with parameters fitted for diesel, for all fuels and operating conditions tested. The plots are split between variation in paraffinic content (left) and oxygenate content (right)

Using this observation, the soot production and oxidation parameters of the model were fitted automatically to the different fuels. The optimization results showed the following:

- The production term decreases linearly with increasing paraffinic content (decreasing aromatic content)
- The oxidation term increases quadratically with increasing oxygenate content, then oxygenate content exceeds a certain value

Using the soot model parameters as a function of fuel composition, the predictive capability of the model for all fuels is very good despite the very wide range of conditions tested and the wide spread in soot concentration. The correlation between the final soot model and measurements for all fuels is shown in Figure 66. The errors relative to the range of soot emissions and the difference between the fuels are very low.

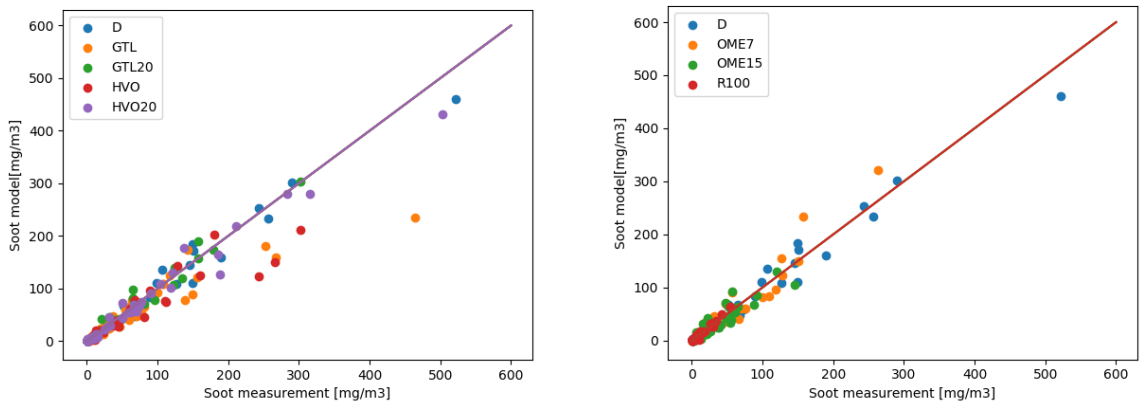

Figure 66: Correlation of predicted and measured soot concentration using the soot model with parameters varying depending on fuel composition, for all fuels and operating conditions tested. The plots are split between variation in paraffinic content (left) and oxygenate content (right)

3.5 WP5: Virtual Sensors in GT-Power (Combustion and Flow Solutions)

3.5.1 MTU base model

A selection of 31 operating points of the available measurement data served for validation of the model with Diesel as the reference fuel. Variations include start of injection, load, oxygen content of the intake charge (dilution) and intake temperature. The chosen operating conditions and their variations for validation ensure the model's capability to account for different fuel masses, system temperatures and reactivities.

Figure 67 shows a comparison of calculated versus measured indicated mean effective pressure values (IMEP) over 12 operating points, with 3 different loads (rising IMEP) and a variation in start of injection (within each load step, from -16 °CA bTDC to -6 °CA bTDC). Good agreement is reached between experiment and simulation, with a small underprediction for low loads and overprediction for higher loads.

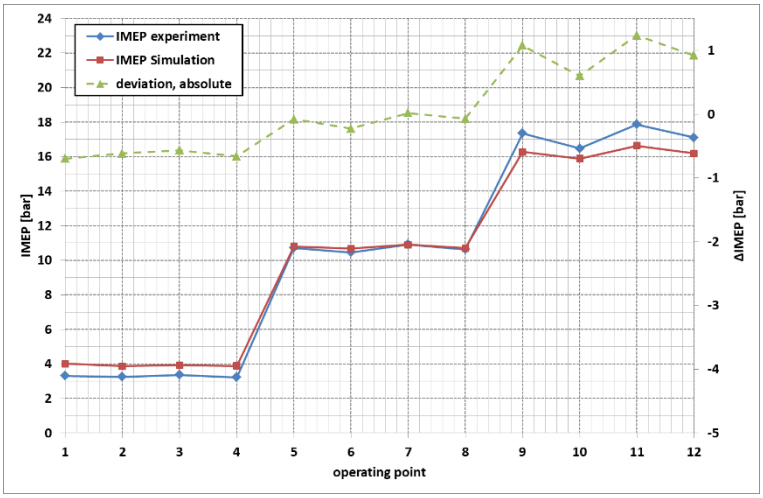

Figure 67: comparison of experimental versus calculated values of IMEP for 12 operating points (variation of start of injection and load)

Figure 68 shows a comparison of calculated versus measured pumping mean effective pressure values (PMEP) over the 12 operating points. The comparison shows good agreement with respect to general trends captured while a difference of 0.2 bar over all operating points is observed which can be attributed to common uncertainties in in-cylinder pressure measurements during pumping cycles.

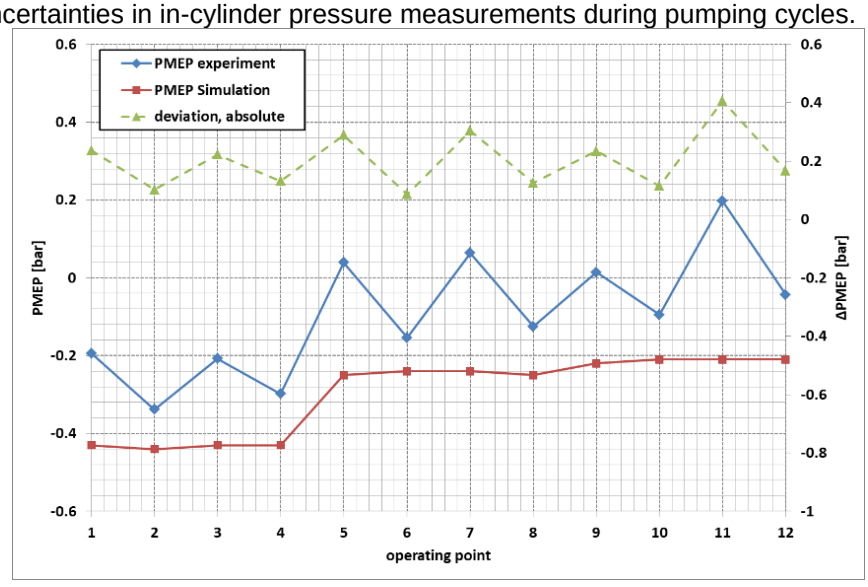

Figure 68: comparison of experimental versus calculated values of PMEP for 12 operating points

Figure 69 shows a comparison of calculated versus measured peak pressure values (p_{max}) over the 12 operating points. Very good agreement is observed, while peak pressure values are slightly underpredicted for low loads and overpredicted for higher loads.

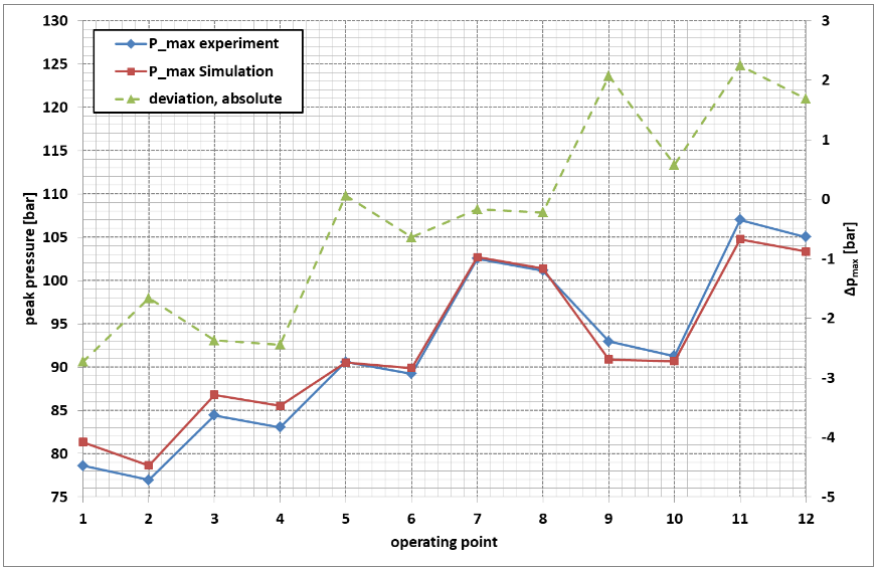

Figure 69: comparison of experimental versus calculated values of p_{max} for 12 operating points

Figure 70 shows a comparison of calculated versus measured in-cylinder and intake pressure for operating point 8. Additionally to the excellent agreement in transient in-cylinder pressure data, pressure pulses and absolute pressure values in the intake port are captured well.

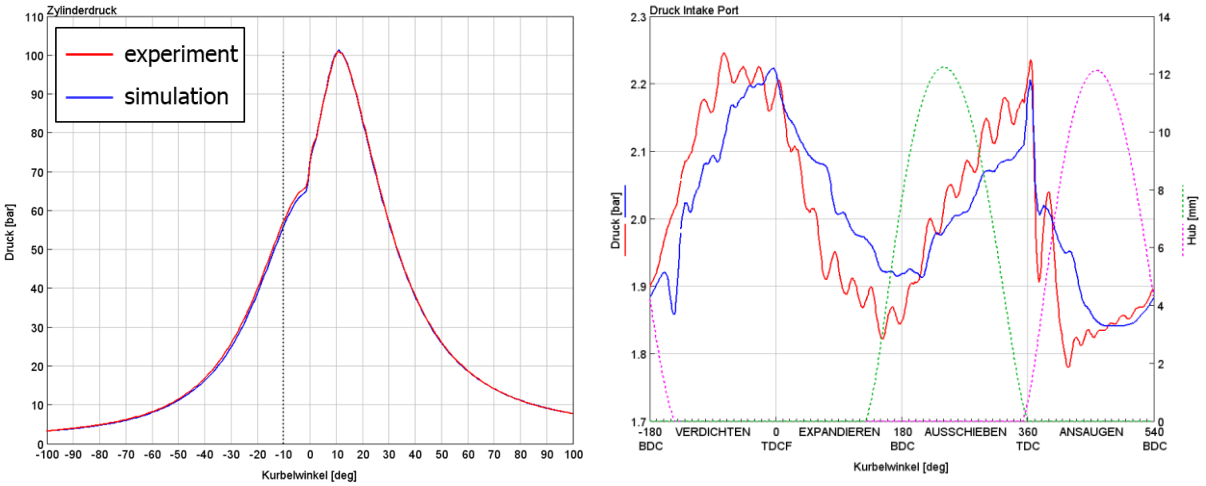

Figure 70: comparison of transient cylinder pressure and intake pressure for experiment (red) versus simulation (blue), operating point 8 (exemplarily)

3.5.2 MTU Fast Running Model

A speed up of 50 was achieved with the FRM (90 s per operating point for the full engine model vs. 1.8 s simulation time for the FRM). Excellent agreement was found between the reduced and full model over a wide range of operating conditions as is shown in Figure 71 and Figure 72.

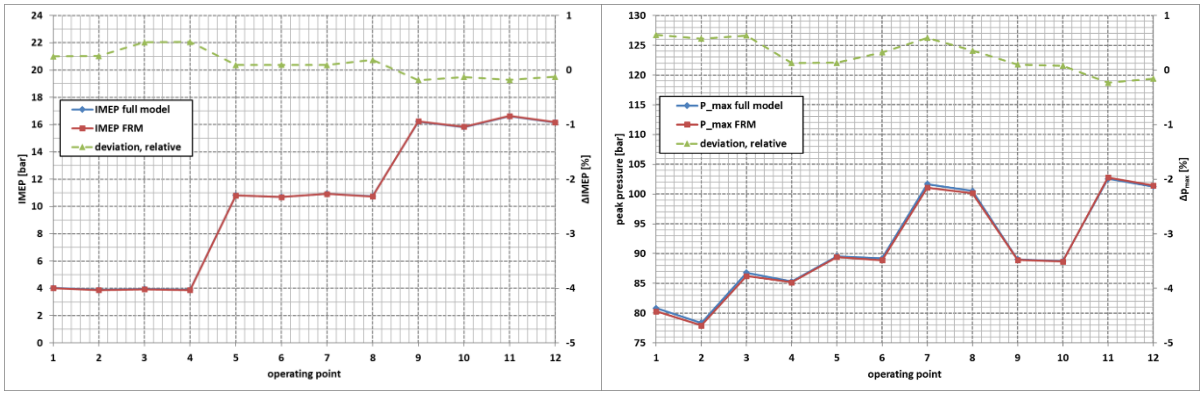

Figure 71: comparison of IMEP (left) and p_{max} (right) for the full model (blue) versus the reduced fast running model (red) a wide range of operating conditions

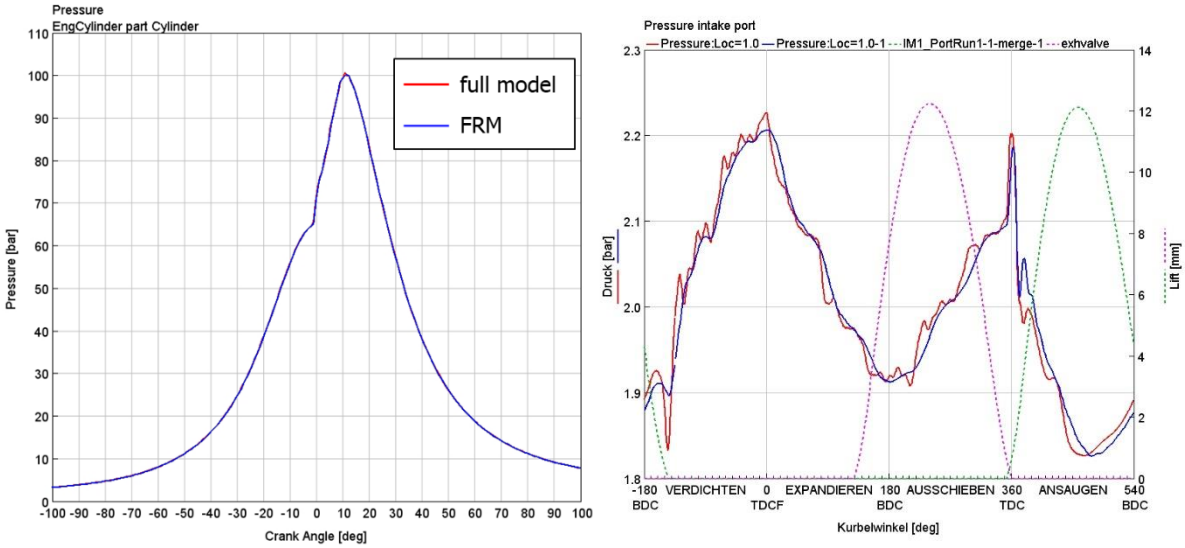

Figure 72: comparison of transient cylinder pressure and intake pressure for the full engine model (red) versus the fast running model (blue), operating point 8 (exemplarily)

3.5.3 MTU FRM with Python

As instantaneous values are passed from and to the python script, certain inputs are not available during the initial few time-steps or even simulation cycles if they are only computed at the end of the respective cycle (result variables). Additional initialization measures were implemented in order achieve numerical stability during these early cycles, which in turn increase the computational time demand. Together with time consuming in- and output procedures which are executed in every time-step, the simulation time increased from 1.8 s for the non-predictive FRM to 5.9 s for the predictive FRM with the python implementation.

The predictive FRM model with python implementation was validated against measurement data to assess prediction capabilities of the external combustion code developed in WP4. Good agreement was found between the measured and predicted heat release rates and pressure evolutions. Injected fuel mass, premixed and diffusion combustion phases and ignition delays were captured well, exemplarily shown in Figure 73.

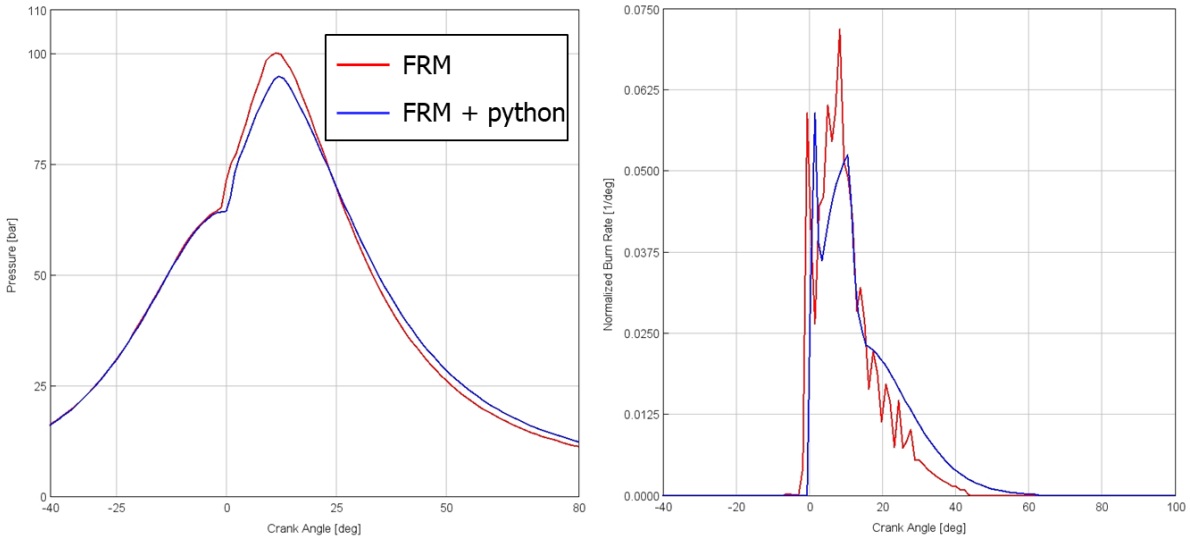

Figure 73: comparison of transient cylinder pressure and heat release rate (normalized by total fuel mass) for the non-predictive FRM (red) versus the predictive FRM with python implementation (blue), operating point 8 (exemplarily)

Differences were observed to be up to 10% in maximum pressure for certain operating points. Ignition delays were slightly overpredicted which causes the difference observed in maximum pressure. Combustion phases including the late stages which are critical for emission predictions are in excellent agreement with test bench measurements. The temporal evolution of the gas mixture in the cylinder during compression is critical with respect to the calculation of ignition delays but very difficult to capture accurately as no means of validation exist with test bench data in general. Trends, however, are predicted well by the developed model which takes into account injection characteristics, fuel type and reactivity of the unburned mixture as detailed in WP4.

3.5.4 Multi cylinder engine model

a) 100% engine load

Table 5 shows the results of the optimization compared to the baseline case at full engine load (P=320 KW) and a variation in fuels. NOx emissions from the baseline case with Diesel fuel are high at 7.8 g/kWh with only a change in injector system which is higher than expected emissions from a EURO IV engine (3.5 g/kWh) which can be attributed to the enhanced mixing and accelerated combustion due to common rail injection compared to a pump injector unit. However, the emissions from the baseline only serve as a means of comparison and to highlight the potential of exhaust aftertreatment and alternative fuels.

Target NOx emissions were achieved over all fuels while keeping engine power output constant. Longer injection durations were observed for fuels with lower heating values compared to Diesel and therefore an increase in break specific fuel consumption resulted. Correcting BSFC values to Diesel equivalent fuel consumption shows minor decrease in consumption for all fuels except HVO. The general increase in BSFC due to exhaust aftertreatment was seen to be small even with a drastic reduction of NOx emissions. The addition of small amounts of EGR enabled a shift to earlier injection timings compared to the base case while lowering NOx emissions. BSFC increase due to DPF regeneration amounts to an average of 0.1% for all fuels due to high exhaust temperatures at full load.

Table 5: comparison of optimized parameters and outputs for 100% load

Case	Diesel (baseline)	Diesel (optimized, aftertreatment)	HVO20 (optimized, aftertreatment)	HVO (optimized, aftertreatment)	OME7 (optimized, aftertreatment)	R100 (optimized, aftertreatment)
Power output [kW]	320.3	321.4	321.4	321	320.3	318.2
BSFC [g/kWh]	195.8	197.9	196	195.8	203.9	222.2
BSFC Diesel equivalent [g/kWh]	195.8	197.9	196.4	198	195	196.5
SOI [°CA aTDCF]	-11	-12.63	-10.84	-12.75	-14.25	-14.25
DOI [ms]	2.77	2.78	2.97	2.78	3.07	3.27
EGR rate [%]	0	2.5	1.38	1.25	1.5	1.5
NOx [g/kWh]	7.8	0.384	0.386	0.394	0.395	0.394
NOx [g/kWh] raw	7.8	6.44	6.287	6.556	6.709	6.886
p_{max} [bar]	178.75	183.1	173.1	186	186.15	185.95
Well-to-wheel CO2 red. [%]	n/a	0	18.6	90.0	5.4	88.1

b) 75% engine load

The comparison in operating conditions for the 75% part load operation is shown in Table 6. The optimization was conducted for different fuels and minimizing BSFC while limiting NOx emissions to 0.4 g/kWh as with the full load operation. Again NOx emissions from the baseline case with Diesel fuel are high at 4.2 g/kWh which can be attributed to the enhanced mixing and accelerated combustion due to common rail injection compared to a pump injector unit.

For part load operation, EGR rates from 0% to 11.25% are used while achieving very low NOx emissions with high rail pressures ($p_{inj,max}$=2000 bar, enabling short injection durations) due to high SCR conversion rates (98%) over all fuels. The influence of exhaust aftertreatment on BSFC was again observed to be negligible but Diesel equivalent fuel consumption showed no increase over fuel variation due to a shift to earlier start of injections as NOx emissions were generally low.

Table 6: comparison of optimized parameters and outputs for 75% load

Case	Diesel (baseline)	Diesel (optimized, aftertreatment)	HVO20 (optimized, aftertreatment)	HVO (optimized, aftertreatment)	OME7 (optimized, aftertreatment)	R100 (optimized, aftertreatment)
Power output [kW]	239.8	239.8	238.2	241.8	239.4	241.6
BSFC [g/kWh]	204.6	203.7	201.9	200.7	212.2	227.1
BSFC Diesel equivalent [g/kWh]	204.6	203.7	203.5	204.2	204.2	202.1
SOI [°CA aTDCF]	-9.2	-9.38	-9.6	-9.61	-10.25	-11.625
DOI [ms]	2.4	2.235	2.4	2.25	2.493	2.65
EGR rate [%]	0	0	0	3.75	11.25	1.25
NOx [g/kWh]	4.2	0.084	0.0856	0.0625	0.0362	0.071
NOx [g/kWh] raw	4.2	4.065	4.172	3.0	1.778	3.55
p_{max} [bar]	143.55	146.2	149.1	147.4	146.2	153.05
Well-to-wheel CO2 red. [%]	n/a	0	18.1	90.0	3.8	88.1

c) 50% engine load

The comparison in operating conditions for the 50% part load operation is shown in Table 7. The optimization was conducted for different fuels and minimizing BSFC while limiting NOx emissions to 0.4 g/kWh. Again NOx emissions from the baseline case with Diesel fuel are higher than EURO IV regulations at 3.38 g/kWh.

Comparable to 75% load operation, NOx emissions are low due to similarly high SCR conversion rates. Therefore, analogous observations are made for EGR rates, short injection durations, a shift to early injection timings and Diesel equivalent BSFC.

Table 7: comparison of optimized parameters and outputs for 50% load

Case	Diesel (baseline)	Diesel (optimized, aftertreatment)	HVO20 (optimized, aftertreatment)	HVO (optimized, aftertreatment)	OME7 (optimized, aftertreatment)	R100 (optimized, aftertreatment)
Power output [kW]	159.8	160.7	161.6	161.9	159.8	159.1
BSFC [g/kWh]	217.1	216.0	214.9	213.1	225.9	244.0
BSFC Diesel equivalent [g/kWh]	217.1	216.0	216.6	216.8	216.5	217.1
SOI [°CA aTDCF]	-9.0	-8.0	-8.125	-7.5	-9.375	-13.125
DOI [ms]	1.995	1.745	1.91	1.745	1.96	2.036
EGR rate [%]	0	0	6.25	5	11.25	11.25
NOx [g/kWh]	3.38	0.076	0.052	0.0522	0.038	0.05
NOx [g/kWh] raw	3.38	3.8	2.6	2.61	1.9	2.5
p_{max} [bar]	116.68	124.35	120.2	117.1	122.35	133.9
Well-to-wheel CO2 red. [%]	n/a	0	17.8	90.0	3.8	87.9

d) 25% engine load

The optimized parameters for engine operation at 25% load are given in Table 8. SCR conversion rates are 97% for all fuels which result in low NOx emissions for all fuels with exhaust aftertreatment compared to the Diesel baseline case with 3.658 g/kWh. Again, high rail pressures could be employed, while the use of EGR rates up to 15% significantly lowered raw NOx emissions (as low as 1.7 g/kWh for HVO operation). Diesel specific BSFC remained constant over all fuels except for HVO20 and R100 with low EGR rates and late injection timings, where a reduction of 1% is achieved. A reduction in raw NOx emissions can be directly related to a reduction in urea consumption. In case of HVO in comparison to Diesel, the reduction in urea consumption is more than 50%.

Table 8: comparison of optimized parameters and outputs for 25% load

Case	Diesel (baseline)	Diesel (optimized, aftertreatment)	HVO20 (optimized, aftertreatment)	HVO (optimized, aftertreatment)	OME7 (optimized, aftertreatment)	R100 (optimized, aftertreatment)
Power output [kW]	78.0	80.7	80.2	81.0	81.9	80.4
BSFC [g/kWh]	257.9	255.9	251.8	251.6	266.3	284.0
BSFC Diesel equivalent [g/kWh]	257.9	255.9	253.8	255.9	256.3	252.7
SOI [°CA aTDCF]	-10	-10.9	-6.97	-11	-13.81	-6.5
DOI [ms]	1.55	1.272	1.4	1.25	1.3	1.45
EGR rate [%]	0	0	0	15	7.8	1.25
NOx [g/kWh]	3.658	0.115	0.082	0.039	0.087	0.0643
NOx [g/kWh] raw	3.658	3.919	2.965	1.702	3.302	2.325
p_{max} [bar]	90.08	95.9	86.06	92.55	82.98	82.4
Well-to-wheel CO2 red. [%]	n/a	0	18.7	90.0	3.8	88.2

In order to investigate the sensitivity of the model to changes in SCR conversion efficiency, the size of the SCR system was reduced by 50%, leading to a drop in conversion efficiency from 98% to 70% at full load due to the resulting high space velocities. The optimization was run again, to obtain corresponding operating parameters for the engine while still fullfilling the exhaust regulation limits for NOx (shown in Table 8).

High EGR rates across all investigated fuels are applied to reduce raw NOx emissions due to the reduced SCR conversion. At the same time, earlier start of injection is needed caused by high EGR rates. BSFC values therefore rose compared to the baseline case without aftertreatment. An increase in fuel consumption compared to the cases with full sized SCR system between 1.6% (HVO) to 3.8% (Diesel) was observed.

Table 9: comparison of optimized parameters and outputs for 25% load

Case	Diesel (baseline)	Diesel (optimized, aftertreatment)	HVO20 (optimized, aftertreatment)	HVO (optimized, aftertreatment)	OME7 (optimized, aftertreatment)	R100 (optimized, aftertreatment)
Power output [kW]	320.3	319.2	320.1	319.6	319.9	319.7
BSFC [g/kWh]	195.8	205.4	200.8	198.9	208.7	227.3
BSFC Diesel equivalent [g/kWh]	195.8	205.4	202.4	202.3	200.8	202.3
SOI [°CA aTDCF]	-11	-14.75	-14.25	-14.63	-14	-15
DOI [ms]	2.77	2.83	3.02	2.84	3.13	3.35
EGR rate [%]	0	15.6	15.1	15.25	14.75	15.2
NOx [g/kWh]	7.8	0.393	0.397	0.397	0.391	0.396
NOx [g/kWh] raw	7.8	1.31	1.323	1.323	1.303	1.32
p_{max} [bar]	178.75	172.7	171.9	172	168.3	169.3
Well-to-wheel CO2 red. [%]	n/a	0	19.2	90.2	6.1	88.2

Figure 74 shows the change in engine efficiency of all operating conditions relative to corresponding operating condition using Diesel. The figure demonstrates, that the potential of fuels with different characteristics in comparison to diesel can be in particular advantageous, if a restriction is added to the system. In the current case, this is the reduction of the SCR size, which forces a high EGR rate

application. Under these conditions, fuels with lower tendency to produce soot are beneficial with regard to particulate filter regeneration energy demand.

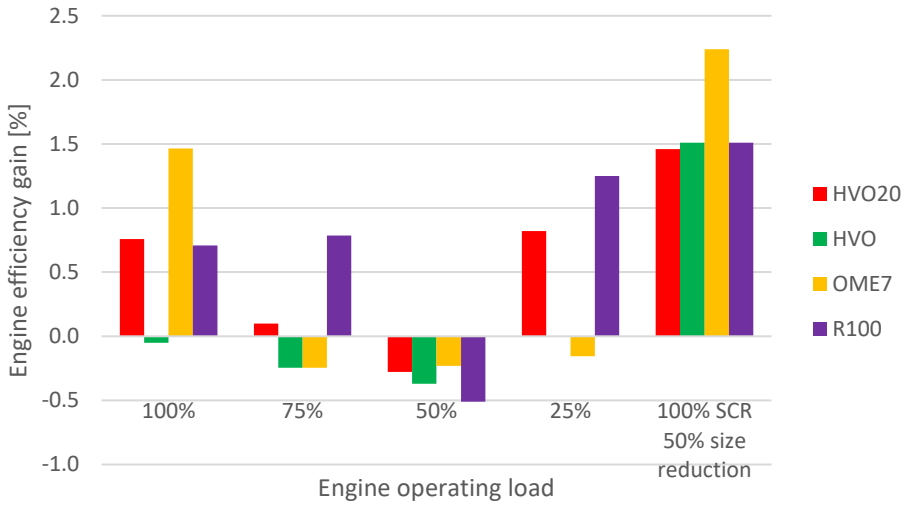

Figure 74: Change in engine efficiency, relative to the corresponding optimized condition using Diesel.

In Figure 75, the total well-to-wheel CO2 reduction potential, relative to the corresponding operating condition using Diesel is depicted. It appears, that the majority of the well-to-wheel CO2 reduction origins from the well-to-tank reduction, respectively from the fuel itself and not from the gain in engine efficiency.

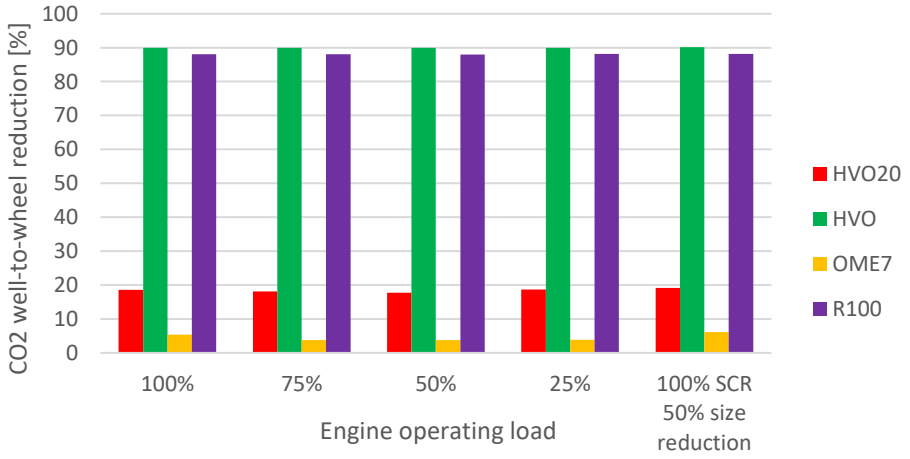

Figure 75: CO2 well-to-wheel reduction, relative to the corresponding optimized condition using Diesel.

Figure 76 shows the contribution of the tank-to-wheel change in CO2, relative to the well-to-wheel change. The figure shows, that only for the blends with relatively low amount of the alternative fuel (i.e OME or HVO) affect the CO2 footprint significantly through the change in engine efficiency. Here it is to note, that the fuel consumption of the blends using the standard engine parameter settings has not been investigated, since these settings would not comply with the target emission standard (EU Stage V). It is remarkable, that the CO2 saving potential of 6.1% for the 100% load operation with a smaller

SCR in combination with OME7, 35% of this reduction origins from improved engine efficiency through the optimization.

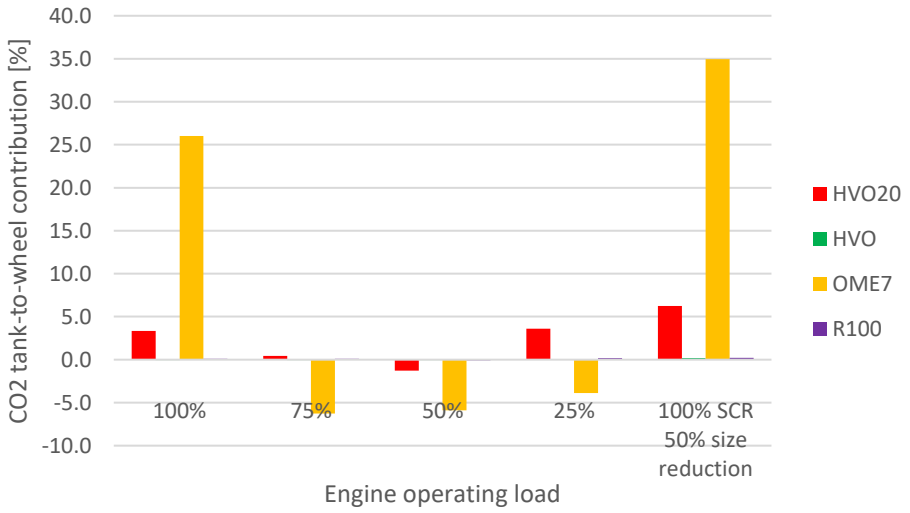

Figure 76:CO2 tank-to-wheel contribution, relative to the CO2 well-to-wheel reduction of the corresponding operating condition.

4 Conclusions

The reduction of CO2 emissions in transport and power generation is a key challenge of the current generation, which can be tackled through the introduction of fuels with a reduced CO2 footprint. The combustion characteristics of such fuels are different and require alterations in the engine settings to minimize energy consumption and maximize efficiency while respecting all other emission limits. The aim of this project is to develop a simulation platform for optimizing the overall engine unit (engine with exhaust gas aftertreatment) of vehicles of all sizes for fuels with different characteristics. The fuels studied in this project beyond diesel were chosen based on their characteristics and reflect the expected future availability of renewable fuels; two paraffinic fuels (Hydrogenated Vegetable Oil and a Gas-to-Liquid fuel), Diesel- Poly(oxymethylene) dimethyl ethers (OME_{3-6}) blends in various compositions and a blend of a paraffinic fuel with OME (R100, the naming indicating that it is a 100% renewable fuel). The project is divided into 5 work packages; the conclusions for each work package are presented below. At the end of the section an overall project conclusion is presented.

The goal of WP1 was to characterize eight fuels for compression ignition engines. To do so, the fuels were tested experimentally in a heavy-duty single cylinder engine. This allowed us to carry out the analysis of the heat release rates of the various compounds, finding out that:

- Both the paraffinic fuels GTL and HVO, due to their high cetane number, strongly reduce the ignition delay. This in turn results in smaller premixed combustion peaks.
- GTL increases the characteristic mixing frequency compared to diesel. This holds true also for GTL20 but with a smaller magnitude.
- The mixing rates of HVO and HVO20 are similar to the one of diesel. This, together with the smaller density, results in a lower heat release rate when the diffusion combustion duration is increased. The reason of the differences between HVO and GTL is to be found in the different distillation curve and in the higher hydrogen-to-carbon ratio of GTL.
- OME has the ability to increase the characteristic mixing rate due to the presence of oxygen content. The reason is the reduced need of oxygen entrainment to reach a flammable mixture, and this leads to a lower EGR sensitivity of the blends containing OME.

- R100, similarly to HVO, has a very good ignitability that reduces the ignition delay and the premixed combustion peak. However, opposite to HVO, the presence of OME increases remarkably the characteristic mixing frequency compared to diesel. This results in a heat release rate in diffusion combustion of the same magnitude of the one of diesel despite the smaller LHV.

According to their composition and to their combustion characteristics, also the emissions of particulate matter and of nitrogen oxides are influenced by the choice of the fuel.

- HVO and GTL, due to the absence of aromatics acting as soot precursors, emit less soot than diesel. Moreover, the smaller premixed combustion portion of HVO and the lower mixing rate are also beneficial for reducing the NOx emissions.
- The oxygen present in OME7 is able to shift the trade-off between soot and NOx at the levels of neat GTL.
- OME15 and R100 benefit from the presence of OME (15*vol*% and 18*vol*%, respectively) and the soot emissions are reduced drastically. R100, moreover, improves also the emissions of NOx.
- The exhaust temperature is dependent on the LHV and the mixing frequency of the fuels. Consequently, R100 and OME15, that have the smallest energy density, have also the lower exhaust temperature. OME7 and GTL also have slightly colder exhaust gases. HVO, HVO20, and GTL cannot be distinguished from diesel.

Due to the differences in mixing frequency (therefore, timing of heat release) and LHV, some fuels have a lower indicated specific energy consumption (ISEC, to compare fuel consumption of fuels with different energy content) under certain conditions while the highest in other cases. R100 is less sensitive to the intake oxygen concentration, allowing strategies with high EGR rates. In general, this result suggests that, depending on the fuel, a proper adjustment of the injection timing is necessary to fully exploit the fuel potential.

The results from WP3, concerning the heat demand of the regeneration of PFs, show a dependency on the soot origin.

- The soot activation energy and the pre-exponential factors were determined for three different fuels:
  - Diesel with 137 kJ/mol (4.62*106 1/s)
  - HVO with 85 kJ/mol (3.59*103 1/s)
  - OME 7 with 152 kJ/mol (1.43*107 1/s)

  The low activation energy of HVO can be caused by the lack of aromatic compounds and therefore a clean combustion in comparison with diesel or OME 7. Diesel is the main component (93 %) and source of the aromatic compounds in OME 7. While OME forms very little soot during combustion, it could have a more ordered structure than diesel soot and therefore requires a higher activation energy for regeneration.
- The amount of finer particles has also an influence on the activation energy. Comparing diesel soot samples with a varying percentage of finer particles, the activation energy increases with an increasing share of small particles. In addition, finer particles influence the regeneration time. Whereas a small amount of finer particles can decrease the needed regeneration time, a sample with a high share of small particles needs significantly longer times, than samples without additional fine particles.
- The regeneration time is inversely correlated to the regeneration temperature, which can be explained by the higher regeneration energy delivered with higher gas temperatures.
- The operational energy demand for a regeneration of a PF, should the regeneration happen at an exhaust temperature of 600 °C, lies in the range of 150 MJ, with a regeneration time of 20 min, for diesel and HVO application, while OME 7 has a significant higher heat demand and

therefore regeneration time (> 50 min). The particle size of soot is strongly influencing the needed regeneration energy and time.

These results were used to calculate the required extra fuel for DPF regeneration.

The objective of WP4 was to develop the fast combustion and emission models, which will be used for the in the optimization of the operating strategy. The models are developed with the aim to accurately depict changes in the heat release rate (HRR) and in the emissions with changes in operating conditions as well as for the different fuels tested. The HRR analysis showed that changes in fuel composition affect mostly the ignition delay as well as the characteristic mixing rate of the diffusion combustion. The observed changes in these parameters were used to change the HRR model parameters, resulting in an accurate depiction of the measured HRR for varying fuel composition. The NOx emission model showed very good predictive capability for all fuels with constant parameters, indicating that any change in NOx emissions between the fuels are mostly due to combustion phasing which is captured by the HRR model. The soot model parameters were shown to be affected by fuel composition, with reducing aromatic content and increasing oxygenate content affecting soot production and oxidation respectively. The resulting soot model shows very accurate estimation of emissions for a very wide range of conditions and for all fuels.
Implementation of the platform developed in WP4 into the commercial software GT-Power by means of an interface with python routines has been successfully performed. Adaptation of the python functions, handling of simulation data between the codes and validation of the predictive combustion and emission model was executed on a single cylinder MTU 396 engine model. Trends were very well represented over a wide range of operating conditions, highlighting the potential of streamlined combustion simulation tools to capture relevant processes.
Subsequent application of the implementation on a 6 cylinder, turbocharged heavy duty Diesel engine (OM501) allowed for efficient optimization of engine parameters to comply with present and future emission regulations. The code is capable of determining an appropriate engine operating strategy depending on fuel composition, thus facilitating the use of alternative fuels towards CO_2 emission and fuel consumption reduction. This has been tested calculating 5 different cases: a load variation with 100%, 75%, 50% and 25% as well as an SCR size reduction at 100% load.
The results show, that engines with DPF (Diesel Particulate Filter) can benefit from fuels which are less prone to form soot. After the optimization, in the case of HVO at low load, a higher EGR (exhaust gas recirculation) rate is applied in comparison to Diesel. The higher EGR rate does not increase DPF regeneration events and results in lower NOx raw emissions without significant penalty in fuel consumption. The reduction in raw NOx reduces urea consumption (more than 50% in this case). However, this result is only valid for this particular setup. The size of the DPF and SCR, the EGR route and many more engine design parameters affect the results. Typically, low sooting fuels are most beneficial with small filters (where regeneration frequency is high), efficient EGR path and small NOx aftertreatement devices (which has been demonstrated).
For the investigated fuels, the following maximum and minimum well-to-wheel CO2 reduction potential was found (well-to-tank in brackets):

- HVO20: 19.2%/17.7% (18%)
- HVO: 90.2%/89.6% (90%)
- OME7 6.1%/3.8% (4%)
- R100 88.2%/87.9% (88%)

The found CO2 reduction of around 90% using HVO or R100 is dominated by the well-to-tank characteristics of the fuel itself and only small contribution originates from changes in engine operation. For fuels with small amount of alternatives (OME7 and HVO20), the contribution to well-to-wheel improvements from the optimized engine operation up to 35%. The optimization well compensates or overcompensates the smaller volumetric heating value of the alternative fuels, which otherwise would result in an engine efficiency decrease.

In all, the results of this project showed that there is potential for engine optimization when using alternative fuels, both in the engine/aftertreatment design phase and during engine operation (online optimization based on fuel characteristics). The work conducted within the project has provided the tools for an engine off-line optimization based on fuel characteristics, which can be of interest for engine manufacturers working on specific applications with different (renewable) fuels.

5 Outlook and next steps

The investigations performed in this study provide sound information concerning the oxidative behaviour of particle matter generated by different fuels. Apart from the kinetic parameters derived, the additional energy required for active regeneration has been assessed. This energy has to be provided to the exhaust gas during active regeneration and increases significantly the efficiency of the powertrain.
During and after the measurements soot samples have been collected for investigating the nano structure of the soot produced by the different fuels. TEM investigations will give some information and may provide sound explanation for the different oxidative behaviour. Therefore the TEM images have to be analysed, first in order to determine the degree of crystallinity of the soot particles. In the regions with clear crystal structure evaluation of the image in terms of average length of carbon atom chains and the average distance among them provide important evidence for the soot reactivity.
In a further step the formulation of an optimal fuel can be envisaged.
On the modelling side, to develop and test methodologies for online control based on fuel identification. For this there is need to work with engine manufacturers.

6 National and international cooperation

During the project, a collaboration has been established with Neste Oil. Neste Oil is also acknowledged for the HVO supply and the co funding. ASG Analytics supplied the OME and the stabilizer to blend R100.
A virtual final event with national and international attendance is scheduled for 22.04.2021.

7 Publications

Parravicini, M., C. Barro., and K. Boulouchos, *Experimental characterization of GTL, HVO, and OME based alternative fuels for diesel engines* Fuel, accepted for publication Jan 2021.

Parravicini, M., C. Barro., and K. Boulouchos, *Strategy for Onboard recognition of GTL, HVO, and OME based alternative fuels for diesel engines* in preparation.

Dimopoulos, P., D. Schreiber, A. Liathi, C. Barro, *Soot oxidation kinetics of alternative fuels in particulate filters* in preparation.

8 References

1. Onder, C., et al., *MOVE – Modellbasierte Optimierung von Verbrauch und Emissionen*. 2015: https://www.aramis.admin.ch/Texte/?ProjectID=33031.
2. Onder, C., et al., *NextICE: Next Generation of Alternative Fuel Converters in the Transportation Sector*. 2018: https://www.aramis.admin.ch/Default?DocumentID=49975&Load=true.

3. Soam, S. and P. Börjesson, *Considerations on Potentials, Greenhouse Gas, and Energy Performance of Biofuels Based on Forest Residues for Heavy-Duty Road Transport in Sweden.* Energies, 2020. **13**(24): p. 6701.
4. Neste Corporation. *Neste Renewable Diesel Handbook*. 2020 15.03.2021.
5. Dusser, P., *The green-house gas (GHG) emission's reduction mechanisms for biofuels in the European legislation ☆.* OCL, 2019. **26**: p. 45.
6. Barro, C., P. Obrecht, and K. Boulouchos, *Development and validation of a virtual soot sensor: Part 1: Steady-state engine operation.* International Journal of Engine Research, 2014. **15**: p. 719-730.
7. Barro, C., P. Obrecht, and K. Boulouchos, *Development and validation of a virtual soot sensor: Part 2: Transient engine operation.* International Journal of Engine Research, 2014. **16**(2): p. 127-136.
8. Mcbride, B., S. Gordon, and M. Reno, *Coefficients for calculating thermodynamic and transport properties of individual species*, in *NASA Technical Memorandum*. 1993, NASA Lewis Research Center: Cleveland, OH, United States
9. Yang, Z., et al., *A Fuel Sensitive Ignition Delay Model for Direct Injection Diesel Engine Operation under EGR Diluted Conditions.* SAE Technical Paper 2018-01-0231, 2018.
10. Barro, C., et al., *Annual Report Reverdi 2019.* 2019.
11. Markus, K., *Verfeinerung des Simulationsmodells des Mercedes-Benz OM 501 Dieselmotors durch Bestimmung der Ventil-Durchflusskoeffizienten.* Bachelorarbeit Fachhochschule Nordwestschweiz FHNW Hochschule für Technik, 2017.
12. Jeffrey D., N. and S. Dennis L., *Effects of Gas Density and Vaporization on Penetration and Dispersion of Diesel Spray.* SAE International, 1996.
13. Parravicini, M., C. Barro, and K. Boulouchos, *Compensation for the differences in LHV of diesel-OME blends by using injector nozzles with diffenrent number of holes: Emissions and combustion.* Fuel, 2020. **259**.
14. Iannuzzi, S.E., et al., *Combustion behavior and soot formation/oxidation of oxygenated fuels in a cylindrical constant volume chamber.* Fuel, 2016. **167**: p. 49-59.
15. Barro, C., et al., *Neat polyoxymethylene dimethyl ether in a diesel engine; part 2: Exhaust emission analysis.* Fuel, 2018. **234**: p. 1414-1421.
16. Barro, C., M. Parravicini, and K. Boulouchos, *Neat polyoxymethylene dimethyl ether in a diesel engine; part1: Detailed combustion analysis.* Fuel, 2019. **256**.
17. Karin, P., et al., *Morphology and oxidation kinetics of CI engine's biodiesel particulate matters on cordierite Diesel Particulate Filters using TGA.* International Journal of Automotive Technology, 2017. **18**(1): p. 31-40.
18. Karin, P., et al., *OXIDATION KINETICS OF SMALL CI ENGINE'S BIODIESEL PARTICULATE MATTER.* Int J Automot Technol, 2015. **16**(2): p. 211-219.
19. Om Parkash, B., et al., *Utilization of HVO Fuel Properties in a High Efficiency Combustion System- Impact of Soot Structure on the Diesel Particulate Filter Regeneration Behavior.* International Journal of Automotive Engineering, 2015. **6**(2): p. 75-82.

9 Appendix

Table 10: WP3 PF segment samples

date of regeneration	PF Segment Label	Length mm	sampled with DOC	Remarks	sampled soot mass g balance	burned soot mass g emission
2/27/2019	1.05	279.4		Diesel	3.64	
2/27/2019	1.06	279.4		Diesel	4.7	3.64
2/27/2019	1.07	279.4		Diesel	3.4	3.64
2/27/2019	1.08	279.4		Diesel		
5/28/2019	2.01	210	x	HVO	5.1	4.33
5/28/2019	2.02	210	x	HVO	3.85	4.38
5/28/2019	2.03	210	x	HVO	4.5	4.29
5/28/2019	2.04	210	x	HVO	4.4	6.72
5/28/2019	2.05	210	x	Diesel	5.85	5.6
5/28/2019	2.06	210	x	Diesel	6.3	5.5
5/28/2019	2.07	210	x	Diesel	7.2	5.7
5/28/2019	2.08	210	x	Diesel		
5/28/2019	2.09	210	x	Diesel fine	5.29	4.13
9/17/2019	3.01	210	x	Diesel fine		
9/17/2019	3.02	210	x	Diesel fine	6.63	7.01
9/17/2019	3.03	210	x	Diesel fine	5.05	4.2
9/17/2019	3.04	210	x	5/6 Diesel & 1/6 Diesel fine	3.8	4.25
9/17/2019	3.05	210	x	5/6 Diesel & 1/6 Diesel fine	5.05	7.44
9/17/2019	3.06	210	x	OME 7	3.64	3.76
9/17/2019	3.07	210	x	OME 7	6.25	5.62
9/17/2019	3.08	210	x	1/6 Diesel & 5/6 Diesel fine	6.86	6.68
9/17/2019	3.09	210	x	5/6 Diesel & 1/6 Diesel fine	6.5	7.4
11/29/2019	4.01	210	x	5/6 Diesel & 1/6 Diesel fine	5.5	7.23
12/23/2019	4.02	210	x	OME 7	2.9	3.76
12/23/2019	4.03	210	x	1/6 Diesel & 5/6 Diesel fine	6.7	6.59
12/23/2019	4.04	210	x	1/6 Diesel & 5/6 Diesel fine	3.95	3.92
12/23/2019	4.05	210	x	OME 7	3.71	3.73
12/23/2019	4.06	210	x	1/6 Diesel & 5/6 Diesel fine	3.85	4.07

Table 11: Operating condition details:

#OC	DOI [ms]	SOI [°CA bTDC]	n_e [rpm]	p_{rail} [bar]	$O_{2,int}$ [vol%]
1	2	10	1000	900	21
2	2	10	1000	1000	21
3	2	10	1000	1100	21
4	2	10	1000	1200	21
5	2	6	1000	1000	21
6	2	7	1000	1000	21
7	2	8	1000	1000	21
8	2	9	1000	1000	21
9	2	11	1000	1000	21
10	2	12	1000	1000	21
11	2	13	1000	1000	21
12	2	14	1000	1000	21
13	2	10	1000	1000	15
14	2	6	1000	1000	15
15	2	10	1000	1000	15.5
16	2	6	1000	1000	15.5
17	2	10	1000	1000	16.2
18	2	6	1000	1000	16.2
19	2	10	1000	1000	16.9
20	2	6	1000	1000	16.9
21	2	10	1000	1000	17.7
22	2	6	1000	1000	17.7
23	2	10	1000	1000	18.2
24	2	6	1000	1000	18.2
25	2	10	1200	1000	21
26	2	6	1200	1000	21
27	2	10	1200	1000	18.2
28	2	6	1200	1000	18.2
29	2	10	1200	1000	17.7
30	2	6	1200	1000	17.7
31	2	10	1200	1000	16.9
32	2	6	1200	1000	16.9
33	2	10	1200	1000	16.2
34	2	6	1200	1000	16.2
35	2	10	1200	1000	15.5
36	2	6	1200	1000	15.5

37	2	10	1200	1000	15
38	2	6	1200	1000	15
39	3	10	1000	1000	21
40	3	6	1000	1000	21
41	3	10	1000	1000	18.2
42	3	6	1000	1000	18.2
43	3	10	1000	1000	17.7
44	3	6	1000	1000	17.7
45	3	10	1000	1000	16.9
46	3	6	1000	1000	16.9
47	3	10	1000	1000	16.2
48	3	6	1000	1000	16.2
49	1	10	1000	1000	21
50	1.5	10	1000	1000	21
51	2.5	10	1000	1000	21
52	1	10	1000	1000	21
53	1.5	10	1100	1000	21
54	2	10	1100	1000	21
55	2.5	10	1100	1000	21
56	3	10	1100	1000	21
57	1	10	1200	1000	21
58	1.5	10	1200	1000	21
59	2.5	10	1200	1000	21
60	3	10	1200	1000	21

In Figure 31, Figure 32, Figure 33, Figure 34, Figure 42 and Figure 35 it can be seen that there are operating conditions not being showed for certain fuels. The reasons are:

- OC 52 Diesel: Intake temperature too low
- OC 50 R100, HVO20: Data acquisition error
- OC14 OME15: Data acquisition error
- OC7 OME7: Data acquisition error